Author:
Rogers, Chris S

Title:
The Taphonomy of Dinosaurs and Birds of the Jehol Biota

The Taphonomy of Dinosaurs and Birds of

the Jehol Biota

Christopher S. Rogers

Supervised by Dr Stuart Kearns, Dr Maria E. McNamara, Dr Patrick J. Orr

and Prof. Michael J. Benton

A dissertation submitted to the University of Bristol in accordance with the requirements for the

award of the Degree of Doctor of Philosophy in the Faculty of Science, School of Earth Sciences.

May 2016

35,592 Words

ABSTRACT

Some of the more outstanding fossils from the Early Cretaceous Jehol Biota of NE China are the early birds and feathered dinosaurs. Compared to studies on the biology of these animals, relatively little has been written on their taphonomy.

Any interpretation of the biology of the birds and dinosaurs from the Jehol Biota and indeed any fossil inherently depends on a full understanding of its taphonomy. To that end, the taphonomy of the birds and dinosaurs from the Jehol Biota must be investigated.

We explore the taphonomy of the Jehol birds and dinosaurs from different deposits through a range of different methods. In particular, we determine the likelihood that volcaniclastic flows were responsible for the death transport and burial of these animals. Through field observations and analysis of *Psittacosaurus* fossil matrices from the fossil-rich volcaniclastic deposits of the Lujiatun Unit, we reveal multiple fossil-bearing horizons. The lithology of these horizons reveals animals including the ceratopsian dinosaur *Psittacosaurus* were not killed by a single volcanic event as had previously been suggested and were instead buried within remobilised volcaniclastic material.

Using semi-quantitative skeletal taphonomy metrics we test the hypothesis of Jiang *et al.* (2015) that the overwhelming majority of allochthonous components of the Jehol Biota were killed, transported and deposited in a lake by a pyroclastic density current. Analysis of the skeletal taphonomy of the early bird *Confuciusornis* and the four-winged feathered microraptorine dinosaurs reveals that these animals were not transported in a pyroclastic or any other kind of turbulent flow.

We also investigate the decay resistance and relative preservation potential of the skin of birds and squamates using modern analogues. The decay process in the skin of birds and squamates is documented for the first time at an ultrastructural level. Results show that decay of skin progresses differently between individuals and within the same individual over short distances.

From this, we develop a predictive model for the likelihood of the various components of the skin being available or unavailable for preservation in the fossil record at different points in the decay process . In addition to imaging decayed bird skin and muscle using standard histological techniques, we also employ micro-computed tomography. The advantages of imaging decay on non-biomineralized tissues using each method in isolation and as part of an integrated approach are then discussed.

ACKNOWLEDGEMENTS

AUTHOR'S DECLARATION

I declare that the work in this dissertation was carried out in accordance with the requirements of the University's Regulations and Code of Practice for Research Degree Programmes and that it has not been submitted for any other academic award. Except where indicated by specific reference in the text, the work is the candidate's own work. Work done in collaboration with, or with the assistance of, others, is indicated as such. Any views expressed in the dissertation are those of the author.

SIGNED _____   DATE _____

CONTENTS

STATEMENT OF COLLABORATION

All chapters were collaborations with Michael Benton, Stuart Kearns, Maria McNamara and Patrick Orr.

- Chapter 2 was published in the journal Palaeogeography, Palaeoclimatology, Palaeoecology Vol 427. For this chapter I carried out fieldwork, analysed the data, and wrote the paper (80% contribution); co-authors (David Hone and Zhao Qi) accompanied me on fieldwork and contributed to writing the paper.

- Chapter 3 has also been formatted for submission to the journal Palaeogeography, Palaeoclimatology, Palaeoecology. For this chapter I photographed specimens with the help of DH. ZQ also contributed to Chapter 3 by helping with accessing and photographing specimens. I assessed skeletal taphonomy, analysed the data and wrote the paper (100% contribution).

- Chapter 4 has been formatted for submission to the journal Paleobiology. I collected and analysed the data and wrote the paper (100% contribution).

- Chapter 5 is a collaboration with Phil Donoghue who scanned samples using the TOMCAT beam line of the Swiss Light Source, Paul-Scherrer Institut, Villigen, Switzerland. I analysed the data and wrote the paper (100% contribution).

Specific collaborations are noted at the start of each chapter.

Introduction

1. Introduction to taphonomy

Palaeobiology has always stood at a nexus between biology and geology, and over the last two centuries, the field has grown to incorporate methods and practices from other areas of science. It could be argued that no aspect of palaeobiology embodies this approach more than taphonomy; the study of the transfer of biological material into the lithosphere (Efremov, 1940; Behrensmeyer et al., 2000). When viewed in a palaeontological context, the primary role of taphonomy is to highlight and assess the extent of taphonomic bias in the fossil record at the level of a community, species, or tissue (Briggs, 1995; Behrensmeyer et al., 2000). Any interpretations based on fossil material concerning ancient biodiversity (Raup, 1976), phylogenetic relationships (Sansom et al., 2010), functional anatomy (Kemp and Unwin, 1999) and ecology (Kidwell and Behrensmeyer, 1988) can be affected by taphonomic bias (Briggs and McMahon, 2016). Therefore, palaeontological analyses must account for the effects of taphonomy on the fidelity of the fossil record. Palaeontological data can only be viewed objectively when the effect of taphonomic bias is considered and in some cases corrected.

The origins of taphonomy can be traced back several hundred years, with, for example, forensic observations of decay in carcases from 13th century China (Tzu, 1924; Benecke, 2001). Later, the palaeontological implications of taphonomy were recognised by Darwin in *The Origin of Species*, when he wrote: "No organism wholly soft can be preserved" and "only organic beings of certain classes can be preserved in

a fossil condition" (Darwin, 1859, p355 & 538). It was not until 1940 that the modern palaeontological approach to taphonomy emerged, when Efremov (1940), coined the field 'tafonomiya'. Once taphonomy was defined in a palaeontological context, a more rigorous approach to recording these types of observations and their impact on fossil data sets was possible. Early studies extrapolated the effects of taphonomic bias using one or more of the following three approaches; (1) reconstructing taphonomic history directly from fossil material (Olsen, 1952); (2) using actualistic observations of the carcassses of modern organisms (actuopalaeontological observations) to infer taphonomic processes in the fossil record (Schäfer 1972); (3) using a more experimental approach to attempt to replicate the conditions under which an individual assemblage formed (Menard and Boucot, 1951; Brenchley and Newell, 1970). But these studies typically focused on mineralized skeletons, paying relatively little attention to the preservation of other tissues. The taphonomy of soft tissues was brought to the forefront during the last decades of the twentieth century and has remained an important aspect of modern taphonomic investigations (Seilacher et al., 1985; Briggs and Kear, 1993b; Briggs, 1995; Briggs and McMahon, 2016).

2. Experimental taphonomy

The use of scanning electron microscopy and chemical analysis techniques such as x-ray diffraction and microprobe to closely monitor and manipulate the conditions under which decay occurs proved to be a breakthrough in the field of taphonomy, allowing the mineralization process to be replicated in laboratory settings (Allison, 1988; Briggs and Kear, 1993b; Hof and Briggs, 1997; Grimes et al., 2000; Briggs and McMahon, 2016). Experimental decay has subsequently been used to investigate how taphonomic bias impacts the preservation and interpretation of phylogenetic data (Sansom et al., 2010, 2011), reinforcing the concept that

information from the fossil record must be viewed through a taphonomic filter. The preservation of soft tissues has been further scrutinised through the application of high-resolution three-dimensional imaging techniques such as micro computed-tomography (CT) (Donoghue et al., 2006; Sanchez et al., 2013). Additionally the use of high sensitivity chemical analysis techniques such as mass spectrometry to study taphonomy at a molecular level has now become widespread; using trace amounts of organic compounds as identifying biomarkers for non-biomineralizing structures in the fossil record (Asara et al., 2007; Lindgren et al., 2012; Bertazzo et al., 2015; Colleary et al., 2015; McNamara et al., 2016b; Clements et al., 2016).

3. Data collection

Ideally studies should aim to use quantitative/numerical measurements to describe taphonomy, not poorly defined qualitative/relative terms, such as 'well preserved' or 'poorly preserved', as their use prevents accurate comparisons between specimens/sites and makes it more difficult to test for relationships between taphonomic variables (Beardmore et al., 2012b). But as noted above, taphonomy is a broad subject that encompasses many variables, and in some cases, the data does not lend itself well to quantitative description. This is particularly true of those studies concerned with mapping the sequence or extent of decay of non-biomineralized tissues (Sansom et al., 2011; 2012, Murdock et al., 2014) where it is more pragmatic to use qualitative descriptive terms. If this is the case, then to ensure the taphonomy of the specimen is faithfully recorded, descriptions need to be detailed. One way to improve the detail of a study is to focus on taphonomy of the same subject/deposit at a variety of scales, from individual tissues (McNamara et al., 2016a) and organisms (Murdock et al., 2014) to fossil deposits (Beardmore et al., 2012b) or entire ecosystems (Gaines et al., 2012; Zhou et al., 2016). Another means to make detailed

descriptions is by using a range of different methods and approaches to collect and analyse the data. As with any hypothesis, those taphonomic models most robust to testing are those based upon a suite of evidence collected at different scales and using different methods aiding researchers in comparing and analysing patterns in larger taphonomic datasets.

4. Lagerstätte and the Jehol Biota

The field of taphonomy is broad. Despite this, most taphonomic studies base their investigations around sites of exceptional preservation, i.e., Konservat Lagerstätten: deposits that contain mineralized soft tissues or impressions of soft tissues (Seilacher et al., 1985). Exceptional preservation is defined as the preservation of the soft non-biomineralized parts of animals and plants (Orr and Briggs, 1999). Studies based on Lagerstätten are usually either reconstructing the taphonomic history of specimens and associated deposits through direct study (McNamara et al., 2010). Alternately the results of experimental decay and/or actuopalaeontological observations can be used to investigate and test hypotheses on the conditions that allow for exceptional preservation in specific Lagerstätten (Briggs and McMahon, 2016). These deposits drive taphonomic research because they present rare opportunities to investigate instances where the processes that control preservation are pushed to their very limit. Understanding these limitations informs us of those tissues and taxa we might expect to be preserved under certain conditions and those, which due to some aspect of their biology or chemistry are unlikely ever to be preserved (Briggs, 1995). Understanding taphonomic processes allows us to test whether the absence of a structure or taxon from certain periods or locations in the fossil record is a reflection of the true distribution/presence at the time or a failure to preserve.

The Middle Cambrian Burgess Shale of British Columbia, a well-known

Konservat Lagerstätte has had its taphonomy extensively studied, with taphonomic

models for its formation widely supported by a range of evidence gathered using

different approaches, including experimental decay (Briggs and Kear, 1993a),

elemental mapping of specimens (Orr et al., 1998) and classic sedimentological

studies and geochemistry (Gaines, et al., 2012). By comparison, taphonomic studies

on the Early Cretaceous Jehol Biota of NE China are underrepresented (Fürsich et al.,

2007; Zaho, et al. 2007; Jiang et al., 2014). Instead most studies to date constitute

taxonomic descriptions of the plants (Sun et al., 1998), insects (Zhang et al., 2010b),

birds (Zhou and Zhang, 2006; O'Connor and Zhou, 2012), feathered dinosaurs (Xu et

al., 2003; Zhang et al., 2010a) and other terrestrial and aquatic vertebrates of the Jehol

Biota (Meng et al., 2006; Wang et al., 2010). This makes the Jehol Biota a key

assemblage for understanding the emergence of our modern terrestrial ecosystem

(Benton et al., 2008). The environment prevalent in NE China during the deposition

of the Jehol Biota has been reconstructed as a series of lakes surrounded by forests in

a temperate climate, with the region experiencing regular volcanic activity (Benton et

al., 2008; Amiot, et al., 2015). Typically the animals and plants of the Jehol Biota are

preserved within laminated fine-grained lacustrine deposits, but some fluvial deposits

are also fossiliferous (Pan et al., 2013). Collectively these sediments are known as the

Jehol Group, which comprises from oldest to youngest; the Yiaxian Formation, the

Jiufotang Formation and the Fuxin Formation (Pan et al., 2013). The level of

preservation, in the Jehol Biota is often limited to carbonaceous compression fossils

with occurrences of phosphatised soft tissues being much more rare (Benton et al.,

2008). Nevertheless, a great deal of ecological and evolutionary information can be

gathered from the preserved non-biomineralized tissues of the Jehol Biota with many

bird and dinosaur fossils sporting feathers or feather-like filaments (Zhang et al., 2008). In reality these are not the feathers themselves but the remains of pigment-containing organelles within the feather that reflect its morphology and position after the original keratin has degraded (Vinther et al., 2008).

It is important to investigate and gather data on the taphonomy of the Jehol Biota in order to test current taphonomic hypotheses and produce a robust taphonomic model. This will reveal the extent to which ecological and phylogenetic data recorded from the Jehol Biota is influenced by taphonomy.

5. AIMS

This thesis aims to address several issues regarding our limited understanding of aspects of the taphonomy of the Jehol Biota: (1) determine the accuracy of general statements concerning the taphonomic history of dinosaurs and birds of the Jehol Biota; (2) investigate the relationship between regional volcanism in Early Cretaceous NE China and the taphonomic processes that formed the Jehol Biota; and (3) discuss the appropriateness of current methods and devise new procedures and analyses for investigating the taphonomy of deposits, specimens and non-biomineralized tissues in greater detail.

Chapter two investigates the sedimentary sequence of the lowermost division of the Jehol Group; the Lujiatun unit of the Yixian Formation, one of the deposits where the Jehol Biota can be found in fluvial deposits. The preservation of the Jehol Biota in the Lujiatun Unit is atypical of the Jehol Group; it is characterised by three-dimensional articulated skeletons with no non-biomineralized tissues preserved. This study determines whether earlier statements about its formation (Jiang and Sha, 2007; Zhao et al., 2007; Hedrick et

al., 2014) are correct. Horizons that yield fossil material are identified, and a new taphonomic model for the vertebrate specimens is presented, specifically for the ceratopsian dinosaur *Psittacosaurus*, which dominates the fossil assemblage.

Chapter three investigates the taphonomic history of two key groups of terrestrial vertebrates from the Jehol Biota, i.e., the bird *Confuciusornis* and microraptorine dinosaurs. The taphonomic history of terrestrial vertebrates from the Jehol Biota has been specifically linked to volcanism (Jiang et al., 2014) but this hypothesis has yet to be tested using a large dataset of multiple specimens. Patterns of skeletal articulation and completeness (Beardmore et al., 2012b) are used to assess the likelihood that these animals were killed, transported and buried by pyroclastic density currents (Jiang et al., 2014). Articulation and completeness data was also used to determine the impact of anatomy on taphonomy and discuss the application of skeletal taphonomy metrics in this and future studies.

Chapter four addresses how the differential effects of decay on individual tissues are often overlooked (Sansom et al., 2010, 2011; Murdock et al., 2014). The impact of the decay process on the likelihood of the skin of birds and squamates being preserved in the fossil record is investigated using an experimental approach. The skin is an ideal subject for this study as it is a highly complex organ composed of multiple tissues.

Chapter five develops a major theme in chapter 4 chapter four by discussing the merits of three different approaches used to document the results of decay experiments. Generally, morphological decay is imaged using photography or electron microscopy (Briggs and Kear, 1993a), making interpretation of changes to complex, often layered tissue ultrastructure difficult

to interpret in three dimensions. The advantages of using micro-CT to study decay in un-mineralized tissues are demonstrated for the first time, and future applications of this technology to study taphonomy are discussed.

Chapters two to five in this thesis will be or have already been submitted for publication, and they have been written and formatted with this in mind. For this reason the main topics of the thesis are included in the introductions of the relevant chapters. Details of publication and author contributions are presented at the start of each chapter.

The Chinese Pompeii? Death and destruction of dinosaurs in the Early Cretaceous of Lujiatun, NE China

A group of *Psittacosaurus* trapped in a slurry of water and sediment by John Sibick

The Chinese Pompeii? Death and destruction of dinosaurs in the Early Cretaceous of Lujiatun, NE China

Christopher S. Rogers[a*], David W.E. Hone[a, b], Maria E. McNamara[a, c], Qi Zhao[d], Patrick J. Orr[e], Stuart L. Kearns[a], Michael J. Benton[a]

[a] *School of Earth Sciences, University of Bristol, Wills Memorial Building, Queens Road, Bristol, BS8 1ND, UK*

[b] *School of Biological & Chemical Sciences, Queen Mary University of London, E1 4NS, U.K.*

[c] *School of Biological, Earth and Environmental Sciences, University College Cork, Distillery Fields, North Mall, Cork, Ireland.*

[d] *Institute of Vertebrate Paleontology and Paleoanthropology, Chinese Academy of Sciences, PO Box 643, Beijing 100044, Peoples Republic of China.*

[e] *UCD School of Geological Sciences, University College Dublin, Belfield, Dublin 4, Ireland*

ABSTRACT

The Lujiatun Unit (Yixian Formation) yields some of the most spectacular vertebrate fossils of the Jehol Group (Lower Cretaceous) of NE China. Specimens are preserved both articulated and three-dimensional, unlike the majority of Jehol fossils, which are near two-dimensional compression fossils. The site has been referred to as the 'Chinese Pompeii' because the dinosaurs and other

---

[*] Corresponding author. Tel.: +44 117 394 1340; fax: +44 117 9253585.
E-mail address: cr8392@bristol.ac.uk

animals were assumed to have been killed and buried by hot, airborne volcanic debris and ash in a single event; this has yet to be confirmed. Field and laboratory evidence for the sedimentological context of the fossils from the Lujiatun Unit is described in detail, and used to assess whether the fossil remains correspond to a single depositional event and whether this event was the direct result of volcanic activity. Fossils of the Lujiatun Unit occur in several horizons of volcaniclastic sediments that represent multiple depositional events. Petrological analysis shows that the fossil-bearing sediments were remobilised and deposited by water. The Lujiatun dinosaurs and other fossils were therefore not killed by a single airborne volcanic ash, but in multiple flood events with a high load of volcaniclastic debris.

1. Introduction

The Jehol Biota from NE China offers an unparalleled window into Early Cretaceous terrestrial ecosystems, yielding highly abundant, exceptionally preserved fossils (Zhou et al., 2003; Benton et al., 2008). The most common Jehol fossils include plants, insects, aquatic invertebrates, fishes, salamanders, and feathered dinosaurs (Zhou et al., 2003), early birds (Zhou and Zhang 2007), and other taxa linked to the Cretaceous terrestrial revolution (Lloyd et al., 2008). These fossils occur in sediments of the Jehol Group, and are typically preserved, as flattened, near-two–dimensional, compression fossils, in laminated fine-grained lacustrine deposits (Zhou et al., 2003; Benton et al., 2008; Pan et al., 2013).

The lowest part of the Jehol Group is the Yixian Formation; its most basal division, the Lujiatun Unit (Fig. 2.1), is known for its unusual fossil preservation. In contrast to other fossils from the Jehol Group, specimens from Lujiatun lack non-biomineralized tissues, and are, instead, partially or fully articulated three-dimensional skeletons hosted within volcaniclastic sediments (Zhao et al., 2007; Benton et al., 2008). The faunal composition of the Lujiatun Unit is also distinct from that of the remainder of the Jehol Group, comprising only dinosaurs, mammals and reptiles (McKenna et al., 2006; Evans et al., 2007; Zhao et al., 2007). Birds and feathered dinosaurs considered capable of limited flight are conspicuously absent suggesting burial affected ground dwelling taxa only. The fossil assemblage is dominated by the ceratopsian dinosaur *Psittacosaurus*, the ontogeny and population biology of which have been studied in detail (Erickson et al., 2009, Zhao et al., 2013, 2014). A semi-arid climate during deposition of the

14

Jehol Group has been proposed on the basis of plant fossils and sedimentology (Fürsich et al., 2007; Jiang and Sha, 2007). However, subsequent analysis of stable isotope ratios from dinosaur fossils suggests a cool temperate climate would have been prevalent (Amiot et al., 2015).

The fossiliferous Lujiatun sediments have been referred to as the 'Chinese Pompeii' because of the suggestion that the dinosaurs and other fossil vertebrates were killed (Zhao et al., 2007; Jiang et al., 2014) and even transported (Jiang et al., 2014) by volcanic debris flows (lahars), suggesting a mode of preservation akin to the historical catastrophe at Pompeii.

A particular problem for study of the Lujiatun specimens is that many lack information on their precise stratigraphic context, often as a result of illegal excavation (Du, 2004). Recent work reporting on the taphonomy and sedimentology of a specimen containing several *Psittacosaurus* from the Lujiatun Unit has reiterated the need for stratigraphic context of specimens in order to properly assess the taphonomy of the unit as a whole (Hedrick et al., 2014). Therefore, identification and analysis of the fossiliferous horizons within the Lujiatun Unit is crucial to testing the 'Chinese Pompeii' hypothesis and understanding the sequence of events that led to such a distinctive mode of preservation. Critically, no study has yet provided a field or stratigraphic context for fossils from the Lujiatun Unit; further, it has yet to be confirmed whether any fossils supposedly from Lujiatun (especially those sourced illegally), actually originate from the Lujiatun Unit.

Here, the first account of the sedimentology of the Lujiatun Unit is presented. Using data from the field and from laboratory analysis of sediments from Lujiatun and from museum specimens of Lujiatun fossils, the stratigraphic

position of the fossils within the logged succession is investigated, and the hypothesis of whether the dinosaurs, reptiles and mammals truly were overwhelmed and transported by volcanic debris flows is tested.

Repository abbreviations. —IVPP, Institute of Vertebrate Paleontology and Paleoanthropology, Beijing. DMNH, Dalian Museum of Natural History.

2. Geological setting

The deposits of the Jehol Group are distributed around the confluence of Liaoning, Hebei and Inner Mongolia provinces, in north-eastern China (Benton et al., 2008). The Jehol Group unconformably overlies the Jurassic–Early Cretaceous Tuchengzi Formation. The Lujiatun Unit is a regional horizon within the Jehol Group (Fig. 2.1), occurring at the base of the succession, and underlying the Lower Lava Unit. Where it is absent, the Lower Lava Unit and even Jianshangou Unit, overlie the Tuchengzi Formation (Hethke et al., 2013). The Lower Lava Unit provides an ideal marker for the top of the Lujiatun Unit; it is traceable over an area measuring 4 km by 8 km, the unit ranges in thickness from 0.7–17 m in distal portions, to 200–300 m in the proximal area in the northwest, close to the presumed volcanic source (Jiang et al., 2011).

The Jehol Group encompasses, in stratigraphic order, the Yixian Formation (125–120 Ma), Jiufotang Formation, and Fuxin Formation (Pan et al. 2013). The group is late Hauterivian to early Aptian in age (Zhou et al., 2003; Benton et al., 2008). Current estimates for the age of the Lujiatun Unit are based on radiometric dates from the overlying Lower Lava Unit, and from tuffs within

the Lujiatun Unit, and range from 124.9 Ma (Yang et al., 2007; Jiang et al., 2011) to 123.2 Ma (He et al., 2006; Jiang et al., 2011).

The fossils from the Jehol Biota have been researched extensively (Xu and Norell 2004; Hu et al., 2005; Dong et al., 2013), but surprisingly little is known about the sedimentological context or taphonomy of fossils from the Lujiatun Unit (Zhao et al., 2007). Studies to date have provided a broad classification of the facies within the Lujiatun Unit, described the context of the unit within the regional geology of the area (Jiang and Sha, 2007; Jiang et al., 2011) and analysed the matrix of two Lujiatun specimens, one a cluster of *Psittacosaurus lujiatunensis* juveniles (Zhao et al., 2007), the second another assemblage of predominantly juvenile *Psittacosaurus* (Hedrick et al., 2014).

The Lujiatun Unit has been repeatedly described as a series of extensive fossiliferous tuffs, which show little to no stratification, but do display lateral variation in thickness (Zhou et al., 2003; He et al., 2006). A more thorough analysis of the area revealed that the Lujiatun Unit additionally consists of sheetflow, streamflow, sheetflood, debris flow and lahar deposits (Jiang and Sha 2007; Jiang et al., 2012). The spatial distribution of the Lujiatun Unit and overlying Lower Lava Unit, in particular their consistent thinning southward (Jiang et al., 2011) and eastward (Jiang and Sha 2007) suggests that they comprise a volcaniclastic, alluvial apron with a shield volcano at its centre (Jiang et al., 2011). In the Sihetun-Huanbanjigou area, this alluvial apron was deposited along the northern edge of a NW–SE trending basin, with the volcanic centre at the northwesternmost edge (Jiang et al., 2011). Whereas this study focuses upon Lujiatun village, the richest site for fossils in the Lujiatun Unit, earlier sedimentological accounts are based on more western locations (e.g. Jiang et al.,

2007, 2011) and thus are not relevant to the unique mode of preservation of the Lujiatun fauna.

In a petrological analysis of the matrix of a cluster of articulated juvenile *Psittacosaurus lujiatunensis* (IVPP V14341), Zhao et al. (2007) suggested that the fossiliferous horizon within the Lujiatun Unit is composed predominantly of remobilised volcanic material that had undergone several cycles of transport and deposition. IVPP V14341 shows no evidence of mixing of bones between individuals; this plus a lack of bioturbation, suggests that there was little to no time between death and burial for disruption of the carcassses via scavenging (Zhao et al., 2007). The host sediment was considered to comprise a high-density cohesive flow and not a turbulent hydraulic flow or aeolian deposit, on the basis of its high clay content, poor size sorting, massive texture and matrix-supported grains (Zhao et al., 2007). This list of characters supports a previous hypothesis that the entire Lujiatun succession represents a single catastrophic depositional event, in this case identified as a lahar (Wang and Zhou 2003; Zhao et al., 2007). In a second study on a different cluster of predominantly juvenile *Psittacosaurus* (DMNH D2156), Hedrick et al. (2014) noted that the sediment appears to have been formed by a rapidly deposited volcaniclastic flow, which they interpreted as a lahar or fluvial deposit on the basis of its clay-rich matrix, and the concurrence of the preferred orientation of specimens and the prevailing flow direction. Though the matrix of DMNH D2156 is rich in volcanic products, a pyroclastic flow origin was rejected by Hedrick et al. (2014), based upon the lack of charring or modification to bone microstructure of the *Psittacosaurus*, expected from exposure to intense heat in a pyroclastic flow (Jiang et al. 2014). The burial of animals in the Lujiatun Unit by a catastrophic volcaniclastic flow has been the

standard view, reiterated through the popular conception of Lujiatun as the 'Chinese Pompeii'. This hypothesis was supported by Jiang et al. (2014), who further suggested that all terrestrial Jehol fossils, not just those at Lujiatun, had been killed by volcaniclastic flows, and that the fossils had been transported by those flows to the site of deposition.

Other studies, however, have proposed alternatives to this 'Chinese Pompeii' model. Some authors have invoked multiple massive catastrophic high-energy depositional events (Jiang and Sha, 2007), whilst others have argued for burial in volcanic debris by a flooding event, or entombment by the collapse of burrows (Meng et al., 2004). It is clear that there is no consensus as to whether or not these events were linked to volcanism, and how the animals died and became buried.. In addition, the sedimentary matrix of some fossils includes mudstone lenses (Evans et al., 2007) and other heterogeneities such as burrow mottling (Meng et al. 2004), suggesting that the genesis of the Lujiatun Unit may be more complex than a single catastrophic volcaniclastic burial event. .

3. Methods

The present work is based primarily on data from two field trips made in 2013, but also includes data from specimens at IVPP (including earlier observations by Zhao et al., 2007). The Lujiatun Unit was logged at four sites near to Lujiatun village, Beipiao, Liaoning Province (41o35'57.3714" N, 120o54'45.0822" E) (Figs. 2.1, 2.2). An extensive section (Fig. 2.3A) was logged 1.4 km to the northwest of the village; samples were collected from individual

beds where possible; larger sedimentary packages composed of multiple beds, which share a similar lithology, were sampled every 0.2 m. Three logs (Fig. 2.3B–D) were made 0.43 km to the north of the village, along a transect of 135 m (Fig. 2.1B).

These logging locations were selected, and the exact horizons from which dinosaur specimens had been recovered were confirmed by three means.

(1) The matrix of two fossils at IVPP that were thought to have originated from the Lujiatun Unit were sampled, so that the fossil matrix could be compared with rock samples taken in the field and keyed to the logs. Samples were retrieved from IVPP V14341, a cluster of juvenile *Psittacosaurus* (Zhao et al., 2007), and another separate single adult *Psittacosaurus* IVPP V14748.

(2) Signs of excavation were observed at several points close to the sites of logs A–C, where specimens had been excavated previously, and these indicated fossiliferous levels (Fig. 2.2B–C). At one of these excavations exposed vertebrate fossil remains were identified in situ.

(3) In 2007, MJB had visited the localities in the company of IVPP palaeontologists Zhou Zhonghe and Zhang Fucheng, and they used their existing knowledge to identify the sites of logs B–D as typical of where the fossils were found (Fig. 2.2A–B). Further, one of us (QZ) has worked extensively on the local fossils (e.g. Zhao et al., 2007). Further, because of the intense activity over many years by illegal excavators, QZ interviewed those informants, and a local collector also identified the locality of log A as a source of dinosaur specimens, on the second field trip (Fig. 2.2C–E).

Prior to thin sectioning, rock samples from the field and those removed from the *Psittacosaurus* slabs at IVPP were dehydrated at 30–40oC in an oven for 12 hours. Samples were subsequently embedded in Epo-fix under vacuum at room temperature and cut using a Buehler ISOMET low speed saw equipped with a diamond wafering blade. Cut surfaces were re-impregnated with Epo-thin, polished and fixed to a frosted glass slide using a further layer of Epo-thin under vacuum, then ground and polished down to a thickness of 30 μm using oil-based lubricants to avoid compromising the integrity of the mud-dominated sediments.

Slides were analysed using a Nikon Eclipse LV100D–U stereomicroscope with NIS Elements software to calculate sediment composition and grain size. Offcuts from the manufacture of slides were polished, sputter-coated with carbon, and examined using a Hitachi S3500N variable-pressure scanning electron microscope equipped with an EDAX Genesis energy dispersive spectrometer (EDS). Rocks and sediments were classified according to the schemes in Hallsworth and Knox (1999).

4. Sedimentary succession

Field observations confirmed the position of the Lujiatun Unit beneath the extrusive vesicular trachyandesites of the Lower Lava Unit (Jiang et al., 2011) and above the underlying green sandstones of the Tuchengzi Formation (Chen et al., 2006; Zheng et al., 2001).

The Lower Lava Unit at the top of each log is a clear stratigraphic marker, whereas each log begins at a different level within the unit;, so the sedimentary log is described from top to bottom. The four logs vary in thickness from 10–19 m and show significant lateral variation. The following sequence of sediment packages was identified beneath the Lower Lava Unit; not all units are present in all sections (from top to bottom): variegated sequence of sandstones, upper grey siltstones, pink tuffaceous sandstones and lower tuffaceous siltstones (Fig. 2.3). The lowest part of the Lujiatun Unit was obscured by debris and vegetation, but its basal contact was inferred by the first appearance of distinctive green sandstones characteristic of the upper part of the Tuchengzi Formation (Chen et al., 2006).

Below the Lower Lava Unit, a variegated sequence of upper sandstones was identified in logs B–D (Fig. 2.3). This is absent in log A. These upper sandstone deposits appear to vary in thickness, with some pinching out laterally over 50 m (Fig. 2.3B–D).

4.1. Lower Lava Unit

The lower boundary of the Lower Lava Unit is in contact with different beds within the Lujiatun Unit at different sites; the underlying sediments at all sites exhibit a clear baked margin implying lateral variation in the thickness of beds between sections. The Lower Lava Unit, typically ca. 10–20 m thick, comprises olivine basalts, basaltic andesites, and trachyandesites (Jiang et al., 2011, 2012).

4.2. Upper grey siltstones (UGS)

The upper grey siltstones (UGS) underlie the variegated sandstones and comprise the majority of sections in logs A–C; they are not present in log D (Figs. 2.3A–C, 2.4C). The UGS is a ca. 7–m-thick package of very fine-grained, tuffaceous muddy siltstones-sandstones, which show normal and reverse grading between beds. There is no evidence of sedimentary structures or bioturbation; subtle variations in grain size occur throughout (Fig. 2.3A). The package is dominated by silt and fine sand-sized grains composed of crystal, glassy ash at various stages of devitrification. In certain horizons, the volume of vitric ash is noticeably higher and can be distinguished by its bright orange–red coloration.

The UGS can be described as a moderately sorted, subangular to subrounded, tuffaceous, vitric-crystal sandy-siltstone to siltstone with very few lithics (<1% of total volume) (Fig. 2.4A). The crystal fraction is dominated by quartz (60–70% total clast volume) and plagioclase feldspar (35–25% of total clast volume), crystals of biotite vary considerably in abundance between different horizons but can constitute up to 15% of total clast volume, K-feldspars are also present but contribute less than 1% of total clast volume. Iron oxides can also be seen and exist both as rims around some crystals and as isolated accumulations. All grains are floating in a matrix of very fine silt grains and clay mostly derived from devitrified vitric shards.

Analysis of thin sections reveals elongate lenses of clay minerals with fiammé-like geometry. These most likely represent post-diagenetic alteration of

vitric fragments that have deformed under the pressure of overlying sediment (Branny and Sparks, 1990). Well-rounded lithic fragments with conspicuous biotite inclusions are up to pebble and cobble size, and are distributed randomly throughout; they contribute less than 1% of the sediment by volume (Fig. 2.4A). Other minor components of the UGS are small (2–3 cm diameter) fragments of carbonised wood; these are randomly distributed throughout the unit.

An isolated limb bone was recovered in log A approximately 3.45 m from the base of this package, and a partial tooth row was identified in thin section from a sample taken 2.45 m below the top of the package (Fig. 2.4A). These suggest that further isolated vertebrate remains are scattered throughout the package (Figs. 2.2B, 2.3B).

4.3. Pink tuffaceous sandstones (PTS)

Below the UGS package lie the 600 mm thick coarser pink tuffaceous sandstones (PTS). The PTS were found only in log A where they consist of five discrete beds (Figs. 2.2C, 2.3A, 2.4B–C). The PTS can be formally described as a poorly sorted angular to sub-angular, vitric-crystal tuffaceous sandstone. As with the overlying UGS, some vitric shards show distinctive orange-coloured rims, the crystal fraction is dominated by quartz (65% of total clast volume) and plagioclase feldspar (25% of total clast volume) with small amounts of biotite (<10% of total clast volume) and K-feldspars (<5% of total clast volume), the majority of crystals are monocrystaline, but others exist as crystal clusters. Lithics are also present, but constitute less than 1% of total volume. Clasts float

in a clayey groundmass of devitrified volcanic glass and very fine silt-sized quartz and feldspar grains.

The top bed of the PTS is 100 mm thick and displays little internal structure and no evidence of bioturbation, but the boundary between the UGS and PTS is gradational and indistinct (Fig. 2.3A). This bed is a poorly sorted, medium-grained, greyish, orange-pink tuffaceous sandstone (Fig. 2.4B–C). As with the UGS, there is abundant volcanic material in the vitreous and crystal fractions; the latter comprises predominantly fragmented plagioclase feldspar and quartz crystals with minor biotite crystals. Many vitric fragments are bright orange in colour in hand specimen (presumably due to oxidation) (Fig. 2.4B). Petrographic sections demonstrate that only the larger vitric fragments are oxidised. Coarse fragments of vitreous ash are common (Fig. 2.4C), and often exhibit distinctive concave to angular margins; larger fragments can contain vesicles up to 0.5 mm in diameter (Fig. 2.4B). Most vesicles are spherical, although elongated examples also occur within pumiceous clasts. Flattened clay pseudofiammé that represent weathered pumiceous fragments are also abundant. Most importantly, a partially articulated skeleton consisting of several ribs, pelvic bones and a partial humerus was exposed within this bed (Fig. 2.4B).

The remainder of the PTS is a succession of deeper pink, poorly consolidated, coarser tuffaceous sandstones. These contain slightly less orange weathered vitric ash than the previous bed, but otherwise are a similar composition. No fossil material was recovered from the remainder of the PTS (Fig. 2.4C).

4.4. Lower tuffaceous siltstones

The lower tuffaceous siltstones (LTS) lie beneath the PTS, but detailed field characterisation of the gross structure of this unit was not possible as it is typically obscured by debris and vegetation. The LTS can be described as a moderately sorted, vitric-crystal, tuffaceous, muddy siltstone with angular to subangular grains of quartz (55% of total clast volume), plagioclase feldspar (35% of total clast volume), biotite (>10% of total clast volume) and sparse volcanic rock fragments of larger biotite phenocrysts within an aphanitic groundmass. These clasts float within a matrix of very fine silt grains and devitrified volcanic glass (Fig. 2.4D). Accumulations of iron oxides are also relatively common compared to the overlying PTS.

A broad difference exists between the uppermost 1–2 m of the unit and the remainder, which are light olive grey and pale red in colour respectively (Figs. 2.2E, 2.3A). Despite the colour contrast, the texture and lithology of both units is similar to the UGS, i.e. the matrix is composed of weathered vitric-crystal ash. Rare small fragments (10–20 mm) of plant material occur. The LTS have a limited number of distinguishing features; unlike the overlying beds, the LTS contain a higher proportion of lithics (though still rare), and almost all volcanic glass components have been totally altered to clay (Fig. 2.4D), and rarely show the characteristic orange rimmed vitric ash present in the upper part of the section.

No vertebrate fossil material was recovered in the LTS. This unit, however appears to be the horizon to which the main excavation pits were dug by locals, with evidence of recent activity.

5. Interpretation of the sedimentary log

In summary, the Lujiatun sections represent the upper reaches of a floodplain environment close to the edges of a basin that experienced multiple volcanic events such as ashfalls, lahars and pyroclastic flows. Various lines of evidence (see below) indicate these volcanic deposits were subsequently remobilised in numerous unchannelised flows. These findings agree with those of Jiang and Sha (2007), Zhao et al. (2007), and Hedrick et al. (2014), who identified a volcaniclastic origin for the Lujiatun Unit, associated with the remobilisation of volcanic material through lahars.

5.1. Lower Lava Unit

The various igneous rocks comprising the Lower Lava Unit are interpreted as the products of a shield volcano (Jiang et al., 2011, 2012) that was located to the northwest of the Lujiatun area, but perhaps less than 5 km away (Jiang et al., 2011).

5.2. Upper grey siltstones

The relative homogeneity of the UGS and the absence of channel structures indicate that these sediments originated in an unchannelised mass movement event. Successive graded intervals (normal and reversed) within the

UGS indicate deposition occurred in multiple events. The silt-grade clastics suggest the events were of low energy, only possessing sufficient energy to remobilise unconsolidated underlying sediment. Such a deposit could be generated in various ways. For example, the distal run-out portions of lahars and debris flows are known to form extensive, poorly sorted, mostly fine-grained volcaniclastic lateral deposits (Castruccio et al., 2010), and these have been recorded previously in the Lujiatun Unit (Jiang and Sha 2007). Alternatively, the UGS could represent post-lahar deposits, which are often associated with high sedimentation rates and fine-grained, remobilised, poorly consolidated lahar sediment (Major et al., 2000; Major, 2003). These overspill-run out deposits can cover extensive areas reaching up 22 km in length, from the source of the flow, to 1 km in width perpendicular to the direction of flow (Castruccio et al., 2010). The basal contacts of lahars and other debris flows are usually sharp, especially on shallow slopes and flat surfaces such as those in the distal reaches of a volcanic province (Fisher and Schminke, 1984). However, the base of the UGS is gradational, which may indicate some other type of mass movement. The style of deposition of a lahar is typically non-erosional and can preserve pre-existing soil surfaces (Fisher and Schminke, 1984), though the basal contacts of some lahars are locally erosive (Brantly and Waitt, 1988), potentially explaining the gradational contact between the lowest bed in the UGS and the underlying PTS.

An alternative depositional mechanism for the UGS is that they represent a series of sheetflood mass movements, a sedimentary feature known to be associated with volcanic deposits (Gernon et al., 2009; Paik and Kim, 2006) and that have been recorded previously at other outcrops of the Lujiatun Unit (Jiang and Sha, 2007). Sheetfloods progress downslope as uniform sheets of water and

sediment slurries, the result of remobilisation of loose material by intense bursts

of rainfall and lose momentum in alluvial areas where they deposit suspended

and entrained sediment (Hogg, 1982). Early Cretaceous NE China has been

considered to have experienced both an arid climate (Fürsich et al., 2007; Jiang

and Sha, 2007) or cool temperate conditions (Amiot et al., 2015). However, both

scenarios would have involved episodes of intense precipitation and so are

compatible with of the occurrence of sheetfloods. Channels can occur, leading to

channelised flood deposits and, if the clay fraction is sufficiently abundant ,

potentially to mudflows or non-volcanically induced lahars (Hogg, 1982).

However, it is notoriously difficult to distinguish pumiceous lahars and other

mudflows from reworked pyroclastic flow and fall deposits, especially

remobilised ignimbrites (Fisher and Schminke, 1984; Sparks, 1976). The

maximum distance travelled by sheetfloods is considerably lower than that for

known lahars (Hogg, 1982). This has implications for the ability of a flow to

entomb hundreds of animals, such as has been suggested at Lujiatun (Xu and

Norell, 2006; Zhao et al., 2007). In spite of this, if pyroclastic material is being

weathered over a large enough area, then a series of sheetfloods could lead to a

repeated build-up of originally upslope material being deposited on top of older

downslope sheetflood deposits. Considering the amount of material deposited in

pyroclastic flows and associated ash falls in general, a great amount of relatively

unconsolidated sediment would have been available for remobilisation in the

Lujiatun area. Though many sheetflood deposits are only a few centimetres in

thickness (Hogg, 1982), single sheetflood events are also capable of forming beds

70–80 cm thick (Hubert and Hyde, 1982), consistent with the range of bed

thicknesses at Lujiatun. Sheetfloods are often a response to intense seasonal

bursts of rain, which would have been likely under either the semi-arid or cool temperate climates envisaged by different authors (Fürsich et al., 2007; Amiot et al., 2015). Repetition of these would generate the multiple stacked individual beds, although the similarity of the beds, and the absence of any other lithology, suggests a single depositional process, and that the series of depositional events was closely spaced in time. (Hogg, 1982). This scenario is plausible given the ongoing volcanic activity in the Lujiatun area at the time (Jiang and Sha, 2007; Jiang et al., 2011). The variation in grain size and vitric-crystal ratios in the beds of the UGS could reflect differences in the precise nature of each eruption and co-occurring weather conditions (Parfitt and Wilson, 2008).

5.3. Pink tuffaceous sandstones

The grading of the PTS into the much finer grained, but otherwise broadly lithologically similar upper grey siltstone, suggests remobilisation of the uppermost parts of the PTS deposit (Fig. 2.3A). A distinct period of greater volcanic activity is suggested by the high abundance of coarse ash through the PTS compared to the PTS suggesting a decrease over time in the extent of volcanic activity (Fig. 2.4C). The predominance of smooth spherical vesicles within vitreous fragments of the PTS suggests a magmatic origin for the ash in all logged beds, as the vitreous fragments (Fig. 2.4B,C) are unlike the blocky shapes characteristic of a more phreatomagmatic eruption (Heiken, 1974). Pumiceous clasts represent regions of cooling magma that formed near the walls of the magma vent, whereas vitreous clasts with spherical vesicles originate in central

vent regions where fluid forces are more equal (Heiken, 1974). The absence of deformed vesicles within the vitreous components indicates that the grain shape of vitreous particles was determined by the air bubbles within the magma, suggesting a melt of high viscosity, and pointing towards a rhyolitic-andesitic composition (Heiken, 1974). Magma composition of this type is not consistent with the hypothesis put forward by Jiang et al. (2011) that a shield volcano is the main source of eruptive and syneruptive deposits in the Lujiatun Unit (Heiken, 1974).

Based upon the abundance of poorly- to moderately well-sorted, fine, angular crystal and vitric ash fragments, the near absence of lithic fragments, and the near absence of clay from a non-diagenetic origin, neither the PTS and the overlying UGS are representative of the matrix of IVPP V14341, shown by Zhao et al. (2007, fig. 2). From this, two conclusions are drawn; firstly, the sediments in logs A–D are not deposits of cohesive lahars, and secondly the matrix of IVPP V14341 and the PTS and UGS represent separate depositional events. The relatively fine-grained matrix and small size of pyroclasts, together with the angular and fragmented nature of the ash, suggests rapid transport of material some distance away from the volcanic source. The poor sorting of the unit is noteworthy. This could result from the breakage of crystals through impact during transport, especially along fractures formed during rapid cooling. Pyroclastic ash fall deposits typically feature such ash fragments, but also large unfractured clasts, but these are characteristically well sorted, (except proximal to the volcanic vent, when larger pyroclasts, such as lapilli and bombs, can occur (Sparks, 1976; Parfitt and Wilson, 2008)). The PTS is therefore unlikely to comprise pyroclastic fall deposits. Both pyroclastic flow and pyroclastic surge

deposits are poorly sorted (Fisher and Schminke, 1984; Parfitt and Wilson, 2008); the latter are characteristically enriched in crystal and lithic fragments (Fisher and Schminke, 1984) and can exhibit wavy or lenticular cross bedding and erosional bases. Pyroclastic flow deposits are also known to form discrete bedded intervals and distally, these deposits can exhibit subtle normal grading in their lower parts (Tucker, 2001) that, when unwelded, can be expressed as compositional or colour changes (Fisher and Schmincke, 1984). The PTS contains abundant crystal fragments, but does not exhibit any of the other characteristic lithological features of pyroclastic surge deposits; it does, however show discrete bedding identifiable by clear colour changes and subtle grading internally ; it is thus interpreted herein as a product of pyroclastic flows, specifically an ignimbrite.

Jiang and Sha (2007) identified volcaniclastic flows in the Lujiatun Unit, but did not consider these to represent ignimbrites because the deposits lacked grading and contained rounded pebbles. It is possible that there may have been some special and/or temporal variation in depositional processes but the evidence from this study confirms the importance of pyroclastic deposition..

An *in situ* partially articulated skeleton found within the PTS in log A (Fig. 2.3B) could have been overcome by such a pyroclastic flow, but the grading of the topmost bed of the PTS (in which the specimen is preserved), into the UGS suggests this bed is formed by the reworking of previously deposited sediments. Therefore the animal may not have been buried within a pyroclastic flow but by a remobilisation of pyroclastic flow deposits. However, extensive weathering of the specimen means it cannot be assessed whether it had been initially buried by a remobilisation of older sediments or itself remobilised from older pyroclastic

deposits. The series of pyroclastic deposits reinterpreted by the PTS are an obvious potential source for the series of remobilised event beds represented by the UGS.

5.4. Lower tuffaceous siltstones

The distinctive light olive grey and pale red coloration of the LTS is likely a weathering effect, and is attributed to the weathering of iron oxide detrital grains (McBride, 1974). Although the sedimentology of this unit was difficult to study in the field, petrological analysis shows that its lithology is broadly similar to that of the UGS, and likely the result of similar depositional processes. Therefore, it is predicted that additional volcaniclastic flows and ash falls occur below the LTS and are the source of the ash within the latter.

In summary, sedimentological and petrological data support a scenario for the genesis of the Lujiatun beds consistent with reported fossil evidence, whereby various members of a terrestrial ecosystem were killed by a series of events depositing primary and remobilised volcanic material in ignimbrites and distal lahars / sheetfloods, respectively (Jiang and Sha, 2007). Significantly, data presented herein reveals that the animals were not killed and deposited in a single cataclysm, as had been suggested (Wang and Zhou, 2003; Zhao et al., 2007; Hedrick et al., 2014).

6. Regional context

Both the pink tuffaceous sandstone and the matrix of IVPP V14341 indicate that volcaniclastic flows were a key depositional mechanism within the Lujiatun sequence. Differences between the two lithologies reflect their different origins, a pyroclastic flow and a lahar (Zhao et al., 2007), respectively, and potentially different source lithologies. Both IVPP V14341 and the PTS appear to have been deposited some distance from the source. Given that pyroclastic flows and lahars are capable of transporting debris several hundreds of kilometres along their course before losing the required energy to keep load in suspension (Sparks, 1976; Vallance, 2000), it remains possible that the relevant flows associated with IVPP V14341 and the PTS came from different volcanic centres. Jiang and Sha (2007) report a trend in the lateral thinning of syneruption deposits southward, but also more importantly westward. Whereas Jiang and Sha (2007) reported fine-grained lapillistones and sheetflood deposits several kilometres to the west of Lujiatun village, they also described coarser pebble- and boulder-dominated deposits (Jiang et al., 2012), which were not recorded by this study. The sediments in logs A–D show smaller grain size, and thus represent lower energy flows. There is no evidence of multiple vents at this stage in the geological evolution of the area. Given a single source, it appears that the sections reported here are distal to both the flanks of the volcanic source itself and the volcaniclastic deposits it yielded (Fig. 2.5). Consistent with this, the eruptive and

34

syneruptive deposits continue to thin radially away from the volcanic centre identified by Jiang et al. (2011).

In the context of the volcanic evolution of the area, the ignimbrite and the highly viscous nature of the vitric ash point towards a period of intermediate-felsic explosive volcanism during deposition of the Lujiatun Unit. Subsequently, the laterally continuous basaltic and andesitic lavas of the Lower Lava Unit were formed by a shield volcano, which was eventually terminated by a post-Lujiatun period of intermediate explosive eruptions (Jiang and Sha 2012). A volcanic centre showing major chemical changes in eruptive material and variation between the two conditions of low viscosity effusive basaltic lava and high viscosity explosive intermediate eruptions could more appropriately be classified as a stratovolcano rather than a shield volcano (Fisher and Schminke, 1984). This was discussed by Jiang *et al.* (2011) who favoured an interpretation of the source as a shield volcano, based on the profile and lateral extent of the deposits of the Lujiatun and Lower Lava units.

7. Fossil matrices

The total number of fossil specimens available to study from the collections for which the field locality is known , and therefore any additional evidence for the depositional context from these fossil specimens is tentative. In addition to those lithological characters reported by Zhao et al. (2007), the matrix of IVPP V14341 has a high clay content and lacks pumiceous vitreous fragments (Fig. 2.4F), both of which exclude an origin as a pyroclastic flow

(Fisher and Schmincke, 1984). The matrix of IVPP V14748 also lacks pumiceous vitric ash fragments, characteristic of pyroclastic flow deposits, ash fall deposits (Fisher and Schmincke, 1984) and of the UGS and PTS, but more resembles the LTS, indicating similar depositional processes, although the matrix of IVPP V14341 is finer grained (Fig. 2.4A, C, E). It appears that the matrix of IVPP V14748 originates either from the LTS, or another series of sheetflood deposits with a similar source. Field and witness evidence of repeated excavations by illegal collectors into the UGS and LTS suggests the likely presence of good quality dinosaur skeletons in these horizons. Additionally, the higher fidelity of preservation of specimens in the UGS makes it unlikely skeletal material was routinely reworked from the underlying PTS; most Lujiatun material is unlikely to originate from the latter. Further, it should be noted that the proposal that some Lujiatun Unit dinosaurs were preserved as partially articulated skeletons within the violent interior of a pyroclastic flow, such as the PTS, is at odds with most other cases in which fossils in volcaniclastic flow deposits generally consist of isolated remains (Siebe et al., 1999; McKenna et al., 2006; Antoine et al., 2012).

The majority of Lujiatun skeletons are nearly fully articulated, suggesting preservation *in situ* and this is probably a result of the high density and low energy of these distal volcaniclastic flows (Evans et al., 2007; Zhao et al., 2007). Fieldwork in the course of this study confirms other specimens are less complete and less well articulated, suggesting they have undergone some degree of disturbance and transport. The discovery of isolated bones in the field, and in thin sections suggests these are not uncommon, possibly more so than hitherto realised, (Evans et al., 2007; Hedrick et al., 2014). The prevalence of nearly fully articulated specimens in museums and institutional collections is almost

certainly a sampling bias, whereby collectors preferentially excavate and sell

articulated specimens instead of individual elements (Benton et al., 2008).

Nonetheless, the high abundance of articulated specimens indicates that the

quality of fossil preservation in the Lujiatun Unit is unusual, and implies the

prevalent sedimentological conditions were favourable. This is inconsistent with

the suggestion that volcanic flows transported the Lujiatun fossils.

8. At-rest postures

Some of the articulated dinosaur skeletons from the Lujiatun Unit exhibit

what has been described as a 'sleeping posture' (Xu and Norell 2004; Wang et al.,

2006; Gao et al., 2012). Here the term 'at-rest' is preferred to describe such

postures, as they may also be adopted while an animal is at rest but alert; the

terms 'sleeping' or 'resting' imply a behaviour that cannot be determined. The

limbs of some Lujiatun specimens are not in 'at rest' positions: some specimens

show other evidence for transportation, including considerable disarticulation

(Evans et al., 2007).

Volcaniclastic flow deposits from other localities worldwide typically

contain fossil material that is poorly articulated and fragmented (Siebe et al.,

1999; McKenna et al., 2006; Antoine et al., 2012). The lahar hypothesis for the

formation of Lujiatun fossil matrices has been challenged by some on the

grounds that the at-rest postures of Lujiatun fossils would be unlikely to be

maintained during even low-energy lahar events (Gao et al., 2012). Although

lahars are capable of transporting large clasts, boulders and entire man-made

structures (Antoine et al., 2012), at gradients below ten degrees their erosional potential is greatly diminished; soil surfaces and vegetation can be preserved underneath a flow (Fisher and Schmincke, 1984). The relatively high degree of articulation of the Lujiatun dinosaur skeletons and the absence of large clasts in the sedimentary matrix (Fisher and Schmincke; 1984) suggest that the fossiliferous localities were in low-gradient regions relatively distal to the source of the flows (Zhao et al., 2007). A lahar hypothesis cannot be excluded on the basis of the postures exhibited by the Lujiatun dinosaurs, although on sedimentological criteria this origin is less likely than other mass movement deposits (see above)..

Death by asphyxiation from volcanic gases (Wang et al., 2006) is consistent with the widespread and repeated occurrence of volcanic episodes during the Early Cretaceous of NE China (Jiang and Sha, 2007; Jiang et al., 2011, 2012). Toxic volcanic gases have been invoked as the cause of death for taxa preserved in other Jehol beds (Guo et al., 2003). In particular, this killing mechanism could generate the at-rest postures of some Lujiatun taxa, (although a mode of burial that preserves the posture is required). For example, the post-mortem at-rest postures documented in humans in volcanically active areas have been claimed to be the result of asphyxia via mass CO_2 release from nearby lakes (Kling et al., 1987; but see Hansell and Oppenheimer, 2004). Within ash sediments from the Jianshangou Unit of the Jehol Group (Fig. 2.1), the concentration of volatiles within phenocrysts correlates positively with the abundance of fossiliferous beds (Guo et al., 2003). These volatiles are hypothesised to originate either via precipitation from volcanic plumes or adsorption onto the surfaces of tephra (Guo et al., 2003) The introduction of

various poisonous eruption products into the environment through gas release, volatile-contaminated tephra, or water could be responsible for the death of the animals in the Lujiatun Unit, and their at-rest postures. Not all of the fossiliferous horizons of the Lujiatun Unit, however, are related to volcanic activity and only some of the Lujiatun vertebrate fossils show resting postures (Zhao et al., 2007). It is therefore unnecessary to evoke the release of toxic volcanic volatiles/gases as a death mechanism for all fossils from the succession. The death positions of the Lujiatun vertebrates within lahars and sheetfloods more likely represent burial *in situ* by the flow.

If the classic 'Pompeii' model were correct, the fossils should be preserved in various postures, as is the case for humans and dogs at Pompeii. Although some animals would perhaps hunker down and die in a curled-up and at-rest or defensive posture (or even be overcome while asleep), others would attempt to flee and thus show signs of being in motion. Some fossil localities show animals remaining *in situ* and presumably being buried alive (especially aeolian deposits showing animals brooding on a nest e.g., Norell et al., 1995) though this would seem less likely as a response to a low-energy waterborne deposit than a sandstorm. If the sediment has been redeposited by water, there should also be a wider range of skeletal postures, some animals lying on their backs or sides, for example, and in particular limbs would be extended rather than flexed (Faux and Padian, 2007). It is possible that the current flows lacked sufficient energy to shift the carcassses, but were strong enough to rework the sediments. At most, it is envisaged that the sheetflood and /or lahar flows lined the carcassses up in stable positions, but did not move them or disturb their protective positions.

Dinosaurs from Lujiatun that show at-rest positions have also been interpreted as having taken shelter within burrows, which were subsequently infilled (Xu and Norell 2004; Gao et al., 2012). The burial of the DMNH D2156 *Psittacosaurus* in burrows was also considered one of several plausible hypotheses by Meng et al. (2004). However, such claims require stronger evidence than simply their having a curled or head-down posture; claims of burrow collapse by Meng et al. (2004) were later rejected, by Hedrick et al., (2014) who claimed the sedimentary textures that would have supported this concept were absent. In the case of unequivocal examples of fossil vertebrates preserved in burrows the burrow walls are distinct and visible as distinct sharply curved margins that cross-cut bedding; there can be scratch marks on the inside walls of the burrow (Groenewald et al., 2001, Krapovickas et al.; 2013; Varricchio et al., 2007). None of these features were observed in the field, or associated with museum specimens.

The preservation of at-rest postures in Lujiatun vertebrates occurred above ground as the animals were rapidly buried *in situ* by a variety of cohesive flow mechanisms (lahars, sheetfloods). Otherwise, the relationship between the mode of deposition of the Lujiatun beds and the posture of the preserved vertebrates is enigmatic. It is possible, but unlikely, that the animals were covered *in situ* while alive, having failed to flee or adopting a defensive posture;– animals in the process of being covered would be expected to move or at least adopt an alternate posture. It seems more likely that these animals had already died in a non-violent manner; volcanic gassing may have been involved. Additional specimens may well demonstrate the frequency of at-rest postures at

Lujiatun, and data from modern burial events of vertebrates in lahars and sheetfloods would be especially valuable.

9. Conclusions

Here, the first systematic description of the sedimentology of the fossiliferous deposits of the Lujiatun Unit is presented and related to the exceptional preservation of the Lujiatun fossils. This study shows that multiple fossiliferous horizons exist within the Lujiatun Unit. In the region of Lujiatun village, most articulated remains are derived from a limited number of beds that represent a series of sheetflood deposits of remobilised pyroclastic material onto the upper reaches of a floodplain. The matrix of IVPP V14341 (Fig. 2.4F) is unlike any of the deposits encountered at Lujiatun village, which suggests that more than a single depositional event was responsible for the burial of the Lujiatun fossils. Field evidence shows that some depositional events occurred as a prolonged pulse of activity. Other fossiliferous horizons, such as the pink tuffaceous sandstones, represent either the remobilisation of partially articulated remains from sheetfloods and lahars or *in situ* burial of remains within a pyroclastic flow.

The absence of channelised facies, as noted by Jiang and Sha (2007) in more proximal areas, indicates that the sediments close to Lujiatun village lay further from the volcanic source than those studied by Jiang and Sha (2007); they most likely represent unchannelised sheetflood deposits. Critically, widespread evidence for sheetfloods indicates that the dense tuffaceous flows that killed the Lujiatun dinosaurs, and other animals, were not necessarily associated with

primary volcanic events/eruptions. This study emphasises the need to elucidate the depositional history of a succession prior to interpreting the taphonomy of any associated fossils. The results of this study will provide a basis for understanding the taphonomy of all fossils from the Lujiatun Unit, and will provide a framework for further investigations into the taphonomy of the Jehol Biota as a whole.

Acknowledgements

The skeletal taphonomy of *Confuciusornis* and microraptorine dinosaurs from the Jehol Biota (Lower Cretaceous, NE China)

A new day in the Jehol, tranquillity disturbed by the distant volcanic activity, by Alice Butt

The skeletal taphonomy of *Confuciusornis* and microraptorine dinosaurs from the Jehol Biota (Lower Cretaceous, NE China)

Christopher S. Rogers[a*], Maria E. McNamara[a,b], Patrick J. Orr[c], Stuart L. Kearns[a], Qi Zhao[d], Michael J. Benton[a].

[a] *School of Earth Sciences, University of Bristol, Wills Memorial Building, Queens Road, Bristol, BS8 1RJ, UK*

[b] *School of Biological, Earth and Environmental Sciences, University College Cork, Distillery Fields, North Mall, Cork, Ireland.*

[c] *UCD School of Earth Sciences, University College Dublin, Belfield, Dublin 4, Ireland*

[d] *Institute of Vertebrate Paleontology and Paleoanthropology, Chinese Academy of Sciences, PO Box 643, Beijing 100044, People's Republic of China*

ABSTRACT

Keywords: Dinosaur, Jehol Biota, Cretaceous, Taphonomy, Articulation

The Early Cretaceous Jehol Biota of NE China is famous for the exceptional preservation of birds, feathered dinosaurs and other vertebrates, but the cause of their death remains unresolved. Jiang *et al.* (2014) hypothesise that the

---

[*] Corresponding author. Tel.: +44 117 394 1340; fax: +44 117 9253585.
E-mail address: cr8392@bristol.ac.uk

terrestrial components of the Jehol Biota were killed and transported by a pyroclastic density current (PDC). We offer the first robust test of the PDC hypothesis, using the skeletal taphonomy of specimens of *Confuciusornis* and microraptorine dinosaurs to test whether their completeness and articulation conform to that predicted by such a killing mechanism. Secondly, we test how similar the skeletal taphonomy of the two groups is, an approach that may shed light on what anatomical functional differences between the two there were. Our results indicate that the specimens of *Confuciusornis* and microraptorine dinosaurs experienced a brief flotation period with minor disarticulation, followed by more extensive disarticulation and loss of completeness on the lake-bed when carcases were disturbed by underwater currents. The skeletal taphonomy of these small theropods and birds is inconsistent with death and transport by a PDC or similar catastrophic event. The cause of death and mode of deposition of the vertebrates in the Jehol Biota is likely to be some process other than PDC; therefore the skeletal taphonomy of other taxa in the biota should be reassessed.

Introduction

The animals and plants preserved within the volcanically influenced fluvial and lacustrine sediments of the Early Cretaceous Jehol Biota (130–120 Ma) of NE China offer an unparalleled view of life at the beginning of the Cretaceous terrestrial revolution (Zhou et al., 2003; Benton et al., 2008; Zhou, 2014b). Most research to date comprises taxonomic descriptions of the invertebrates, plants, enigmatic feathered dinosaurs and early birds and their ecological context (Zhou, 2014b). Recent efforts have been made to understand the Jehol Biota in a taphonomic context, specifically the cause of the mass mortality events responsible for the accumulation, and also the preservation of the world famous vertebrate fossils (Jiang et al., 2014; Rogers et al., 2015).

Mass mortality accumulations of different taxa in the Jehol Biota are the result of various environmental events. Autochthonous components of the Jehol Biota, by far the most commonly encountered died and accumulated following relatively high-frequency, low-level perturbations to the lake environment. For example, rich mass mortality horizons of aquatic mayfly nymphs have been tied to seasonal fluctuations in anoxia levels in the lake (Pan et al., 2011). Accumulations of the teleost *Lycoptera* are also common and are linked to localised mass mortality event caused by plumes of toxic bottom waters rising during periodic lake overturn events (Pan et al., 2015).

2.1 Catastrophic death hypothesis

In contrast, the accumulations of allochthonous vertebrates in the lacustrine and fluvial deposits of the Jehol Group have been attributed to various

catastrophic events related to contemporary regional volcanism (Zhou et al., 2003; Guo et al., 2003). Volcanism has long been invoked to explain the exceptional preservation of the Jehol Biota (Jiang et al., 2011; Zhou et al., 2014b). Recently death, transport and burial of the bulk of the terrestrial vertebrates been linked directly to volcanigenic events, specifically attributed to pyroclastic density currents (PDCs) (Jiang et al., 2014; Sulpizio et al., 2014). This model is termed here the catastrophic death hypothesis (CDH). The evidence in support of this hypothesis by Jiang *et al.* (2014) includes (1) the preferred E–W orientation of multiple specimens of the Early Cretaceous bird *Confuciusornis* at the Sihetun locality, (2) flexed limbs in numerous specimens of avian and non-avian dinosaurs (typical postures of PDC victims), and (3) cracks in the bones of two specimens of *Confuciusornis* that resemble those in human bones exposed to the 79 AD eruption of Mount Vesuvius.

A PDC is a fast-moving turbulent cloud of heated gas and volcanic material, including shards of volcanic glass, pumice, lapilli, and fragments of lithic material. PDC speeds can range from 10 ms^{-1} to 300 ms^{-1} (Dufek, 2016) and speeds of 100 ms^{-1} are common (Parfitt and Wilson, 2008). They can travel for hundreds of km and are capable of transporting large clasts measuring 1m in diameter (Dufek, 2016). A PDC is formed either through the collapse of an eruption column, low-pressure release of a gas-charged magma at an open vent or the explosive release of gas and lava under high pressure (Fisher and Schmincke, 1984; Parfitt and Wilson, 2008). There is little relevant experimental data concerning the transport of carcasses within a PDC. Experiments on modern taxa indicate freshly killed carcassses are highly resistant to disarticulation during transport (Allison, 1986), albeit these results were generated under

conditions unlike those inside a PDC. Reports of injuries suffered as a result of a pyroclastic flow almost exclusively refer to human casualties, the majority of which have either died or suffered life-threatening injuries as a result of exposure to extreme heat (Baxter, 1990; Loughlin et al., 1990). Most reports often refer to individuals at the periphery of the flow where impact or transportation-related physical trauma is lessened or those that had access to some form of shelter, specifically individuals who were not transported by the flow. The most common injury among these people is severe thermal damage to soft tissue. Transported individuals buried by the PDC and exposed to the centre of the flow (direct flow zone) show fractured bones or dismemberment (Baxter, 1990; Loughlin et al., 2002).

If PDCs are responsible for the aggregation of the bulk of terrestrial vertebrates in the Jehol biota, animals from a variety of habitats, then the transport of animals over a variety of distances (Jiang et al., 2014), and trauma to the bodies of those transported animals (Baxter, 1990) is implied. Animals such as *Confuciusornis* and microraptorines, which are considered to be arboreal (Zhang et al., 2009; O'Connor et al., 2011), presumably have been carried through the coniferous forests around the lake shore (Ding et al., 2016), impacting and being impacted by other objects caught in the PDC during the process. Logically transport within a PDC would have resulted in considerable damage to the carcasses, specifically resulting in the disarticulation and loss of completeness of parts of the appendicular skeleton (Loughlin et al., 2002), such as the limbs, within the flow. This transport would be followed by rapid burial of the carcassses within the crystal and lithic particles entrained by the flow.

A large dataset of specimens of different taxa can be used to test the CDH. The CDH assumes two things about the skeletal taphonomy of terrestrial vertebrates in the lake. Firstly, skeletons should show loss of completeness and articulation consistent with transport of freshly killed specimens in a turbulent flow e.g. strong linear relationships between articulation and completeness, no effect of specimen orientation on skeletal taphonomy, dismemberment of appendicular parts of the skeleton (Loughlin et al., 2002). Secondly, the taphonomy of the skeletons should be consistent with rapid burial; i.e. immediately upon deposition within the lake. Specifically, there should be no evidence for elements having moved from the position in which they originally came to rest. Both these assumptions must be met to accept the CDH, if either is rejected we must accept the null hypotheses that terrestrial components of the Jehol biota were not transported by PDCs and that less spectacular scenarios are responsible for the formation of the biota.

The aims of this paper are: (1) to test whether the taphonomy of key vertebrates, i.e., the bird *Confuciusornis* and the microraptorine dinosaurs is congruent with the CDH; and (2) if the skeletal taphonomy of these animals does not support a CDH then to what extent can differences between the skeletal taphonomy of the two taxa be explained by anatomical differences.

2. Methods

2.1 Sampling

High-resolution photographs were taken of specimens of *Confuciusornis* and microraptorines (Supplementary information 3.1) in collections at the Institute of Vertebrate Paleontology and Paleoanthropology, Beijing (IVPP) and the Chaoyang National Geopark (CYNG). Images of additional specimens were sourced from the literature (Chinsamy et al., 2012; Gong et al., 2012; Pei et al., 2012; Li et al., 2014; Han et al., 2014) and internet. *Confuciusornis* and microraptorines originate from either the Yixian or Jiufotang Formations of the Jehol Group, though the precise stratigraphic origin of the majority of specimens included is unknown. Absence of stratigraphic information does not impact assessment of the CDH, which applies to the bulk of terrestrial vertebrates in the Jehol Biota and makes no distinction between specimens from the Yixian or Jiufotang formations. In the context of this study 'microraptorines' is treated as a single taxon that includes all specimens with a body plan that closely resembles that of *Microraptor zhaoianus.* Microraptorines includes those specimens of *M. hanquingi* and *M. gui* considered to be synonymous with *M. zhaoianus* (Pei et al., 2014) as well as various specimens that have yet to be officially described or assigned to the genus *Microraptor* plus other closely related genera such as *Changyuraptor* (Han et al., 2014).

Confuciusornis is ideal for studies of this kind as it is one of the most abundant terrestrial vertebrates in the Jehol Biota; thousands of specimens are

known (Jiang et al., 2014). It is unknown whether the different skeletal

anatomies of *Confuciusornis* and microraptorines would pass through similar

taphonomic pathways given identical conditions of transport and burial.

However, due to the extreme amounts of energy involved in a pyroclastic density

current (Baxter, 1990; Loughlin et al., 2002) we assume that transport in such a

turbulent flow would produce a similar pattern of disarticulation/

dismemberment and trauma in both taxa. Therefore any differences in anatomy

would have a negligible effect on this pattern. The collections of museums and

other academic institutions are likely to be biased towards more complete and

better-articulated specimens. Intuitively, this biases the dataset in favour of

models (including the CDH hypothesis) that envisage entombment and transport

of specimens while alive and geologically instantaneous burial.

2.2 Assessing skeletal taphonomy

The semi-quantitative skeletal completeness and articulation metric

presented by Beardmore et al. (2012b) was applied in this study to assess the

skeletal completeness and articulation of specimens of *Confuciusornis* and

microraptorines from photographs. This method has several advantages over

other approaches: (1) it can be easily adapted to assess the skeletal taphonomy

of any tetrapod, including *Confuciusornis* and microraptorines; (2) data collection

is efficient; and (3) it provides numerical values for completeness and

articulation, hence allowing quantitative comparison among specimens. In the

context of this study, articulation refers to the life position of skeletal elements, if

two adjacent skeletal elements are no longer in *in vivo* position relative to one

another then they are considered disarticulated. Completeness refers to those skeletal elements near the immediate vicinity of the carcas i.e. within 30mm. Preparation of the sediment around the specimen extends to ~20–60mm, and so skeletal elements that were present but not within 3cm of the carcas (and therefore complete) were not apparent.

A skeletal taphonomy metric that can be applied to different taxa must account for variations in the numbers of bones, so that similar scores represent similar proportion of loss of completeness or articulation for each taxon. A metric that can be applied to different taxa must accommodate variations in the actual number of bones between taxa. In order to do so, values for the different categories of completeness and articulation are defined on the basis of percentages (Beardmore et al., 2012a).

Each specimen was divided into nine skeletal units, i.e., the left forelimb, right forelimb, left hindlimb, right hindlimb, skull, cervical vertebrae, dorsal vertebrae (including the thoracic and sacral series), caudal vertebrae, and ribs (Fig. 3.1–3.2). The gastralia were not included in this scoring system as they were often too small or faint to identify or might have been removed during preparation. Similarly, the sternum was not included in the completeness or articulation metrics as it is also often difficult to identify, particularly in specimens with the uppermost dorsal surface exposed in which the sternum remains covered by sediment. Further, the sternum is difficult to assign to a particular anatomical unit since it could be associated with the forelimbs, the dorsal vertebrae, or the ribs. Throughout this study 'left' and 'right' refer to the body plan in life, irrespective of the orientation of the specimen on the surface of the slab; the way-up of the latter is not always known (Fig. 3.1). Each unit was

scored between 0–4 for completeness and articulation according to predetermined categories (Tables 3.1–3.6); a score of 0 indicates that the unit is absent/fully disarticulated, whereas 4 represents a complete/fully articulated unit (Beardmore et al., 2012b). The overall score for the specimen is the mean of the nine scores for the individual skeletal units. Scores of completeness and articulation for each specimen were produced by independently averaging the completeness and then the articulation scores of the anatomical units (Supplementary information 3.2). It could be argued that the median is a more accurate representative of average specimen completeness or articulation as scores for individual anatomical units in a specimen are in general not normally distributed, therefore an outlier or extreme value is more likely to pull the mean away from the typical value for the specimen as a whole. However, the range of possible scores for completeness and articulation (0–4), and the number of data points that constitute an average score for a specimen (7–9) are low. As a result, the representative nature of the median value is highly susceptible to specimens in which just under half the anatomical units are scored at the opposite extreme of the completeness/articulation scale to the remaining anatomical units. For example, if the median is used then the average score for completeness of a *Confuciusornis* specimen missing the head, cervical and dorsal vertebrae and the ribs, but retaining fully complete left and right forelimbs and hindlimbs and complete caudal vertebrae would be 4 (fully complete). If the mean is used it would instead be scored as 2.2. For this reason we consider the mean to be a more appropriate way to average the data for each specimen.

The completeness of each limb of *Confuciusornis* and microraptorines is the average score for the presence/absence of four subunits (Table 3.1). In the

forelimb, these are the humerus, the radius and ulna combined, the metacarpals and the phalanges (Fig. 3.4). In the hindlimb, these are the femur, tibia and fibula combined, the metatarsals and the phalanges. A subunit is coded as more than 50% complete if more than 50% of the elements that comprise it are present. For example, the both the radius and ulna must be present for that unit to be complete and if only one is present that subunit is absent. The humerus and femur each comprise a single element and are thus scored as either present or not. Articulation is scored as the average of scores of four articulation points. For the forelimb, these are the shoulder, elbow, wrist and phalanges, and for the hindlimb the hip, knee, ankle and phalanges. For any one of these points to be coded as more than 50% articulated 50% or more of the constituent elements need to be articulated. For instance, the shoulder is either articulated or not, whereas more than 50% or both of the articulation points of the elbow must be articulated in order to be considered mostly articulated.

For the vertebral units (Tables 3.2–3.4), i.e., the cervical, dorsal and caudal vertebrae, completeness was scored using the system published by Beardmore *et al.* (2012a). For articulation of vertebral units, the system used by Beardmore *et al.* was replicated and is clarified as follows; a score of 4 denotes skeletal units in which all elements are articulated; a score of 3, one or two breaks in the vertebral series; a score of 2 , between 3 and 50% of the number of total articulations rounded up to a maximum of 10; a score of 1, >50% of the number of total articulations are disarticulated or if more than 10 breaks are present in a vertebral series; a score of 0, no articulations. This scheme summarised in Tables 3.1–3.6, enables comparison among studies and taxa. For example, *Confuciusornis* possess eight cervical vertebrae, if there are four breaks

articulation would be scored as 3, if there are five breaks then articulation would

be scored as 2 as more than 50% of the articulations have become disarticulated.

Disarticulation involves the displacement and separation of skeletal

elements– either via collapse before or during burial or due to physical processes

before burial. The many small bones that constitute the skull are often displaced

so that they are juxtaposed over the top of one another making their

presence/absence and articulation/disarticulation difficult to determine. For this

reason, the skull of all nine skeletal units is the most difficult to assess for

articulation and completeness. Therefore, scoring for articulation and

completeness in the skulls of microraptorines and *Confuciusornis* must by

necessity be more qualitative than the other eight units (Table 3.6).

Completeness of the skull, is based on the presence/absence of each of the

following elements or group of elements: the left and right mandibles (each

made of a dentary, angular and surangular bone); maxilla and pre-maxilla;

frontal and nasals; parietal complex (post-orbital, parietal, squamosal and

occipital bones); jugal complex (jugal, lacrimal); and quadratojugal bone. A score

of 4 is given if all elements are present, a score of 3 if ~80% of elements are

present (i.e. one-two elements are absent, typically the mandibles), a score of 2 if

between ~80% and 50% of elements are absent (typically the maxilla, frontal

and nasals, and parts of the parietal complex), a score of 1 if less than 50% of

elements are absent and a score of 0 if the skull is entirely absent. Articulation is

scored in a similar fashion. A score of 4 is given if all elements are articulated, a

score of 3 if ~80% of elements are articulated (typically all elements but the

mandibles), a score of 2 if between ~80% and 50% of elements are articulated

(what elements are articulated usually varies between taxa), a score of 1 if more

than 50% of elements are disarticulated (typically the jugal and post-orbital remain articulated) and a score of 0 if the skull is entirely disarticulated.

The nine skeletal units represent one of two groups. The first grouping includes the four limbs, skull and ribs, none of which can be scored with a higher value for articulation than for completeness. For example, loss of completeness of distal elements of the limbs implies disarticulation of those elements from more proximal parts of the limb. Units in the second group, which comprises the cervical, dorsal and caudal vertebrae, can in certain circumstances be coded with a lower completeness than articulation value. For instance, the vertebral series can only be assessed for articulation based upon which elements are present; if the posterior half of the tail is absent, but the anterior half is fully articulated, then only a single point of disarticulation can be proved, and the absent half of the tail could potentially be fully articulated (Beardmore et al., 2012b). In these cases, all combinations of scores are possible except a completeness value of 0 and articulation between 1 and 4, or articulation value of 4 and completeness between 0 and 3.

Skeletal units obscured by overlying bones could not be assigned a completeness or articulation score and were coded as 'xh', whereas skeletal units truncated by the edge of the slab or not fully exposed during preparation were coded as 'xp' for consistency according to Beardmore et al. (2012b). An exception to this is if the number of elements present in a truncated unit, (for example a hand or foot) is sufficiently high to warrant being scored as fully complete or fully articulated; it is coded as 4 not 'xh'. Any specimen with three or more skeletal units coded as 'xh' or 'xp' was not included in the analysis of whole specimens but was included in analyses of those skeletal units not affected.

Using the methods of Syme and Salisbury (2014), the articulation between units, the inter-unit articulation (IUA), was also investigated. There are seven points of IUA: one between the axial skeleton and each of the right forelimb, left forelimb, right hindlimb and left hindlimb (rfl-a, lfl-a, rhl-a, lhl-a, respectively); the skull and first cervical vertebra (s-cv); the cervical vertebrae and dorsal vertebrae (cv-d); and the dorsal vertebrae and caudal vertebrae (d-cu) (Fig. 3.1). Each of the seven IUA points was scored qualitatively for the degree of articulation as follows: fully articulated, partially articulated, and fully disarticulated. The IUA between the ribs and the dorsal vertebrae was not included in this analysis, as this would comprise multiple articulation points and thus is not directly comparable with the other IUA values. This aspect of skeletal taphonomy is already treated in the intra-articulation metric.

The orientation of each specimen was also assessed. The way up of most specimens is unknown, and thus orientation was assessed on the basis of the angle between the sagittal plane of the specimen and the bedding plane. Each specimen was assigned to one of three categories: dorsoventral, in which the sagittal plane is perpendicular to the bedding plane; oblique, in which the sagittal plane is oblique to the bedding plane; and lateral, in which the sagittal plane is parallel to the bedding plane.

2.3 Determining taphonomic pathways

Relating the skeletal taphonomy data to a particular taphonomic pathway follows the method used by Beardmore *et al.* (2012b). The relationship between articulation and completeness was measured by plotting articulation vs.

completeness for all specimens of each taxon. A linear trend line forced through the taphonomic origin sensu Beardmore *et al.* (2012b) at (4, 4) was fitted to the data. Using the statistical programming package R, a Pearson's product-moment correlation test of the trend line was used to assess the strength of the linear relationship between articulation and completeness and was given by the r^2 value. The intercept of the linear trend line with the y-axis (completeness) gives the trend line value (T), and allows us to identify the taphonomic data as one of three linear trends (Fig. 3.3): Trend 1, varying values of articulation with consistently high levels of completeness; Trend 3, positive linear relationship between articulation and completeness; and Trend 2, values falling between Trends 1 and 3 (Beardmore et al., 2012b). Trend 4, values of articulation higher than values of completeness, this is only possible for the second group of units, therefore in order for a specimen to be placed in Trend 4 at least one unit from group two must be present and must also be scored higher for articulation than completeness. If the r^2 value indicates the relationship between completeness and articulation is not linear then it is possible the relationship between the two variables is not described by any of the three possible trends. In this instance, the T value is not descriptive of the data. Instead, the relationship between articulation and completeness can be visualised by a non-linear trend line. The strength of the relationship between the two variables, whether linear or non-linear can be given by the Spearman rank r_s value and p-value. To confirm any particular trend, it is necessary to identify corroborating taphonomic signals using other methods on other subsets of the skeletal taphonomic dataset. The distributions of articulation and completeness scores for each taxon were compared using two-tailed Kolmogorov-Smirnov tests.

The taphonomic pathways of specimens in the Jehol Biota were investigated further by separating the skeletal taphonomy data into various subsets. First, the taphonomic trends shown by each anatomical unit were investigated using the methods for entire specimens described above (Figs. 3.5–3.6 and Table 3.7). Additionally, the similarity of the completeness and articulation data between each possible pair of the nine units was assessed using statistical software program PAST (Hammer et al., 2001) to perform non-parametric multiple analysis of variance (NPMANOVA). This was followed by an investigation of the patterns of element loss and disarticulation in each of the limbs (Fig. 3.7). Lastly, the similarity of completeness and articulation scores between limbs in a pair were compared using a paired appendage analysis (Fig. 3.8) (Beardmore et al., 2012b).

The total articulation and completeness dataset was separated by orientation for both taxa and represented graphically as a pair of scatterplots (Fig. 3.9). The impact of specimen orientation on articulation and completeness scores was investigated using NPMANOVA. Completeness and articulation data follow a Poisson distribution, therefore a generalised linear model (GLM) with a Poisson distribution was used to investigate whether orientation or limb anatomy are better predictors of differences in completeness or articulation scores between each side of the body.

The relationships between intra- and inter-unit articulation in both taxa were investigated as follows (Fig. 3.10A). The distribution of disarticulated, partially articulated, and fully articulated elements at each IUA point was plotted. Chi-squared tests were performed on the *Confuciusornis* and microraptorine IUA data sets to determine whether the three possible scores for IUA were

distributed equally amongst the seven possible IUA points. Finally, the percentage of IUAs with one of the three scores found in the same specimens as another identically scored IUA were tabulated and expressed graphically as a bubble plot. It is impossible to infer the sequence of disarticulation from a single fossil since each specimen represents a 'snapshot' of a time during the disarticulation process. However, using a larger data set of specimens a causation between the loss of articulation at one point in the body and disarticulation at another point and therefore a sequence of disarticulation, can be inferred. This is achievable if it can be shown that within a subset of specimens in which the latter is disarticulated, that the percentage in which the former is also disarticulated is higher than the percentage of a different subset of specimens in which the former is disarticulated where the latter is also disarticulated (Fig. 3.11). This can be visualised using IUA bubble plots. Six bubble plots were produced: three for *Confuciusornis* and three for microraptorines, and two for each set of IUA scored as fully articulated, partially articulated and fully disarticulated according to the definitions presented by Syme and Salisbury et al. (2013). 'Full articulation' refers to the maintainance of in vivo position; 'partial articulation' is where all elements of the articulation maintain in vivo proximity to one another but not in vivo position and 'full disarticulation' refers to points of articulation where elements are neither in position nor proximity as is in vivo (Fig. 3.11). The radius of each circle in the bubble plot represents what percentage of IUAs in a specimen that co-occur with another IUA that is scored the same. The percentage of the first point of IUA (1°), is not necessarily the same as the percentage of that second point of IUA (2°), which has been scored the same as the first point. This is because the number of

the first IUA with a certain score could be higher or lower than the number of the second IUA with that same score. For instance, if nine specimens of *Confuciusornis* have the articulation between the right forelimb and axial skeleton (rfl-a) scored as disarticulated, and of those nine specimens, there are three with disarticulated s-cv, the percentage of disarticulated s-cv joints in the same specimen as articulated rfl-a joints is 33%. However, if the total number of specimens with disarticulated s-cv joints is six, then the percentage of articulated rfl-a joints found in the same specimen with articulated s-cv joints is 50% (Fig. 3.11).

3. Results and analysis

3.1 Similarity of scores between taxa

Articulation and completeness scores are not obviously different between the two taxa (Fig. 3.3). Both taxa show high levels of skeletal completeness with variable levels of skeletal articulation, although the average completeness score for *Confuciusornis* is slightly lower than for microraptorines. Most *Confuciusornis* specimens sit in the upper half of Trend 2, but most microraptorine specimens sit in the lower half of Trend 1. Despite this difference, two two-tailed Kolmogorov-Smirnov tests demonstrate that the distribution of completeness and articulation scores is similar for both taxa (*p*-values: 0.5314–0.723). Therefore the distributions of completeness scores and articulation scores in *Confuciusornis* and microraptorines could be randomly drawn from a single population.

3.2 Taphonomic trends of anatomical units

The taphonomic trends exhibited by all units in both taxa show weak to no linear relationship (Figs. 3.5, 3.6; Table 3.7). In *Confuciusornis* the relationship between completeness and articulation in both forelimbs, the left hindlimb, the cervical vertebrae, dorsal vertebrae and skull is one where values for both completeness and articulation are variable, but values for the former are consistently higher than for the latter. Of the remaining three anatomical units the caudal vertebrae show the greatest variation of articulation and completeness scores. Whereas the non-linear trendlines of the right hindlimb and ribs seem to closely follow the path of fitted linear trend lines, but deviate at one end due to a relative abundance of units identified as having zero articulation but a higher average completeness than units scored 1 for articulation. This suggests the possibility of two distinct taphonomic pathways exist in the right hindlimb and the ribs. Using NP MANOVA the patterns of articulation and completeness in the nine skeletal units in *Confuciusornis* can be split into two groups; group one represents units in which the articulation and completeness values are not significantly different from each other (p-values 0.1311–0.826); it comprises all four limbs, the skull, the cervical vertebrae and the dorsal vertebrae. Group two includes the caudal vertebrae and the ribs. These units show significant differences in articulation and completeness values compared to several of the other seven units but not to each other (p-values 0.0071–0.0427).

In microraptorines, adherence to linear taphonomic trend lines for all units is weak to absent except for the left and the right forelimb; which follow the linear trend more strongly (Figs. 3.5, 3.6; Table 3.7). As with *Confuciusornis*, the trends for the left forelimb, right forelimb left hindlimb and the ribs show strong relationships between articulation and completeness. NP MANOVA reveals only the articulation and completeness values of the dorsal and caudal vertebrae are statistically different between the two taxa (*p*-value 0.0142).

3.3 Sequence of disarticulation in the limbs

It cannot be known which points in the limb have disarticulated first by observing a single specimen. The sequence of element loss or disarticulation in a limb can be inferred somewhat by grouping limbs based upon completeness/articulation score (0–4) and then counting the relative abundance of joints that remain articulated/ elements that remain present in limbs for each group. In specimens with only one missing element or point of disarticulation, this is simple. For example, if the shoulder is identified as the only point of disarticulation in a large dataset of *Confuciusornis* forelimbs in which the other three joints remain articulated, logically in *Confuciusornis* the initial disarticulation occurred at the shoulder. For limbs in which there are two missing elements or points of disarticulation, this approach becomes less robust. This is because it is impossible to distinguish in these limbs which was the initial point of element loss/disarticulation and whether they are the product of a different taphonomic sequence compared to that which produced limbs with only one point of disarticulation. Broader patterns in element

loss/disarticulation can be inferred by observing whether distal or proximal elements are more commonly missing/disarticulated. Specimens of *Confuciusornis* with less complete forelimbs are more often missing distal elements than proximal elements. The taphonomic trend in the hindlimbs is similar, though less striking (Figs. 3.7). Patterns of disarticulation are more complex than those of completeness. Initial disarticulation of the forelimb occurs at the elbow joint. In limbs with lower completeness scores disarticulation usually, occurs in the phalanges. In the hindlimbs, disarticulation is more likely to occur in proximal joints (the hip or knee), than distal joints (the phalanges and ankle).

Patterns of completeness loss are similar in the forelimbs of microraptorines and *Confuciusornis*. Completeness patterns in microraptorines are, however, less clear, and likely reflect the small number of specimens in the dataset. Overall there is no recognisable pattern as to how completeness is lost in the hindlimbs of microraptorines. However, in specimens with lower articulation scores, there is a consistent pattern; phalanges are more commonly encountered articulated than other points of articulation in all limbs.

3.4 Paired appendage analysis and specimen orientation

Paired appendage analyses for *Confuciusornis* and microraptorines show completeness and articulation scores of limbs rarely match the completeness or articulation scores with the other limb in the pair. The relationship of scores between limbs is revealed to neither be linear, nor particularly strong (Fig. 3.8). Subsetting paired appendage analyses by specimen orientation may more clearly

reveal the impact of specimen orientation on articulation and completeness of different sides of the body. Unfortunately, sample numbers are too low to identify any meaningful taphonomic trend when data is split by orientation and then by limb. The lowest scores for completeness and articulation are in laterally oriented specimens of *Confuciusornis* (Fig. 3.9A; Table 3.8). Oblique specimens show the highest completeness and articulation values. None of the relationships for articulation and completeness of the three orientation subsets (dorsoventral, oblique and laterally oriented) fit linear trends. Inspection of non-linear trend lines (Fig.3.9C) shows dorsoventrally, and obliquely oriented specimens of *Confuciusornis* show a relationship of decreasing completeness with decreasing articulation (rho 0.62–0.66, p=0.006–7.8x10^{-5}). Conversely, spearman rank correlations indicate there is no significant relationship between completeness and articulation in laterally oriented specimens (rho 0.49, p=0.12). NP MANOVA indicates that when p-values are corrected for multiple comparisons using Benjamini-Hochberg (Benjimini and Hochberg, 1995) (Table 3.9) none of the orientation datasets is significantly different from one another (p-values= 0.1895–0.0555). However, if the low completeness / low articulation outlier in the *Confuciusornis* dorsoventral dataset is removed the dorsoventral and lateral datasets are significantly different from one another (p-value 0.0360). For these two orientations, an increase in the angle between the sagittal plane and bedding plane does lead to a significant increase in skeletal completeness and articulation but only between laterally and dorsoventrally oriented specimens. Completeness and articulation scores for obliquely oriented specimens are not significantly different from either laterally or dorsoventrally oriented specimens.

GLM analysis of the *Confuciusornis* data set reveals that neither limb type, nor specimen orientation is a significant predictor of the difference or similarity in completeness or articulation scores between limb pairs (Table 3.11). Additional tests of the suitability of the GLM (Chi-square; likelihood ratio, and comparison of Akaike information criteria) demonstrate that, although the GLM suggests that orientation and limb type impact completeness scores, it cannot describe the difference in articulation scores. The fit of the GLM to articulation data was not improved by transforming the articulation data (log-transformed, squared, z-transformed). The conflict between the results of the NP MANOVA and the GLM indicates that orientation impacts on total specimen completeness and articulation but not on the difference in completeness scores between limbs on different sides of the body. Presumably, factors not considered by the GLM control the difference in completeness scores between limbs.

Laterally orientated microraptorines have the lowest average completeness value, whereas dorsoventrally orientated specimens have the highest mean articulation and completeness value (Fig. 3.9B). NP MANOVA reveals no significant difference between any of the three datasets, which may reflect a small sample size (Table 3.9).

3.5 Inter-unit articulation

In both *Confuciusornis* (rs 0.31, *p*-value 0.02) and microraptorines (rs 0.48, *p*-value 0.03) spearman rank tests demonstrate the relationship between articulation and inter-unit articulation is weak (Fig. 3.10A).

The IUA of *Confuciusornis* is characterized by the following features: (1) most of the seven points of IUA (rfl-a, lfl-a, rhl-a, lhl-a, s-cv, cv-d & d-cu) are usually either fully articulated or fully disarticulated, not partially; (2) some skeletal units are more likely to remain attached to the body than others (Figs. 3.1, 3.9B) with some exceptions. These exceptions are (1) the s-cv joint, which is fully articulated (63% of 60 specimens) more than it is partially articulated (13%), or disarticulated (23%) and (2) the cv-d joint, which stands out, as partially articulated (37% of 57 specimens) much more often than fully disarticulated (19%) (Fig. 3.8). The chi-squared test confirms that the distribution of IUA scores among the seven IUAs is not random (p = 0.009). Standardised residuals indicate that the distribution of IUA scores among the s-cv and cv-d joints differs significantly from the expected scores (Table 3.11), and thus s-cv and cv-d are more likely to be found articulated and partially articulated than the other anatomical units. Relatively few IUAs were coded as partially articulated and therefore require no further analysis (Fig. 3.10)

The only similarity in the distributions of the three IUA scores in microraptorines (Fig. 3.10C) and *Confuciusornis* (Fig. 3.10B) is that most IUA points are rarely partially articulated. In microraptorines, the rfl-a stands out as the only IUA to be scored as partially articulated (50% of 20 specimens) more frequently than fully disarticulated (40 %), or fully articulated (10%). The lfl-a is much more likely to be found disarticulated (65% of 21 specimens) than partially articulated (10%) or fully disarticulated (25%). The distribution of IUA scores in the s-cv is also found fully articulated more frequently (60% of 20 specimens) than partially articulated (15%) or fully disarticulated (25% specimens). The cv-d is the only IUA in microraptorines to be found articulated

(50% of 20 specimens) and partially articulated (40%) more frequently than fully disarticulated (10%). A chi-squared test demonstrates the distribution of IUA scores is not random (p = 0.007). The standardised residuals indicate that the IUAs contributing most to this difference are the rfl-a, lfl-a, s-cv and cv-d (Table 3.11).

The IUA values can inform on the sequence of disarticulation. In *Confuciusornis*, limbs usually disarticulate as pairs of wings or legs (65–90%) rather than a single wing and leg (32–58%) (Fig. 3.11). Unlike modern birds where the hindlimbs often disarticulate before the forelimbs (Davis and Briggs, 1998) the disarticulation of wings in *Confuciusornis* is not usually accompanied with the disarticulation of the legs.

There is a correlation between the disarticulation of the limbs from the axial skeleton and disarticulation of the head from the neck. Specimens with articulated s-cv joints rarely possess articulated limb-axial skeleton joints (39–53%). This suggests the s-cv joint remains articulated after the limbs have disarticulated from the body. Therefore in *Confuciusornis* the limbs are more likely to disarticulate before the s-cv than vice versa.

Disarticulation patterns in microraptorines are less obvious than in *Confuciusornis* because of the small sample size (Fig. 3.11). Overall, microraptorine specimens exhibit similar patterns of limb IUA as *Confuciusornis* except for the forelimbs, individual examples of are rarely found articulated to the axial skeleton (20–50%). The relationship between disarticulation of the s-cv joint and disarticulation of the limb-axial skeleton joint in microraptorines is identical to that in *Confuciusornis.* Disarticulated s-cv and cv-d joints are found alongside disarticulated limb-axial skeleton joints (0–50%) more often,

compared to fewer limbs disarticulated from the axial skeleton found alongside disarticulated s-cv & cv-d joints (0–33%). This reinforces the concept that disarticulation of the limbs is more likely to occur before disarticulation of the axial IUAs. However, the microraptorine dataset is limited, and the results should be treated with caution.

4. Discussion

4.1 Evaluating the catastrophic death hypothesis

To accept the CDH the skeletal taphonomy of *Confuciusornis* and microraptorines must demonstrate loss of completeness and articulation consistent with transport of freshly killed specimens in a turbulent flow followed by rapid burial. These can be tested by determining whether carcasses disarticulated prior to or after settling on the lake floor.

The relationship between the articulation and completeness data in both taxa suggests that disarticulation occurred on the lake floor. If disarticulation had occurred prior to the specimens arrival at the lake floor, articulation and completeness scores would decrease in tandem, as disarticulation of joints such as a shoulder or hip would automatically involve the separation of all more distal elements (Beardmore et al., 2012a). However, the principal taphonomic trend is that articulation decreases faster than loss of completeness (Fig. 3.3), with many units showing high levels of articulation except in cases of extreme completeness loss (Fig. 3.5). Confirming carcasses must have arrived at the bottom of the lake before extensive decay of the soft tissues and subsequent disarticulation and limited loss of completeness. This is supported by the pattern of disarticulation

shown by the limbs, these show progressive loss of articulation of proximal parts of the limb before distal parts, i.e. the femur is disarticulated before the phalanges (Fig. 3.7), indicating whole limbs did not drop off a carcass prior to settling on the lake bed.

Detailed analysis of specific subunits reveals some potential complexities in the model. Some of the skeletal units in *Confuciusornis* (ribs and caudal vertebrae) show an equal loss of completeness if articulation is high (3 or 4) but a greater loss of articulation relative to lower completeness values (1 or 2), as a non-linear trend this does not fit perfectly within the definition of Trend 2. Still, an equal loss of articulation during an early loss of completeness could be interpreted as potential evidence for disarticulation prior to deposition such as in a floating carcass, or one still undergoing transport (Fig. 3.5). If disarticulation of these skeletal units had occurred within the water column or during transport, other equally exposed parts of the appendicular skeleton such as cervical vertebrae or limbs might be expected to display similar patterns. However, in *Confuciusornis* the forelimbs, the left hindlimb and the cervical vertebrae exhibit patterns of high completeness, indicating that they did not undergo extensive disarticulation until after arrival at the lake bed.

There are alternatives that explain the initial equal decreases in articulation and completeness localised to the ribs and caudal vertebrae. The pattern of disarticulation and loss of completeness exhibited by the ribs could result from a buildup of internal gases, or exposure due to decay of the integument around the abdomen (Schwermann et al., 2012; Syme and Salisbury, 2014), and exposed caudal vertebrae but not other, body regions. However, the taphonomic trend in *Confuciusornis* could be produced if the ribs and caudal

vertebrae were disarticulated only after deposition of the carcass on the lake floor (and bones in other body regions were not). In contrast to previous studies (Pan et al., 2015), recent evidence suggests that during deposition of the intervals bearing the *Confuciusornis* and microraptorine specimens, the lakes were completely oxic (Zhou et al., 2016). Therefore scavengers could have caused the disturbance and removal of some elements of the ribs and tail. However tooth marks have not been noted on any skeletons, so this displacement was more likely the result of current activities.

In microraptorines, the limbs, skull, cervical, dorsal and caudal vertebrae show lower values for articulation while completeness remains relatively high generally mirroring similar trends observed in the units of Confuciusornis. However, significant relationships between the two variables could not be demonstrated in the right hindlimb, cervical vertebrae or dorsal vertebrae. Although absence of correlation could be used to support the hypotheses that these units disarticulated at the lake bed, it is also possible that absence of a relationship is the result of low sample size (Fig. 3.6).

Microraptorines and *Confuciusornis* are bilaterally symmetrical, so both sides of their bodies should respond identically to the forces within a turbulent flow such as a PDC. However, the carcases evidently broke up asymmetrically, as indicated by the completeness and articulation analyses of all four paired appendages (Fig. 3.7), favouring disarticulation of specimens at the bottom of the lake. This is further supported by differences in taphonomy having occurred between specimens in different orientations. Decay fluids produced via the decomposition of soft tissues (Bickart, 1984; Davis and Briggs, 1998) and microbial mats (Zhou et al., 2016) would contribute to the adherence of certain

elements of the carcas to the sediment and prevent movement or loss of

completeness (Bickart, 1984; Davis and Briggs, 1998). If specimens

disarticulated at the lake-bed, laterally oriented specimens might be expected to

show lower articulation values since one side of the body will be exposed to the

water column whereas the other side will be protected from currents or the

actions of scavengers by being in contact with the sediment. Laterally oriented

specimens of both *Confuciusornis* and microraptorines support this hypothesis in

showing the lowest values for articulation and no significant relationship

between articulation and completeness (Fig. 3.9). This further supports the

suggestion that disarticulation disproportionately affects one side of the body

more than the other. It is possible that a pattern of unequal disarticulation

between different sides of the carcass could also occur if there were an unequal

distribution of decay gasses in the carcasses during a period of floatation prior to

deposition on the lake bed. This too would rule out the CDH as it would preclude

instantaneous burial. If carcasses did experience a period of floatation it could

lead to carcases preferentially floating with one side of the body higher in the

water column. The limbs on this side would have their weight supported and are

likely to undergo less extensive disarticulation compared to those limbs on the

other side of the carcas which would experience greater stress due to gravity. If

disarticulation of the limbs had occurred during floatation, we would expect

there to be evidence for prolonged floatation in other anatomical units such as

the skull. Stress due to gravity on the articulation between the skull and the rest

of the carcas will be greater in a floating carcas than in a carcas that is supported

by the sediment. Actuopalaeontological observations suggest that the first unit

likely to disarticulate from the carcass of a modern bird is the skull, both in

floating carcasess (Schäfer, 1972) and in carcasses resting on sediment (Bickart, 1984). The high number of specimens with skulls (59 out of 63), and the large number of specimens in which the skull is articulated (37) is telling evidence for carcass decay and break-up on the lake bed. It is possible that an uneven build up of decay gasses could also affect which side of the body would more frequently come into contact with the surface of the substrate. This could explain why the paired appendage analysis indicates an unequal loss of articulation and completeness between the left and right limbs despite the skeletal taphonomy as a whole not supporting disarticulation within a PDC or during an extended period of floatation (Fig. 3.8).

In summary, the skeletal taphonomy of *Confuciusornis* and microraptorines strongly indicates carcases did not undergo disarticulation during transport within a turbulent flow such as a PDC, instead disarticulation occured after carcasses settled on the lake bed, possibly after a short flotation period. This suggests that any loss of completeness that has occurred is the result of the movement of elements out of their original position. Therefore both assumptions of the CDH have failed to stand up to analysis of the skeletal taphonomy of a large number of specimens, thus we reject the CDH on these grounds.

4.2 Effects of anatomy on skeletal taphonomy

Although the flight capabilities of *Confuciusornis* and microraptorines are debated (Nudds and Dyke, 2010; Paul, 2010; Wang et al., 2011), their morphology nonetheless resembled that of modern birds. Therefore, their carcasses might be expected to follow the same sequence of disarticulation and

element loss as modern birds. It is possible to infer the similarity of the functional anatomy of these extinct taxa to one another and to that of modern animals through comparison of their skeletal taphonomy.

The pattern of disarticulation inferred in the limbs of modern birds is similar to that observed in other modern animals (Brand et al., 2003). This pattern can be characterised by the separation of limbs from the axial skeleton in pairs followed by disarticulation of the individual limb bones from one another. This sequence of disarticulation is consistent between carcases decayed under natural conditions that have disarticulated while floating (Schäfer, 1972) and carcasses that have disarticulated after coming to rest on the sediment (Bickart, 1984; Davis and Briggs, 1998). However, detailed observations of the sequence of disarticulation of individual elements of the wing of modern birds are limited (Brand et al., 2003; Bickart, 1984). Therefore only general comparisons between the sequences of disarticulation of the limbs in modern birds with those of the limbs in *Confuciusornis* and microraptorines can be made.

The pattern of disarticulation in the forelimbs of the majority of *Confuciusornis* specimens is similar to modern birds in that the initial disarticulation occurs at the shoulder, separating the limb from the body (Fig. 3.7). The loss of articulation in more proximal parts of the limb before distal points of articulation may have occurred via two pathways: (1) the shoulder disarticulates from the floating carcas but retains its association with the remainder of the carcas due to a strong integument (Brand et al., 2003); (2) in cases where the tissue around the joints has undergone some decay the shoulder disarticulates from the force of impact with the sediment (Syme and Salisbury, 2014). In forelimbs scored lower for articulation, there is little difference in the

76

distribution of disarticulations among the four points of articulation. We are unable to infer the next point of articulation in the forelimbs as it is unknown if the disarticulation pattern in limbs scored as 2 for articulation is part of a continuum with the pattern of disarticulation observed in limbs scored as 3. It is equally likely that they instead represent a separate sequence of disarticulation. The data does indicate that in limbs scored lower for articulation that the phalanges and wrist are more likely to be found disarticulated than more proximal joints. The small bones of the wrist and phalanges and their position at the periphery of the skeleton make them more susceptible to movement by scavengers or currents and exposure due to soft tissue decay. This pattern differs from that observed in the forelimbs of modern birds by Bickart (1984) where the elbow is commonly found disarticulated while the phalanges remain articulated. However, the carcases observed by Bickart (1984) were exposed intermittently to subaerial conditions and so are not directly comparable to the conditions experienced by *Confuciusornis* carcasses in the Jehol Biota.

We can infer that the initial point of disarticulation in the hindlimbs of *Confuciusornis* specimens is split relatively evenly between the hip and knee. (Figs. 3.4, 3.7). The maintenance of articulation of the phalanges in limbs scored lower for articulation is related either to internal anatomy or differences in the decay resistance of the skin of the distal portions of the leg. Modern birds have a covering of scales on the lower half of their hindlimbs (Dhouailly, 2009), these scaly coverings are also known from some birds in the Jehol Biota, but the absence of these scales in *Confuciusornis* has been argued by other authors (O'Connor and Chang, 2013). The scaly skin of modern reptiles has been demonstrated to maintain the in vivo position of bones within the limbs of small

squamates in a subaqueous environment (Brand et al., 2003), similar

taphonomic effects have also been suggested to be present in Coelurosaurian

dinosaurs (Casal et al., 2013), it is possible the scaly leg coverings of birds feet

too would be resistant to decay and similarly prevent disarticulation of bones in

the phalanges. The difference in the pattern of disarticulation between forelimbs

and hindlimbs may result from a more substantial feather covering in the

forelimbs; this does not explain why the hindlimbs of *Confuciusornis* show a

different pattern of disarticulation from the hind limbs of modern birds where

the phalanges are among the first elements found disarticulated alongside

separation of the legs from the carcasss (Brand et al., 2003).

It is problematic to infer any patterns of disarticulation in the

microraptorine dataset which is reduced compared to *Confuciusornis.* This is

likely the result of a lack of similarity in the general taphonomic patterns

between the forelimbs of microraptorines. However, we can still infer two

things: (1) the proximal-most joint, the shoulder/ hip, is more commonly found

disarticulated compared to other points of articulation in limbs with a single

point of disarticulation, (2) the phalanges are often articulated relative to other

points of articulation in limbs with overall lower articulation scores. This is

similar to the general pattern in modern animals where initial disarticulation is

from the axial skeleton (Brand et al., 2003).

The clear differences between the taphonomic patterns in the forelimbs

and hindlimbs of *Confuciusornis* may represent their different functions in life,

namely aerial and terrestrial locomotion. The arms and legs of microraptorines

might be expected to disarticulate in a similar manner because both shared the

same function, that of wings for gliding (Dyke et al., 2013). Further, if the

function of a limb does dictate the sequence of disarticulation then the fore- and hindlimbs of microraptorines might also be expected to share a similar taphonomic pathway with the wings of *Confuciusornis.* However microraptorines were gliders, while *Confuciusornis* was likely capable of powered flight (Wang et al., 2011), therefore it is also possible that the anatomical changes to the skeleton necessary for powered flight could produce a different taphonomic pattern in the wings compared to the wings of a glider. At present, there is insufficient data to properly address whether the functional similarities in the wings of these animals impacted the skeletal taphonomy.

The taphonomic pathways of the sacral and caudal vertebrae are also affected by their functional anatomy. For example, compared to more basal theropods such as *Archaeopteryx,* the sacral vertebrae of *Confuciusornis* are fused together to form a synsacrum similar to modern birds (Zhou and Zhang, 2003). Therefore, the sacral vertebrae of a more derived bird may remain articulated for longer than more basal taxa in which the sacral vertebrae are less completely fused. Additional functional adaptations to flight such as the numbers and function of caudal vertebrae can also result in differences in skeletal taphonomy. The data suggests the caudal vertebrae of microraptorines are on average less likely to disarticulate and lose completeness than those of *Confuciusornis* (Figs. 3.5–3.6) implying the connective tissue around the caudal vertebrae of microraptorines was more decay resistant. Microraptorines like other dromaeosaurs (Norell and Makovicky, 1999) likely had a well developed network of tail tendons to improve the stability of the tail, for numerous functions, such as a counterbalance during running or climbing (Gatesy and Dial, 1996), as a flight stabiliser (Alexander et al., 2009), or as a flexible but stable rod

to help in negotiating landings (Han, et al., 2014). This connective tissue may have reduced the rate at which the tail disarticulated, however this depends on the decay resistance of tendons compared to the presumably less dense connective tissue that surrounds the caudal vertebrae of *Confuciusornis*.

The relationship between the function of the caudal vertebrae of *Confuciusornis* and their taphonomy is less apparent. Unlike the tail of microraptorines, the primary function of the caudal vertebrae in modern birds is as an anchor for the dense network of muscles responsible for the manipulation of tail feathers for flight (Gatesy and Dial, 1996). The tail of *Confuciusornis* may have acted as a site of muscle attachment, but this was unlikely to be as a flight stabiliser as *Confuciusornis* did not possess a fan of caudal pennaceous feathers (O'Connor et al., 2013). Nor did the tail aid balance during locomotion, as in microraptorines, but it may have acted as a site for muscle attachment for the elongate tail feathers probably used for display (Chiappe, et al., 2008; O'Connor et al., 2011). It is likely that the more extensive disarticulation and loss of completeness of the caudal vertebrae of *Confuciusornis* compared to those of microraptor and to the cervical and dorsal vertebrae in *Confuciusornis* relates to the absence of tendons for stability or large muscles for feather manipulation.

Our evidence suggests that, although *Confuciusornis* and microraptorines shared many aspects of body size and functional anatomy, and passed through similar taphonomic pathways in the Jehol lakes, there were sufficient differences in their anatomy to lead to some differences in the disarticulation of their carcases.

4.3 Skeletal completeness metrics

Until recently, most studies of the taphonomy of vertebrate skeletons relied on qualitative classification systems (Smith, 1993; Oliver and Graham, 1994; Bandyopadhyay et al., 2002; Soares, 2003). Often these studies used terms such as 'semi-articulated' and 'scattered' to describe the preservation of a specimen, but such terms were hard to use in comparisons between studies and taxa. One quantitative approach is to document each bone (Kemp and Unwin, 1997), but this requires extensive work to document little more than a few specimens (Beardmore et al. 2012b). Less time intensive methods were required in order to gather data to address wider questions of taphonomic bias in the fossil record, and these included qualitative metrics of completeness (Benton, 2008), as well as percentages of element completeness (Mannion and Upchurch, 2010; Brocklehurst et al., 2012; McNamara et al. 2011, 2012). Division of the vertebrate skeleton into several skeletal units (Fig. 3.1) allows rapid collection of taphonomic data and facilitates the assessment of taphonomic patterns for each anatomical unit (Mannion and Upchurch, 2010; Beardmore et al., 2012a; McNamara et al 2012a,b). Also, a measure of articulation is required, and this can be done with minimal modification of the scoring system for completeness (Beardmore et al., 2012b; McNamara et al., 2012). It is important to apply the same method to all specimens and taxa so that the data sets can be compared.

However, current methods can only describe the amount of decay that has taken place in relative terms ('more decayed', 'less decayed'). Without decay experiments on modern taxa, the relationship between the extent of soft tissue decay and quantified levels of skeletal taphonomy will remain unclear.

Understanding the anatomy of extant organisms is important to understanding how biology impacts upon the skeletal taphonomy of a fossil organism (Schwermann et al., 2012; Syme and Salisbury, 2014). Logically an animal's functional anatomy must affect its skeletal taphonomy, the fusing of bones for instance forms a stronger more durable structure in life and will reduce the chances of those bones disarticulating from one another post mortem. Bones not fused to one another too may maintain articulation longer into the disarticulation process if in life their articulation was maintained by decay resistant connective tissues such as ligaments. Experiments on extent taxa have demonstrated the skin, in particular, may be a major contributor to maintaining articulation and completeness of the skeleton (Schwermann et al., 2012; Syme and Salisbury, 2014), logically the more resistant the skin is to decay the more likely that articulation and completeness are maintained longer post-mortem. The effects of functional anatomy must be considered when determining taphonomic pathways in fossil specimens, especially when comparing two taxa of different ecologies. Otherwise, it is possible that a causal relationship may be drawn between a taphonomic trend in a particular anatomical unit and a feature of the depositional environment, rather than a feature of the animals functional anatomy that better explains the pattern being observed.

However, when using extant taxa to interpret taphonomic patterns in extinct taxa, it is important to consider whether phylogenetic comparisons or functional comparisons are more appropriate. For instance, logically modern elephant skeletons are a better analogue for understanding taphonomic patterns of large dinosaurs such as sauropods (Dodson et al., 1980), than their closer living relatives, birds and crocodilians. In general, the best approach is probably to

consider the anatomy and biology of several modern analogues to understand the impacts of function and phylogeny on the skeletal taphonomy of fossils.

5. Conclusion

Multiple lines of evidence strongly suggest that *Confuciusornis* and microraptorine dinosaurs experienced minimal disarticulation prior to deposition on the floor of the Jehol lake; there, carcasses were not immediately buried, but disarticulated while exposed to the water column. The specimens studied show patterns of skeletal taphonomy inconsistent with the hypothesis that they were transported in a catastrophic event such as a PDC. While this does not rule out the likelihood of at least some specimens having been killed, transported by a pyroclastic density current and then instantaneously buried, it does indicate that this taphonomic history cannot be applied as a general statement to all or even the bulk of allochthonous components of the Jehol Biota.

The skeletal taphonomy of *Confuciusornis* and microraptorine dinosaurs is broadly similar. The taphonomy of specific skeletal units shows that functional anatomy impacted on patterns of completeness and disarticulation. We recommend the standardisation of skeletal taphonomy metrics to improve understanding in single case studies, but also to allow comparisons between locations and taxa.

Acknowledgements

Experimental decay of avian integument: implications for the fossilization of skin

Two Zebra finches by Emma Kerridge

This chapter was formatted for publication in the journal Paleobiology. C Rogers contributed 100% to the writing of this paper.

Supplementary information can be found in the appendix for Chapter 4.

Experimental decay of avian integument: implications for the fossilization of skin.

Christopher S. Rogers[a][*], Maria E. McNamara[b], Patrick J. Orr[c], Stuart L. Kearns[a], Michael J. Benton[a].

[a] *School of Earth Sciences, University of Bristol, Wills Memorial Building, Queens Road, Bristol, BS8 1RJ, UK*

[b] *School of Biological, Earth and Environmental Sciences, University College Cork, Distillery Fields, North Mall, Cork, Ireland.*

[c] *UCD School of Earth Sciences, University College Dublin, Belfield, Dublin 4, Ireland*

ABSTRACT

Keywords: Preservation, Taphonomy, Decay experiments, Bird Skin, Feather, Muscles

The preservation potential of non-biomineralized tissues is often investigated using decay experiments but rarely do the results of such experiments consider how the decay of different component tissues affects the decay of the animal as a whole. This inhibits our ability to make accurate interpretations of anatomical features preserved in organs such as the integument of vertebrates in the fossil record. The skin is a major control on skeletal taphonomy and examples in the fossil record can inform on the coloration, physiology and ecology of extinct animals. Despite its palaeobiological importance in

---

[*] Corresponding author. Tel.: +44 117 394 1340; fax: +44 117 9253585.
E-mail address: cr8392@bristol.ac.uk

studies of fossil vertebrates, the taphonomy of skin is poorly characterised and has yet to be analysed systematically. Here we use histology techniques and scanning electron microscopy to compare the taphonomy of the skin of the zebra finch *(Taeniopygia guttata)* with that of the skin of fan-footed geckos *(Ptyodactylus hasselquisti)*. The decay of tissues in bird skin usually occurs relatively rapidly with fractures and fragmentation of the epidermis commonplace and loss of coherence of the dermis identifiable in the skin that has experienced minimal decay. Results demonstrate that reptile skin is markedly more resistant to decay than bird skin most likely due to its thicker dermis with densely packed collagen fibres. Preservation of avian integument with a high degree of fidelity is likely to require replication in minerals early in the decay process.

1. Introduction

Decay is an important control on the preservation of non-biomineralized tissues in the fossil record (Sansom et al., 2011; Briggs et al., 2016). The processes involved are complex, but experimental programmes have shed light on the various environmental and biological controls involved (Briggs and Kear, 1993a, 1993b; McNamara et al., 2010; Briggs and McMahon, 2016), and established the sequence in which tissues decay for a wide variety of taxa (Sansom et al., 2010; 2011, Murdock et al., 2015). However most previous studies have focused upon the effects of decay on the organism as a whole. The taphonomy of the individual components of tissues, and how these contribute to the taphonomy of that tissue is unknown. The taphonomy of important tissues that comprise multiple components or layers with different composition and chemistry, e.g. skin, remains poorly characterized.

1.1 The structure of skin

Skin is an organ, it fulfils many important biological functions, first and foremost the protection of internal organs and tissues from physical damage or invading microorganisms (Stettenheim, 2000). It also often houses pigments crucial for visually communicating with other animals (McNamara et al., 2016a). Further, it has been shown that skin is important for maintaining the cohesiveness of a carcasss after death, often described as a skin bag, and so has implications for the taphonomy of other tissues (Schwermann and Wuttke, 2012; Syme and Salisbury, 2014).

Fundamental integumentary anatomy is conserved amongst all amniote clades (Bellairs, 1969; Lucas and Stettenheim, 1972; Albardi, 2003). The skin of amniotes comprises three layers (Fig. 4.1A– B): (1) An outermost epidermis. This is the thinnest of the three integumentary layers and comprises an outer desquamating layer of keratin-rich cells (keratinocytes) that arise from the lower stratum germinativum, a generative basal layer (Micali et al., 2001). (2) An inner dermis comprised primarily of collagen that is arranged into several layers that support and aid in mechanical support and protection of the body (Micali et al., 2001). The dermis also houses nerves, various glands, blood vessels, and small muscles for manipulation of epidermal appendages such as feathers and hair (Lucas and Stettenheim, 1972; Micali et al., 2001). (3) The subcutis (hypodermis) comprises a network of connective and adipose tissues that support large blood vessels and nerves; it also functions to protect the body from damage, but its primary function is storage of fat (Micali et al., 2001).

The anatomy of bird skin differs from that of other amniotes (compare Fig. 4.1A and 4.1B). The most obvious difference is the possession of feathers

that are restricted to defined tracts (pterylae) and their support structures, the epidermal and dermal tissues that surround the feather are known as the feather follicle. Feathers are found mostly in the pterylae but also in non-feathered regions (apterylae) (Lucas and Stettenheim, 1972). The dermis of pterylae houses networks of muscles (Fig. 4.1B) which co-ordinate the movement of feathers by linking individual rachi (Homberger and DeSilva, 2000). This supporting musculature enables precise manoeuvres during flight, and manipulation of non-flight feathers, including those for display and thermoregulation (Homberger and De Silva, 2000). The subcutis is also involved in feather manipulation by providing a buffer between the underlying skeletal muscle and the dermis, which helps to return the feathers to their resting positions (Homberger and De Silva, 2000). The evolution of feathers has been studied using evolutionary-developmental and fossil evidence (Prum, 1999; Xu et al., 1999; Dhouailly, 2004; Zhou, 2014a). Feather tracts, dermal musculature and other tissues that support feathers such as the subcutis are crucial components necessary for the development of flight in birds; fossil evidence for their evolution is, however, unknown. Fossilised examples of bird skin thus have the potential to reveal stages in the evolution of flight not revealed by the feathers or skeletal anatomy of the animal.

1.2 Integument in the fossil record

Vertebrate skin has been recovered from numerous taxa in the fossil record, including frogs (McNamara et al., 2008), lizards (Evans and Wang 2007; Edwards et al. 2011), snakes (McNamara et al., 2016), pterosaurs (Martill and Unwin, 1989; Kellner et al., 2010), marine reptiles such as Icthyosaurs and

Mosasaurs (Lindgren et al., 2012, Lindgren, 2014) and dinosaurs (Horner, 1984; Kim et al., 2010). Many are external moulds but some include preserved tissue remains (Coria and Chiappe, 2007; Manning et al., 2009; Godefroit et al., 2014, Vinther et al., 2016). Feather-bearing skin is relatively rare (Homberger and DeSilva, 2000; Navalón et al., 2015), suggesting that feathered skin has a low preservation potential. Decay is an important control on the preservation of non-biomineralized tissues in the fossil record (Sansom et al., 2011; Briggs et al., 2016). This prompts the hypothesis that the structure and biochemistry of bird skin predispose it to rapid decay.

To elucidate why bird skin is poorly represented in the fossil record and with what fidelity it is likely to be preserved, we must first establish how the structures unique to it decay. To do this, we compare how feathered and non-feathered skin from the same animal decay, then compare the decay process in bird skin with that of a non-feathered animal, in this case, squamate skin.

The aim of this study is to characterise the morphological decay of the integument in birds and squamates and to construct a detailed atlas of decay sensu Sansom e*t al.* (2013) to elucidate why bird skin is poorly represented in the fossil record and with what fidelity it is likely to be preserved. Such data will also help to constrain possible interpretations of structures preserved in fossilised skin.

2. Methods

2.1 Materials

We selected two taxa of comparable size: the Zebra Finch (*Tanyoptera guttata)* and the Fan-footed gecko (*Ptyodactylus hasselquisti)*. As a result comparisons between the skin of animals of different scales is avoided (Peters,

1983). The thicknesses of the different layers of the skin undoubtedly affect the decay process. Presumably, the ratio of thicknesses of the layers in the skin differs depending on the size of the animal. To avoid confusing aspects of the decay process related to differences in scale with differences in taxa, choosing two taxa of similar size is preferable. All animals had their health assessed prior to delivery. All animals were euthanized by asphyxiation in CO_2 (finches) or anaesthetic (geckos) according to United Kingdom Animals (Scientific Procedures) Act of 1986. One zebra finch (finch Q) and one gecko (gecko A) had their tissues fixed immediately after death. All other specimens ((n=12 finches); (n=9 geckos)) were placed in individual sterilised 250 ml screw top ointment jars filled with 220 ml of bottled mineral water (Table 4.1). Jars were sealed within plastic zip lock bags and placed in a constant temperature incubator at $20^oC \pm 0.1^oC$. Carcassses (n=3 (finches), n=3 (geckos) were sampled after one week (finches F,G,H & geckos B,C,D), two weeks (finches I,J,K & geckos E,F,G) and one month (finches L,M,N & geckos H,I,J); sampling terminated the experiment. In addition, isolated contour feathers removed from the breast, neck and wing of the finches were placed in separate ointment jars also filled with 220ml of bottled water and decayed for one month. Multiple samples of integument and muscle were retrieved from the feathered and un-feathered parts of the pectoral region of each of the zebra finches. Multiple samples of skin without muscle were retrieved from the anterio-dorsal region, and legs of the geckos. Multiple samples were obtained from each finch in each sampling interval. Up to eight thin sections were produced from each sample. The orientation of all skin samples was kept consistent, sections were cut perpendicular to the plane of the surface of the skin to allow for direct comparison between transverse cross-sections of

the tissue. The muscle was sectioned in multiple orientations to observe the changes to muscle fibres in longitudinal and transverse cross section. Every thin section was then scored individually. Therefore a single animal can yield from two up to five samples of tissue. Between one to eight thin sections can be produced from each piece of dissected tissue, therefore each individual provides from four to thirteen sampling points, though each individual could, in theory, produce many more sampling points (Table 4.3–4.4).

2.2 Tissue preparation and imaging

Tissue samples were immersed in 10% neutral-buffered formalin for 24 hours and dehydrated using standard histological techniques (Bancroft and Gamble, 2002).

(1) –Thin sections were prepared for light microscopy and stained with Fontana-Masson to highlight the epidermis, dermis, adipose tissue, and, in the finches, feathers and their support structures (Fig. 2). Lipids such as adipose are lost during the fixation process, in fresh tissue this does not alter the ultrastructure of adipocyte cell membranes or surrounding tissues. It is likely that extensively decayed tissue with lower levels of structural integrity is affected by dehydration. However, the appearance of tissue structure between decay stages remains comparable as the same fixation and dehydration process was applied to all tissue samples.

(2) –For scanning electron microscopy (SEM), dehydrated tissue samples (~5 mm wide) were immersed in Hexamethyldisilazane (HMDS), and affixed to Al stubs using double-sided carbon tape. Samples were then

sputter coated with gold and imaged using a Hitachi S3500N variable-pressure scanning electron microscope (Fig. 4.3).

2.3 Characterising decay stages

Observations on the changes over time to the ultrastructure samples were collected for each of four tissue categories: (1) epidermis and dermis, (2) feather including rachis, follicle and dermal muscles, (3) adipose tissue and (4) skeletal muscle. Each tissue category is composed of multiple tissue components (Fig 4.1C; Fig 4.4A–4.4D). The appearance of the tissue components in each thin section was described, and this data was then categorized as one of three stages of decay, based on the amount of original detail that remained; (1) evidence for decay having been initiated, (2) moderately decayed and (3) decay well advanced. The ultrastructure of the adipose tissue exhibited greater variation in its decay over the course of the experiment that did the others; to reflect this, a fourth decay stage was added: (4) ultrastructure absent. The results of this analysis are an idealised model that summarises what detail is lost between successive decay stages for each tissue category.

If a tissue category could not be identified in a particular thin section, it was not assessed, because its absence could not be proven to be real (due to decay) as opposed to a sampling artefact.

Important points to note are: (1) tissue categories do not progress between decay stages at either a constant or the same rate; (2) decay stages are a qualitative description of decay relative to the ultrastructure of a fresh sample; (3) the same tissue could exhibit different decay stages, even among samples

taken at the same time; and (4) a single tissue category is capable of passing though one of multiple decay pathways; in these cases the tissue in question can have multiple but distinct appearances in some of the decay stages in the sequence (Fig. 4.4E–4.4L).

Each sampling point represents a value that describes the decay stage of a tissue category within a thin section. Each value is recorded separately (1–3 above, 1–4 for adipose). The same tissue category from two different thin sections can be assigned different values for decay despite both thin sections originating from the same sample of tissue. When assessing the relative rate at which tissue categories progress through various decay stages it is prudent to group all sampling points of a tissue category by the sample of tissue that they originate from to produce an average decay value for that tissue category for the sample as a whole. Note that this average value for the decay stage is reported to one decimal place; i.e. is not a whole number (Fig. 4.4).

The change in the dimension of certain tissue components was analyzed. The thickness of the dermis zebra finches and geckos, the pigmented layer in geckos and the average thickness of muscle fibers in the skeletal muscle of zebra finches were measured from photographs (Supplementary information 4.1 & 4.2). To account for the variation in thickness of the epidermis, dermis and pigmented layer measurements were taken randomly from photographs. Five measurements were taken for each tissue when present from each photograph. Width values presented for muscle fibers are an average of three measurements, all obtained from transverse sections. Measurements were grouped by the decay value for the corresponding tissue component. All measurements recorded from each photograph were included in the analysis. The contribution of

measurements from individual finches (Q, F–N) and geckos (A–J) to the distribution of tissue component dimensions is shown in figure 4.5. Data for each set of measurements was subset by decay stage and tested for normality using shapiro wilks tests (Table 4.2), non-normality for data in the majority of subsets suggests non-parametric statistics are appropriate for comparisons of distributions. After comparison of distributions of measurements in boxplots to assess trends in the data, one-tailed wilcoxon rank sum-tests were performed using the statistical programming software R to assess the direction of any change in thickness of the dermis between decay stages.

A pixel count analysis was used to estimate the area of skeletal muscle in each decay stage. Images containing muscle tissue were overlain by a 100 μm by 100 μm grid. A black/white threshold was applied, white pixels represent areas occupied by muscle and /or other tissues, and black pixels represent areas where no tissue is present. The number of white pixels in a grid square was converted to μm^2; values approximate the extent of muscle tissue present. Only images in which the entire field of view was occupied by muscle tissue had their areas measured. This was done to avoid sampling spaces that appear between fasciculi that may be possible preparation artefacts.

3. Results

3.1 Zebra Finch epidermis and dermis

Fresh tissue -The thickness of the epidermis (6–14um) is consistent between pterylae and apterylae. The outermost layer of the epidermis (stratum corneum) is made of several thin layers of flat disc-like keratinocytes ~5 μm

thick. Groups of up to 30 keratinocytes have been shed from the rest of the skin during the animal's life and occur trapped within the zebra finch feathers. In SEM images the stratum corneum is a continuous multi-layered sheet, individual keratinocytes occur as round to ellipsoid discs with central depressions marking the former position of the nucleus (Fig. 4.3). Locally, particularly in areas of the epidermis that have been fractured. Beneath the stratum corneum, the stratum germinativum occurs as a layer one cell thick, with prominent nuclei at the center of each cell (Fig. 4.1). The dermis is ~10–30 µm thick in the apterylae and ~10–20 µm in the pterylae. However, the dermis is often considerably thicker where feathers are close to the surface of the integument. Collagen fibers in the dermis are predominantly oriented parallel to the surface of the integument, and the upper surface of the dermis is clearly defined by densely packed, well-stained fibres. The majority of collagen fibres in the dermis undulate along their length and pass over and under one another in a web. Circular voids within the dermis of the apterylae are rare and closely resemble adipocytes. The collagen fibers are more widely spaced in the lower part of the dermis than in the upper half.

Decay stage one -The stratum corneum separates in whole or part from the underlying stratum germinativum (Fig. 4.2B, 4.4E). Under SEM the upper layers of the stratum corneum are continuous but distinctly flaky (Fig. 4.3). Individual keratinocytes cannot be identified unless they have detached from the stratum corneum as small flakes or clusters, and become trapped in the barbs and barbules of the feathers. Commonly the stratum germinativum is a distinct layer of nucleate cells; cell boundaries are faint and recognised only locally. The layer locally separates from the underlying dermis. Collagen fibers within the dermis show a limited number of transverse breaks. The collagen fibers in the

outermost part of the dermis remain more densely packed than those in the remainder of the dermis and still define the upper boundary of the dermis. One-tailed Wilcoxon rank sum tests reveal the dermis in the pterylae (W = 37, p = 5.331 x10^{-10}) and apterylae (W = 43, p = 1.924 x10^{-4}) is statistically thicker than fresh tissue (Fig. 4.6A).

Decay stage two – In SEM images fractures in the outer layers of the stratum corneum are noticeable, locally these expose the tissues of the dermis. Individual keratinocytes cannot be observed, but the abrupt, angular; nature of many of the fractures suggests the constituent keratinocytes are also fractured (Fig. 4.3). The stratum germinativum is no longer recognisable (Fig. 4.2C, 4.4E). Though collagen fibres in the dermis are generally identifiable, the fibres closest to the surface are easier to identify and subtly stain more than fibres deeper in the dermis. Some fibres show transverse fractures; individual fibrils separating from one another can be recognised at some of these fracture points. The upper surface of the dermis is not clearly defined; where fibres are fractured, they locally project above the remainder of the dermis. Despite this irregularity, the majority of collagen fibers in the dermis are orientated parallel to the surface of the skin. Despite an apparent decrease in thickness from stage one to stage two, the thickness of the dermis in the pterylae (W = 814, p = 1.105 x10^{-7}) and apterylae (W = 169, p = 1.5 x10^{-4}) is unchanged from stage one (Fig. 4.6A– B).

Decay stage three -The stratum corneum as a whole is cohesive and tightly packed except for the outermost layers and the edges that are flaky with angular fissures. Isolated cells or clusters of keratinocytes have disassociated from the stratum corneum. Central depressions marking the former position of nuclei are absent in these keratinocytes, some of which show small fibres that measure <

1μm thick, which extend outward from their edges. These keratinocytes are angular and not at all disc like. Stratification is no longer evident as collagen fibres vary widely in orientation. The majority of collagen fibers in the dermis are weakly stained, overlap one another and in many places are fractured making it difficult to trace the path of a single fibre. Collagen fibres in the uppermost part of the dermis are more densely packed, are more strongly stained and can be traced along their length more easily than those deeper in the dermis. Collagen fiber thickness does not show a noticeable increase nor decrease in comparison with previous decay stages or fresh tissue. Results of One tailed Wilcoxon rank sum tests reveal the thickness of the dermis is the pterylae is greater than in fresh tissue ($W = 29$, $p = 2.526$ x10^{-10}), but not compared to the thickness of the dermis in decay stage one ($W = 342.5$, $p = 0.568$) or decay stage two ($W = 427.5$, $p = 0.014$). Dermis thickness in the apterylae is also greater than in fresh tissue ($W = 55$, $p = 8$ x10^{-4}) but not compared to the other decay stages ($W = 208$–229, $p = 0.22$–0.80) (Fig. 4.6A–B).

3.2 Feathers and feather support structures

During dissection of decayed finches, feathers would often separate easily from the body as a cohesive mat with minimal manipulation, likely held together via the intricate network of barbules and hooks on each of the barbs of the rachis. This indicates the cohesion between feathers is stronger than the connection to the skin of the zebra finch. The epidermal and dermal tissues that surround the feather are known as the feather follicle. The shape of the follicle epidermis and feather support apparatus varies depending on whether or not the feathers are removed prior to fixation of the tissues in neutral buffered

99

formalin; their removal can result in the collapse of the follicle epidermis (Fig. 4.4F–G).

Fresh tissue -The follicle epidermis as with the rest of the epidermis has a corneous layer and a germinative layer that can be recognised by its prominent nuclei (Figs. 4.2E, 4.4F–4.4G). Thin keratinous strands project from the corneous layer into the follicular cavity and connect the feather to the follicle wall. At the base of the follicle lies the dermal papilla a diffuse network of fibrous material that connects the feather to the rest of the skin. Surrounding the length of the follicle epidermis is a thin dermis; a ring of multiple collagen fibers, with the appearance and arrangement seen in dermal tissues towards the surface of the integument (Fig. 4.1B, 4.2E). Muscles necessary for the manipulation of feathers project into the dermis and are fixed to the follicle epidermis. Transverse fractures of adjacent muscle fibers are rare and most likely represent damage incurred during dissection of the tissue or sectioning (Figs. 4.4F–4.4G). If the feather has developed fully and remained in situ during preparation, the corneous connection between the feather and follicle partially separates from the follicle epidermis. Developing feathers appear as a ring of dense granular material surrounding a more diffuse perforated tissue; the follicle epidermis encapsulates both. Obvious evidence of a thick keratinous follicle is absent.

Decay stage one -The thin corneous layer, and the stratum germinativum of the follicle epidermis is locally present; nuclei within the stratum germinativum can be recognised clearly (as in other areas of the epidermis) (Figs. 4.2F, 4.4F–4.4G). The attachment between the follicle and follicle epidermis is intact, but there are gaps between the dermal feather muscles and the follicle. In decay stage one, the dermal muscles are cohesive but exhibit subtle undulations and /

or transverse breaks. Locally there are spaces between the fibres of dermal collagen surrounding the follicle; individual fibrils can be recognised in some of these fibres. If the feather has not developed fully, the follicle epidermis is deformed around the dense and diffuse material of the developing feather (Fig. 4.3G).

   Decay stage two -The follicle is poorly defined, and the stratum germinativum is not visible (Figs. 4.2G, 4.4F–4.4G). The follicle and the dermal feather muscles can be separated, at least locally, by a small gap (~10 μm). Some muscle fibers are separated from each other (~1–2μm). The space between is not completely empty; locally the surface of muscle fibres appears frayed and smaller diameter fibrous structures (likely myofibrils) project outward from the main body of the fibre. Transverse fractures in individual muscle fibers are numerous and easily identified. Separation of the feather follicle epidermis from the surrounding dermal collagen is extensive, and individual fragments of collagen fibers are difficult to identify.

   In follicles with a fully developed feather, the corneous layer between feather and the rest of the follicle is now fully separated, and the germinative layer absent (Figs. 4.2G, 4.4F–4.4G). The follicle epidermis and dermis are deformed around undeveloped feathers, which appear as locally diffuse deformed material at the centre of the feather follicle. In samples where the feathers were removed prior to decay the follicle epidermis is markedly different from the near circle of epidermal tissue present in sections where the feather is present. Some fragments of the corneous layer of the follicle epidermis can be observed in the center of the irregularly shaped follicle. In follicles where the feather has been removed, or the feather is undeveloped, fragmentation of the

surrounding collagen fibers can lead to projection of collagen fibers into the empty space of the follicle.

Decay stage three -In decay stage three the corneous layer is recognisable in some sections around the internal edges of the feather follicle, but is heavily fragmented (Fig. 4.2H, 4.4F–G). The muscle fibers responsible for feather manipulation stain weakly and are difficult to identify, where present dermal feather muscles appear in patches with poorly defined boundaries. Some fibrous structure can be observed but whether this is collagen or muscle tissue is unknown. Surrounding collagen tissue is heavily frayed and fragmented, neighboring fibers cross each other's paths. Collagen fibres closest to the feather follicle are more densely packed and show more ordered orientation but are still fragmented. The pulp of undeveloped feathers can be distinguished from the surrounding collagen as it is denser and often separated by a mostly empty feather follicle; nevertheless it is very faint, and little evidence of any structure can be recognised.

3.3 Zebra Finch subcutis and adipose tissue

Fresh tissue -Adipose tissue comprises a densely packed array of polygonal adipocytes with thin intact cell membranes. Many of these cell membranes have visible nuclei (Figs. 4.2 I, 4.4H–I). Most of the adipose contained within each adipocyte has presumably been lost to treatment with ethanol during the preparation of the tissue. The amount of collagen present in subcuticular adipose tissue varies. In some areas adipocyte cell membranes are in contact with one another (Fig. 4.4H); elsewhere adipocytes are separated by several layers of collagenous tissue (Fig. 4.4I).

Decay stage one –Most adipocyte cell membranes are intact and maintain contact with one another; nuclei are absent (Figs. 4.2J, 4.4H–I). Some adipocytes have filamentous material projecting from the cell membrane into their center that may be parts of the cell membrane. Isolated strands are also present within the center of the adipocyte and may originate from adipocytes with more fragmented cell membranes. The diffuse material is present surrounding some adipocytes and may be adipose. Adipocytes surrounded by collagen also show isolated strands projecting into the center of the adipocyte and diffuse indeterminate material at their edges (Fig. 4.4I). The surrounding collagen fibers also cut across one another and project into the adipocyte spaces.

Decay stage two –The cell membranes of many adipocytes are fragmentary, but can still be identified by their basic polygonal outline; junctions where more than two cell membranes meet separately less than junctions between two cell membranes, (Figs. 4.2K, 4.4H–I). Some adipocytes are completely infilled by the diffuse indeterminate material.

Decay stage three –The outline of adipocytes is difficult to recognise; their cell membranes are largely fragmentary (Figs. 4.2L, 4.4H–I). However, some isolated complete or near-complete adipocytes can be identified by their polygonal outlines and junctions between several adipocyte cell membranes can be recognised in fragments. Diffuse indeterminate material could not be identified at the center of any adipocytes. The center of intact or partially intact adipocytes were filled with granules and filament-like material thought to be the remnants of cell membranes. The collagen surrounding some adipocytes maintains their polygonal outline; the cell membranes cannot be identified (Fig. 4.4I). The collagenous matrix is itself much more diffuse than in previous decay

stages and is fragmented and frayed, allowing individual collagen fibers to project into the spaces occupied by the adipose tissue along with other detrital material derived from sources such as the adipocyte cell membrane.

Decay stage four –Adipose tissue comprises only small fragments of cell membrane; junctions between more than two adipocytes are absent, thus the regular polygonal texture cannot be recognised (Figs. 4.2M, 4.4H–I). The outline of adipocytes surrounded by collagen also cannot be recognised. All adipose tissue regardless of supporting collagen fibers becomes a diffuse homogenous mass, with no discernable structure.

3.4 Skeletal muscle

Fresh tissue -Muscle fibers are composed of smaller myofibrils bound within a cell membrane, which defines the edge of the fiber. The fibers themselves vary in diameter from ~5–8 µm (Fig. 4.6C). Muscle fibers are held within a network of collagen. The collagenous tissue that bundles multiple fibers together to form the fasciculus is the endomysium; several fasciculi are then held together by collagen in the epimysium (Fig. 4.4J–K). In fresh samples of muscle tissue, the majority of the endomysium and epimysium is obscured by the dense packing of muscle fibers. Transverse fractures across the muscle fibers and separations between groups of fibres were observed in fresh tissue, this might be damage incurred during the dissection process. In areas where groups of neighbouring muscle fibres have become separated the epimysium and endomysium can be observed as a faint web of fibers on groups of muscle fibers. In some cases, individual collagen fibers connecting laterally between muscle fibers can be seen, but this is uncommon. Preparation of the tissue reveals that

the skin in the apterylae is more easily separated from the underlying skeletal muscle than the skin in the pterylae. The amount of muscle tissue present in a fresh sample is ~70–80%, measured as area occupied in a 100 μm by 100 μm square (Fig. 4.6D). The amount of muscle tissue is not 100% due to gaps between bundles of muscle fibres. Presumably in fresh tissue these gaps were incurred during preparation of the tissue.

Decay stage one -The most recognisable feature of decay stage one is the local absence of nuclei; The edge of the muscle fibres is only connected locally to the collagenous endomysium that surrounds them; therefore there is a space locally between the muscle fibers and the endomysium. The muscle fibers themselves are ~3–5 μm across (Figs. 4.4O, 4.6C). In transverse and longitudinally cut muscle fibers myofibrils can be recognised as faint striations. In some places fibers are fragmented into sections ~100–300 μm long. The area occupied by muscle tissue in decay stage one is ~50–70% (Fig. 4.5D).

Decay stage two –Muscle fibers measure ~2–4 μm across and are almost completely separated from the endomysium. Spaces between bundles of muscle fibers are apparent (Figs. 4.2P, 4.4J, 4.6C–D). Fragments of epimysium are partially connected to the muscle fiber bundles. Some of the collagen fibers that comprise the endomysium and epimysium are separated from one another locally along their length; these are noticeably fraying where they line the void formerly occupied by the muscle fiber and in the spaces between muscle fiber bundles. Myofibrils can no longer be identified. Fragmentation of muscle fibers is extensive. Most fragments are ~30–100 μm long. Muscle tissue occupies only ~20–60% of a 100 μm by 100 μm square in decay stage two (Fig. 4.6D).

Decay stage three –Few muscle fibres can be recognised. The vast majority reduced to irregularly shaped slivers of tissue ~15–30 μm long with a larger diameter compared to decay stage one and two at ~4–6 μm across (Figs. 4.2Q, 4.4K). In decay stage three pixel count analysis of the tissues reveals that ~14–25% of a 100 μm by 100 μm square is occupied by muscle tissue. Muscle tissue present is weakly stained, with little structure and indistinct boundaries. Partial contact with the endomysium is common, but some muscle fiber fragments are detached fully from the endomysium. Myofibrils were not present. The collagenous tissues that bind muscle tissue together also stain weakly and are diffuse. There are noticeable gaps between collagen fibres in the endomysium and epimysium, and the fibers themselves are heavily frayed and unorientated.

3.5 Gecko epidermis, dermis and adipose tissue

Fresh tissue -Gecko epidermis is composed of two keratinous layers: an outer β-keratin layer which forms the surface of the scale, which lies atop a layer of **α**-keratin (Figs. 4.1, 4.4L). The β-keratin layer easily separates as a cohesive sheet during preparation of the tissue for microscopy, while the a-layer remains adhered to the remainder of the integument. The stratum germanitivum the lowest layer of the epidermis is a layer one cell thick with prominent nuclei (Figs. 4.2R, 4.4L). Beneath this lies the dermis, approximately 30–100 μm thick. The dermis is predominantly composed of collagen fibers, which are commonly oriented parallel with each other and with the surface of the integument. Collagen fibers in the dermis undulate, often cutting across the paths of several other collagen fibers along their length. Within this network of collagen fibers

are circular adipocytes that can be isolated or associated into groups (normally of around three to four); their nuclei are absent in thin section. Two types of pigmentary structure occur in the upper part of the gecko dermis. First, Chromatophores, possibly iridophores or xanthophores (~1–2 µm in diameter) are yellow-brown in color, and form a near constant layer at the surface of the dermis; they occasionally form localised projections (10–30 µm deep) into the rest of the dermis. In other sections, chromatophores permeate almost the entire thickness of the dermis but become more diffuse, and less numerous with depth. Black or brown melanophores, another type of chromatophore, contain the pigment melanin (~10–30 µm in length). Their outline is often irregular as it includes projections into neighboring areas of the upper part of the dermis. Melanophores are irregularly spaced and never found in the hinge region of a scale

  Decay stage one -The β-keratin layer of the stratum corneum has separated from the remainder of the integument (Figs. 4.2S, 4.4L). The α-keratin layer is intact and adheres locally to the stratum germinativum, following the outline of the scale surface. Commonly the stratum germinativum has also separated locally from the dermis, or in rare cases is completely absent. The stratum germinativum that is still partially connected to the dermis is diffuse and stains weakly; some nuclei can be recognised. Collagen fibers in the dermis are un-fragmented or frayed and oriented parallel to each another. In hand specimen it is clear that gecko skin is pigmented. Diffuse connective tissue at the base of the dermis is partially separated from the dermis and from the underlying muscle. Adipocytes within the dermis are well defined by the surrounding

collagen fibers and their nuclei are absent. The dermis is ~60–100 μm thick (Fig. 4.6E).

Decay stage two -The sheet of epidermal α-keratin remains largely intact but the total absence of the stratum germinativum means the epidermis is not in contact with the dermis. The epidermis is rippled and does not follow the outline of the scale surface (Figs. 4.2T, 4.4L). Dermal collagen fibers are fragmented in some sections and noticeably frayed at the outer surface of the dermis and the boundaries of adipocytes, making it impossible to assess the level of decay of adipocyte cell membranes. The upper boundary of the dermis is hummocky and defined by chromatophores; between the hummocks are fissures that permeate ~10 μm into this pigmented layer. Locally, groups of chromatophores bound by dermal collagen are separated from the dermis. Additionally in some sections beneath the lower boundary of the pigmented layer collagen fibres are more weakly stained. In some samples small, irregularly shaped, aggregations of melanin are also separated from the rest of the integument; the original source of this melanin cannot be identified. The outline of the melanophores is irregular with projections into the surrounding dermis common, including in sections of tissue where the disassociated melanin is present. A peripheral void is present between the center of some of the melanophores and the outer surface of the melanosomes and its projections. The total thickness of the dermis is ~70–120 μm (Fig. 4.6E). One-tailed Wilcoxon rank sum tests reveal the dermis is statistically thicker than the dermis in fresh tissue (W=996, p=3.26x10^{-2}) and decay stage one (W=1814, p=1.95x10^{-3}).

Decay stage three -In decay stage three, most β-keratin scale coverings are incomplete, the layer of α-keratin is intact and detached from the dermis. The

dermal collagen fibers are heavily frayed and fragmented with clear breaks in multiple adjacent fibers. The majority of the fibers are randomly oriented with respect to one another (Figs. 4.2U, 4.4L). The majority of adipocyte boundaries within the dermis can be recognised, but the boundary may be slightly irregular. Areas of multiple adipocytes not bound by collagen fibers appear diffuse, their boundaries are more difficult to identify. Chromatophores are faint and the pigmented layer is locally interrupted (Fig. 4.6F). The upper boundary of the chromatophores is hummocky, but the outer surface is permeated with collagen fibers that project above the pigmented layer. Most melanophores are prominent, with processes that project into the surrounding dermis. The edges of a minority of melanophores are circular and do not possess external projections into the surrounding tissue. Collagen fibres directly beneath the pigmented layer are noticeably more weakly stained compared to collagen fibers lower in the dermis. The thickness of the dermis is ~80–150 µm (Fig. 4.6E). One-tailed Wilcoxon rank sum tests reveal the dermis in decay stage three is statistically thicker than the dermis in fresh tissue (W=129, p=0.0282) and decay stage one (W=261, p=0.0149).

4. Discussion

In general terms, the results confirm previous studies in demonstrating the resistance to decay of the four tissue categories (Goff, 2009; Syme and Salisbury, 2014). More specifically, this study reveals how this decay resistance does not apply to all the tissue categories of the integument equally (Figs. 4.2,

4.4, 4.5) and what impact the differing distribution of certain tissues has on the decay of integument with different functions.

4.1 Epidermis

This study demonstrates clearly that in both birds and squamates the epidermis and dermis are more resistant to decay than the subcutis (Figs 4.5A–B). The recalcitrant properties of these integumentary layers can be attributed to their being largely composed of keratin and collagen molecules (Schweitzer, 2011). Both keratin and collagen molecules are built of tightly bound cross-linked polymeric fibrils, making them particularly resistant to decay. Keratin is further strengthened against the effects of decay by the hydrophobic nonpolar amino acids within its molecular structure. This makes keratin insoluble and therefore particularly difficult to degrade by all enzymes except those specifically adapted to the task (keratinases), which are not widespread in nature (Matikeviciene et al., 2009; Schweitzer, 2011; Lange et al., 2016).

The initial stage in the decay of the integument in the zebra finches and geckos is the separation of the various epidermal layers from one another and also from the dermis; the same process occurs in humans decomposing in wet or moist environments and is known as skin slippage (Goff, 2009). Skin slippage is the result of the production of hydrolytic enzymes from the cells at the junction of the two layers by exposure to water and can lead to the separation of the epidermis locally from the dermis (Lillywhite and Maderson, 1982; Goff, 2009) as seen in this study. Although water can retard decay through lowering

temperatures and enhancing anoxia, when necrotic tissues are exposed to water they begin to break down through enzymatic activity (Gill-King, 1997).

In life the reptilian epidermis is less permeable to water than the epidermis of birds because it has a more effective hydrophobic lipid layer (Lillywhite and Maderson, 1982; Menon and Menon, 2000). Feathers, improve water resistance of bird skin by trapping air close to the surface (Menon and Menon, 2000), logically these will eventually be waterlogged, and bird skin will remain more permeable than squamate skin. Considering the important role water plays during decay, one might expect skin with a relatively permeable epidermis such as bird skin to be more susceptible to the action of hydrolysing enzymes when exposed to external water. The results suggest the epidermis in bird skin decays more readily than in reptilian skin because the reptilian epidermis is much thicker and less likely to fragment and fracture.

4.2 Dermis

In both the zebra finches and geckos the dermis is predominantly composed of collagen fibers which protect the body from damage (Micali et al., 2001) (Fig. 4.1A–B). The thicker the dermis, the more collagen is present and therefore the more resistant the dermis is to damage. The relatively low thickness of dermis in the zebra finch provides little mechanical protection relative to reptilian skin and makes the zebra finch skin delicate and particularly susceptible to damage, as observed during dissection. It seems that, in birds, feathers contribute significantly to the physical protection of the skin, and the animal as a whole, making a thicker, reptilian style, dermis redundant

(Stettenheim, 2000). The increase in thickness of the pterylae and apterylae during decay occurs relatively early in the decay process (Fig. 4.6A). The dermis in the apterylae and pterylae in bird skin shows a statistical increase in thickness after decay stage one. There is also a statistically supported increase in thickness of the reptilian dermis during decay (W = 129, p = 2.824 x10^{-2}) (Fig. 4.6), suggesting this post-mortem response may be common to the skin of both birds and squamates if not the skin of all vertebrates. It is clear that in birds and squamates, the dermal layers of skin separate from one another in response to decay, resulting in an increase in overall thickness of the dermis, while collagen fiber diameter remains constant. The dermal layers of the apterylae show a greater increase in thickness compared to the pterylae, making it less cohesive during decay than those in the pterylae. Both the dermis in the pterylae and apterylae is less cohesive than the dermis in squamate skin, which demonstrates a much smaller increase in thickness during decay relative to its condition when fresh.

The uppermost part of the dermis in bird skin is the most resistant to decay; it is less likely to show heavily fragmented or randomly oriented collagen fibres. We attribute this to the denser packing of collagen fibres leaving less room for them to separate and a reduction in surface area exposure to water, enzymes and microbial action. The dermis of geckos is similarly composed of tightly packed collagen fibres but this is not limited to only the uppermost part of the dermis and extends far into the skin. Ultimately squamate skin is thicker and more compact than bird skin, and so is more resistant to decay.

Collagen is particularly resistant to degradation, but the breakdown of collagen fibers in this study on a relatively short timescale indicates that even

relatively thick reptilian dermis will readily decay over a period of 1 month under the experimental conditions used. Other studies have observed in several animals, including birds, that the outermost layer of dermal collagen is responsible for the mechanical strength of the skin as a whole, and therefore more resistant to damage post-mortem than those beneath it (Ramshaw et al., 1986). In our study dermal collagen layers could not be identified, but constituent fibers in the uppermost part of the dermis appear less fragmented and often retain their parallel orientation with the outer surface of the dermis, while collagen fibers in the lower part of the dermis undergo more extensive fragmentation. It is possible that the compact arrangement of collagen fibers in the upper dermis presents a smaller surface area on which bacterial enzymes could act, reducing the rate at which collagen in the upper dermis degrades relative to collagen in the lower dermis which is more exposed.

The decay resistance of individual collagen molecules is due to the organisation of the constituent amino acids into a triple helix (tropocollagen), but it is the covalent bonds that form between tropocollagen molecules that provide the most strength to the collagen complex as a whole (Chang and Tanaka, 2002). This suggests that the initial physical break down of collagen tissues is likely to occur between the fibrils and fibers early in the decay process, whereas breaks within the tropocollagen molecules are likely to occur later unless they are exposed to considerable stress (Craik and McNeil, 1964). It is possible for the strong bonds within the tropocollagen structure to be split through the action of enzymes such as collagenase released as a result of autolysis or produced by microorganisms (Janko et al, 2010). On the other hand, it seems unlikely these enzymes would cause transverse breaks in the

tropocollagen molecule before the neighboring collagen fibers and fibrils had been separated from one another. This is what would happen at a biomolecular level, how this relates to difference between the upper and lower part is problematic.

Several processes could be responsible for the breakdown of collagen in the dermis and other tissues; enzymes such as collagenase, which have been released into the intercellular space via autolysis, can begin to break down the collagen molecule, but these enzymes will only be able to function for a few hours after cell death (Janko et al., 2010). The breakdown of collagen over the longer term could be the result of collagenase producing bacteria, but these are rare even in environments considered to promote decay such as soil (Suzuki et al., 2006; Janko et al., 2010), and are unlikely to be present in the decay medium (mineral water). This suggests any bacteria present within the decay vessel were introduced on the surface of the animal or in the body and likely to be associated with the digestive system, may be responsible. Endogenous bacteria are known to spread rapidly from the gut to other areas of the body after death, through the blood (Goff, 2009), and inevitably through the spreading soup of decayed internal organs and muscle. After the expiration of enzymes derived from cells in the integument, internal bacterial floras must be a major contributor to decay in the integument of the animals in this study. Exogenous bacteria and fungi, in particular keratin degrading bacteria such as *Chryseobacterium sp.* (Riffel et al., 2003) and *Bacillus licheniformis* (Williams et al., 1990) are known to be associated with poultry waste and could reasonably be expected to be present on the feathers of the animal during life. In conjunction with the adaptive immune system integument presents a physical barrier to external bacteria in vivo,

preventing infections (Stettenheim, 2000). Though the immune system ceases to function soon after death, the physical barrier of the integument n remains cohesive and intact and therefore continues to present a barrier to exogenous bacteria during decay stage one and presents a mostly complete barrier during decay stage two (Figs. 4.2, 4.3, 4.4). This suggests exogenous bacteria play a limited role in the decay of the dermis until later stages of decay, when they have access to the full thickness of the skin. Additionally, the upper part of the dermis shows limited evidence of decay relative to deeper dermal layers. If exogenous and endogenous bacteria were contributing equally to the decay of the dermis, we might expect the evidence of decay in the upper surface of the dermis to more closely resemble the effect of decay on the lower part of the dermis. Whereas this differential response to decay is in part explained by the more compact arrangement of collagen fibers in the former, the noticeably more cohesive and intact surface of the dermis suggests exogenous bacteria are incapable of making noticeable changes to the tissue structure until decay stage three. This suggests that the majority of decay observed in the tissues of finches and geckos is likely the result of endogenous bacteria. While the analysis of bacterial floras could have indicated the extent to which exogenous bacteria had penetrated the skin at each sampling interval it was beyond the scope of this study.

Unlike the skin of the zebra finch, the outer layers of the dermis in geckos are pigmented by yellow/brown chromatophores and black melanophores. The loss of yellow-brown chromatophores from the dermis is the result of the breakdown and fragmentation of the collagenous matrix in which they are housed (Fig. 4.4L). The same processes could also impact a tissue housing the other chromatophores, such as melanophores, which could explain the irregular

aggregations of melanin above the surface of the integument. However, melanophores have not been observed as being lost whole from the surface of the integument, nor having their position within the dermis altered by decay. Melanophores may have lost melanosomes from their edge but not to the extent necessary that their shape was affected.

From this study, it is clear that the reptilian dermis responds to decay in an identical manner to dermis in bird skin, but its greater thickness means that tissue cohesion is maintained further into the decay process. It is possible that the presence of a dense collection of chromatophores in the upper layers of the reptilian dermis may also contribute to the cohesion of the upper part of the dermis post mortem.

4.3 Feathers and feather support structure

Feathers are highly resistant to decay (Fig. 4.5C) and in some cases are known to remain associated with the body of the animal for several months post mortem (Davis, 1994). The results of this study suggest that body feathers will only remain in situ if they are undisturbed, as even small amounts of manipulation such as those during dissection are enough to pull feathers out of position. Developing feathers remain beneath the surface of the integument and so are less likely to be removed when exposed to manipulative forces during dissection, additionally developing feathers are not fully keratinised (Lucas and Stettenheim, 1972) making them more pliable, and potentially less likely to remain pristine during the decay process. In life, the only connection of the feather to the follicle is via the dermal papilla which projects through the base of

the epidermal collar, but this does not maintain the feather's position during life or death (Lucas and Stettenheim, 1976). The retention of the feather within its follicle during life is thought to result in part from the constrictive action of the dermal feather muscles (Buhr et al., 1996; Lucas and Stettenheim, 1976), and this continues for a short period immediately following death, potentially as a result of rigor mortis. It is possible that stresses in the muscle associated with rigor mortis (MacNaughton, 1978) could be responsible for small transverse breaks in the muscle and could also lead to the breaks between the muscle and the feather itself. Presumably after rigor mortis the corneous sheets of the follicle and collagen fibers of the upper dermis take over from dermal feather muscles as the primary forces causing feather retention (Buhr et al., 1996). The results of this study imply that, unless some exterior force disturbs the feather during the decay process, it will remain housed within the integument until the disintegration of the feather follicle epidermis.

As with the outer epidermis, the first stage of decay of the epidermal collar is the hydrolyzation of the bonds between the stratum corneum, stratum germinativum and dermis (Goff, 2009), but in feather follicles the various epidermal layers are prevented locally from physically separating from one another, giving the feather follicle greater cohesiveness than the epidermis on the external surface of the integument. In some cases, a slight expansion of the epidermal collar during decay allows space for the corneous layer to separate partially from the germinative layer of the epidermal collar.

Though not observed in the time frame of this study, if decay were to continue indefinitely, it is likely that the feather and the corneous layer, as the most recalcitrant tissues, would be the last structures to survive of the feather or

feather support apparatus. Furthermore, if the feather has yet to fully develop or has been removed prior to decay, the collapse of the follicle and fragmentation of the corneous layer during decay would make identification of the original feather follicle improbable.

4.4 Subcutis and adipose tissue

Adipose, the least durable of all the integumentary tissues (Fig. 4.5D), is mainly composed of adipocytes associated with small amounts of more decay resistant connective tissue (Lucas and Stettenheim, 1972). The collagen fibres surrounding some adipocytes maintains their shape longer into the decay process than those adipocytes not surrounded by collagen even once the adipocyte cell membranes have degraded. Despite its susceptibility to decay, the retention of junctions between several adipocytes in decay stage three demonstrates that cell membranes can still contribute to tissue cohesion after substantial decomposition. However, these remnants of adipose ultrastructure do not persist for long; unlike the other integumentary tissues studied, the decay observed in some samples of subcuticular adipose tissue was extensive enough that all ultrastructure was obliterated. A fourth decay stage was necessary to incorporate this information, as it was distinct from extensively decayed adipose that still retains some recognisable ultrastructure.

The rapid breakdown of the subcutis may be correlated to the increase in thickness of the dermis of zebra finches. An acidic environment formed from the hydrolyzation of fatty acids in the subcutis (Fiedler and Graw, 2003) can increase the breakdown of more cells thereby increasing the progression of decay overall.

The exposure of collagen fibers in the lower dermis to this acidic mixture of water, enzymes and cellular detritus may cause further loss of cohesion and separation. Presumably this additional decay-related stress would affect the pterylae more than the apterylae, as the former possess much larger quantities of adipose tissue and in turn, could reduce the likelihood of it being identified in later stages of decay. The greater effect of decaying adipose on the structural integrity of the pterylae more than the apterylae may be correlated with the higher relative increase in mean thickness of the dermis and separation of dermal collagen fibers of the former compared to the latter (Fig. 4.6). In some circumstances, adipose tissue is known to improve the decay resistance of other tissues; certain anaerobic conditions cause the adipose within the tissues of the subcutis to be broken down into fatty acids to form a material with anti-microbial properties known as adipocere (Fiedler and Graw, 2003). The absence of adipocere in thin section and samples prepared for SEM could be a preparation artefact from the immersion of the tissue in ethanol. However, adipocere was not observed within the carcasss during dissection. Further the observations of others indicate that adipocere rarely forms in birds (Schroger, 1944), and is unlikely to form in reptiles due to low amounts of fatty tissue (Reisdorf and Wuttke, 2012).

4.5 Skeletal muscle

The skin of the geckos displays higher cohesion with the underlying musculature than does the skin of birds. The ready separation of bird skin from underlying muscle during decay presumably represents a functional necessity in

birds for the skin to move independently from the forces of muscle contraction. However, this is not to say that non-feathered regions of bird skin are more securely anchored to the muscle, as this is not the case. For instance, the skin of the pectoral apterylae displays a much lower cohesion to the pectoral muscles than does the neighboring pterylae.

Compared to other tissue categories skeletal muscle is moderately more resistant to decay than adipose tissue but less resistant to decay than the epidermis and dermis in zebra finches and geckos (Fig. 4.5E). In contrast to other tissue types, the response of muscle to the early stages of decay is well understood from its importance to the food industry, and as a result the shrinkage, transverse breaks and loss of definition in the myofibrils and fibers in this study have all been previously reported in other animals, including birds (MacNaughton, 1978; Pearce et al., 2011). The first stage in muscle decay is rigor mortis, where the ATP in the muscle is depleted leading to contraction of the muscle as a whole, and as a result transverse breaks in the muscle fibers can occur alongside degradation and structural disintegration of the collagen in the surrounding endomysial and epimysial spaces (MacNaughton, 1978; Ando et al., 1992). Eventually, rigor mortis ends, as bonds between the actin and myosin begin to break down and the body becomes more flexible. In some places, individual muscle fibers lose alignment with one another and show an undulating or wavy appearance suggesting they are no longer under tension (McNaughton, 1978), and that there may be additional breaks or deformations to the fiber elsewhere.

Previous results on muscle decay in *Xenopus* tadpoles also demonstrated the separation of muscle fibers from one another during decay (Redelstorff and

Orr, 2015); the results herein indicate this is due to muscle fiber shrinkage (Fig. 4.6) and not relative movement of fibers away from one another. In agreement with other studies where muscle shrinkage has been observed post-mortem (Pearce et al., 2011), we demonstrate that this shrinkage occurs only in the muscle fibers not involving the collagenous endomysium that surrounds the fibers. A one-tailed wilcoxon rank sum test shows the increase in muscle fibre diameter between decay stage two and three is significant (W=2438.5, p=<0.0005), the reason for this is unknown. It may be due to the formation of localised fissures within the muscle fibre separating fibrils from one another. This could lead to an artefact where a greater muscle fiber diameter is measured than in fibers where fissures are absent. This would explain why the area occupied by muscle continues to decrease from stage two to stage three as any fissures would not be recorded as muscle (Fig. 4.6C). The pericellular collagen of the endomysium and epimysium remains in place between the muscle fibers during decay, but unlike the dermal collagen fibers undergoes considerable fragmentation. The increased rate of degradation and decay of this collagen may be due to the thinner fibril diameters of the collagen type V that is thought to compose the majority of pericellular collagen in vertebrate muscle tissue (Ando et al., 1992; Adachi and Hayashi, 1986). Despite the fragmentation of the endomysium, the bonds between collagen and the surfaces of some muscle fibers seem to persist after considerable decay and may contribute to keeping fragmented muscle tissue in position.

A large amount of water is released by the denaturing of proteins in skeletal muscle post-mortem (Pearce et al., 2011), which can contribute significantly to the decay of surrounding muscle and integumentary tissues by

facilitating transport of decay-inducing bacteria (Goff, 2009). The massive

pectoral muscles of the zebra finch presumably contribute proportionately

enormous amount of water. As a result, the transport of various degradative

components around the carcasss via this former intracellular fluid could be much

higher in the area immediately surrounding the pectoral muscles of the finches

than the geckos. Furthermore, obvious pathways for endogenous bacteria and

other degradative components into and around the pectoral muscles of the zebra

finch should be expected on account of their having an extensive blood supply

and associated vasculature (Goff, 2009) necessary to maintain flight. Different

muscles have different distributions of muscle fiber types depending on their

function, which translates to different levels of metabolic activity. Muscles with

different distributions of muscle fiber types are known to have different post-

mortem metabolic rates during the first 45 minutes of decay (Ryu and Kim,

2005), but the effect of different muscle fiber types on long-term decay is

unknown. Presently, the distribution of muscle fiber types in the zebra finch and

gecko is unknown, so this cannot be investigated, but it is worth remembering

that metabolic differences intrinsic to the function of certain muscle groups

could influence their resistance to decay and chances of preservation in the fossil

record.

4.6 Implications for fossilization

Skin is relatively well represented in the fossil record and is variously

preserved as external moulds (Kim et al., 2010), carbonaceous compressions

(Zheng et al., 2013) and mineralized remains (McNamara et al., 2009). Bird skin

is preserved both as carbonaceous compression fossils (Zheng et al., 2013), and phosphate, but only a single specimen (MCCMLH31444); the wing of a Lower Cretaceous bird shows ultrastructural detail. The specimen preserves dermal muscles, tendons and ligaments, and the general outline of the dermis and epidermis in the patagia in calcium phosphate (Navalón et al., 2015). Our results suggest preservation of soft tissue in MCCMLH31444 began during the earlier stages of decay due to the presence of a continuous and cohesive epidermis and dermis, this interpretation is strengthened by the presence of dermal musculature which is likely to undergo phosphatization early in the decay process as a reflection of their high phosphate content. Preservation of the patagia suggests the depositional environment was rich in phosphate and that bird skin can be preserved when not underlain by large underlying skeletal muscles such as the pectoral flight muscles.

Generally, examples of carbonized skin do not preserve ultrastructure in great detail; usually preservation is limited to structures such as scales in reptilian skin (Foster and Hunt-Foster, 2011; Godefroit et al., 2014), with some of these exhibiting structures interpreted as either collagen fibers or keratin fibers (Lindgren et al., 2009). The ultrastructure of soft tissue is more frequently replicated in phosphate; examples of muscle are especially common (Dornbos, 2010; Navalón et al., 2015; Parry et al., 2015), where specific structural details including individual fibers and nuclei are commonly preserved (Martill, 1990; Wilby and Briggs, 1997). Components of skin including collagen fibers are commonly preserved in phosphate (McNamara et al., 2009). Melanosomes are also repeatedly encountered within fossil phosphatized and carbonized skin,

preserving evidence of original color patterning (Lindgren et al., 2014; Vinther et al., 2016).

There are a number of features of decay in bird skin that promote its replication in phosphate: (1) the pectoral flight muscles are particularly large relative to the animal's mass and contain large reservoirs of phosphate, which could be enough to initiate internal mineralization of the overlying skin; (2) the low-pH environment caused by the decomposition of the adipose tissue is conducive to phosphatization; (3) bird skin is relatively thin and permeable to water compared to squamate skin, this presents much less of a barrier for phosphate rich fluids in the external environment to infiltrate the complete thickness of the skin. However, the breakdown of tissue in more recalcitrant integument will take longer than for more labile tissues and internal organs. Also if the primary source of phosphate is internal rather than environmental thicker, impermeable squamate skin would help concentrate that phosphate within the carcasss, preventing it from dissipating into the external environment. As a result, there is a longer period over which phosphate can accumulate in a squamate carcasss, thus when phosphatization occurs there is a greater likelihood that more ultrastructural details of squamate skin will be preserved (Wilson et al., 2016).

Most importantly, skin is an organ composed of multiple intricately intertwined tissues, the decay process in some tissues could impact the preservation of the skin as a whole. Phosphatized tissues often show a preservational gradient with more detail preserved at closer proximity to the source of phosphate and less detail farther away from (Wilby, 1993, Wilby and Briggs, 1997). Examples include tissues where replication is restricted to

surfaces lying on the substrate (Martill and Unwin, 1989). Logically these gradients could also be present in bird skin. Therefore if bird skin was phosphatised in an environment rich in phosphate ions, then the epidermis and dermis are far more likely to become phosphatised than the deeper adipose tissue of the subcutis. However, because bird skin is more likely to undergo fragmentation compared to the skin of squamates during the later stages of decay, it is less likely large contiguous sheets will be preserved. But this does not rule out the existence of smaller fragments of phosphatised skin in the fossil record.

4.7 Implications for the preservation of fossil bird skin: a predictive model.

The results presented in this study have implications for the preservation of the ultrastructure of bird skin in the fossil record. Early in the decay process, many of the tissue components would be available for preservation although there will be some structural differences relative to their appearance in vivo: (1) the separation of collagen fibers in the dermis of the pterylae will have increased and the in vivo arrangement and orientation of these fibers may have changed now that their movement is less constrained by surrounding fibers; (2) some collagen fibers in the lower dermis will be fractured; (3) the dermis and epidermis of the feather follicle will be deformed; (4) muscle fibers in the dermis and in the underlying skeletal muscle will have decreased in diameter and may also show transverse fractures (Fig. 4.7). There are several features that are unlikely to be preserved due to their susceptibility to decay: (1) the stratum germinativum –non-keratinised cells in the outer epidermis and the feather

follicle; (2) nuclei in the muscle; and (3) large contiguous sheets of the epidermis.

Later in the decay process, the vast majority of ultrastructure and tissue components of bird skin would not be available for preservation. In those tissue components that are present the following details will be apparent: (1) the epidermis is present but fragmentary, groups of keratinocytes may be entangled in the feathers, but their outlines will no longer appear disc-like; (2) the dermis is more likely to be represented by collagen fibers from uppermost part of the dermis and from the apterylae which remain cohesive in later stages of decay; (3) feather follicles can only be identified by the position of the rachis in the case of fully developed feathers and concentrations of melanosomes or thinly distributed pulp in the case of developing feathers; (4) remnants of dermal feather muscles cannot be distinguished from remaining collagen fibers; (5) evidence of adipose tissue is completely absent, any cell membrane material remaining is detrital and so ultrastructure cannot be inferred; (6) skeletal muscle is absent but the original presence of skeletal muscle can be identified by the collagenous framework of the endomysium and epimysium. Superimposed upon the tissue components available for preservation is a taphonomic gradient related to their biochemistry in vivo.

5. Conclusion

Broadly speaking, the results of this study suggest that the integument of squamates is less susceptible to decay than the integument of birds, and that

feathered sections of skin in birds are less susceptible to decay than the feather-bearing skin. Collagen is the most important tissue for maintaining cohesion in the skin during the decay process; the amount of collagen and the more densely packed it is, the lower the likelihood that skin will progress to later decay stages. For these reasons, squamate skin with its compact arrangement of dermal collagen fibers will remain intact or near intact much longer than bird skin. The loss of cohesiveness of the dermis and fragmentation of the epidermis during later decay stages suggests that if bird skin were phosphatized after extensive decay, then the epidermis and dermis may be preserved as a higher number of small fragmentary pieces. If phosphatization occurs early in the decay process, it is likely the dermis and epidermis will be preserved as large contiguous sheets observed in MCCMLH31444 the one example of feathered skin so far discovered (Navalón et al., 2015)

More specifically, our results indicate that the integument has limited fossilisation potential and under most environmental conditions rapid mineralization would be necessary to preserve ultrastructural detail. The experiments constrain the relative preservation potential of both the categories of tissue comprising the integument, and the different components of each. This predictive model can be used to test candidate examples of fossil tissue to ascertain whether the absence of specific details is taphonomic or real.

Acknowledgements

Studying decay: a review of available imaging techniques for taphonomic studies

Volume rendering of decayed bird skin with feather

Studying decay: an assessment imaging techniques for taphonomic studies.

Christopher S. Rogers[a]*, Maria E. McNamara[b], Patrick J. Orr[c], Stuart L. Kearns[a], Michael J. Benton[a].

[a] *School of Earth Sciences, University of Bristol, Wills Memorial Building, Queens Road, Bristol, BS8 1RJ, UK*

[b] *School of Biological, Earth and Environmental Sciences, University College Cork, Distillery Fields, North Mall, Cork, Ireland.*

[c] *UCD School of Earth Sciences, University College Dublin, Belfield, Dublin 4, Ireland*

Keywords: Taphonomy, Decay, Histology, Imaging, Micro-CT

ABSTRACT

Keywords: Experimental decay, Micro-CT, Bird Skin, Taphonomy

The experimental decay of extant organisms is a well-established method for understanding the exceptional preservation of non-biomineralized tissues in the fossil record. The techniques used to image the results of these experiments, however, are limited and rely heavily on light and scanning electron microscopy (SEM). Here we integrate a suite of methods - SEM, light microscopy and micro-computed tomography (Micro-CT) - to image tissue components of the skin and muscle of birds. The relative

* Corresponding author. Tel.: +44 117 394 1340; fax: +44 117 9253585.
E-mail address: cr8392@bristol.ac.uk

merits of each technique in documenting morphological change during decay are assessed. Whereas SEM allows rapid assessment of decay-related changes on the surface of specimens, and light microscopy in conjunction with histological stained tissue sections, enables specific tissue types to be identified in section, the ability of Micro-CT to produce high-resolution complete volume scans makes it the ideal method for tracking decay related changes of non-biomineralized tissue morphology in three dimensions.

1. Introduction

Fossils that show exceptional preservation of non-biomineralized tissues are proven to radically improve our understanding about the biology of extinct organisms. The first studies to investigate the decay of animals in a palaeontological context were concerned with decay-related changes to the entire carcass and the difference in preservation between biomineralized and non-biomineralized tissues (Schäfer, 1972; Allison, 1988). Subsequently, the study of taphonomy has focused upon the decay of specific non-mineralized tissues (Briggs and Kear, 1993, 1994). Although decay is not the only factor influencing the preservation of a non-biomineralized tissue, its impact on preservation potential is critical and requires further study (Sansom et al., 2011, 2013; Murdock et al., 2014; Briggs and MacMahon, 2016). The decay of non-biomineralized tissues is typically investigated under experimentally controlled conditions with the level of resolution rarely progressing further than that of whole organs. Often these are simply viewed at limited magnification either with the naked eye or the use of binocular microscopes. The changes in the appearance of an anatomical feature from fresh to decayed tissue can then be assessed. This approach improves our ability to predict what non-biomineralized tissues are more or less likely to be preserved in the fossil record, it also helps to identify fossilized non-biomineralized tissues by comparison with decayed modern analogues (Sansom et al., 2013; Briggs and MacMahon, 2016).

The decay process, of course, does not affect all tissues equally; certain tissues are more recalcitrant than others, loss of fidelity does not occur at an equal rate for all tissue categories equally (chapter 4). For instance, muscle

tissue can retain its cohesion and structure for several weeks before breaking down into a paste (Briggs and Kear, 1993, 1994). Whereas collagen fibres are more recalcitrant and though fragmented maintain their shape throughout the decay process (chapter 3; section 3.1). Decay is variable within and between different categories of tissue, and the appearance of non-biomineralized tissues post decay can vary over short distances within the same individual (chapter 4; section 3.1–3.5). Therefore when investigating the decay process in some cases it is appropriate to record decay related changes to soft tissue with ultrastructural resolution.

Accurate records of the effects of decay on the anatomy of non-biomineralized tissues at the level of tissue ultrastructure require: (1) high-resolution images capable of visualizing structural details such as cell walls or collagen fibres at a μm to nm scale; (2) record information on the interior and exterior morphology of decayed tissue with minimal or no damage; (3) visualize tissue structure in three dimensions (3D), by inferring it from either multiple images of two-dimensional (2D) slices with different orientations or by scanning the complete volume of a sample; (4) produce images in which different structures can be recognised post-decay (Table 5.1). Traditionally SEM has been used to image decayed tissues at high resolutions (Briggs and Kear, 1993, 1994), whereas standard light microscopy remains underutilised. Micro-CT has previously been used by others to image the results of experimental decay (Schwermann et al., 2012; Meyer et al., 2014), however, the opportunities it presents to distinguish the response to decay of different tissues from one another is only beginning to be explored.

The aim of this paper is to demonstrate the usefulness of micro-CT as a tool for investigating the decay of non-biomineralized tissues at the ultrastructural level.

2. Methods

Samples of bird skin and skeletal muscle at different stages of decay are ideal candidate tissues for this study: (1) skin is composed of several tissue components with distinct chemistries and densities, including keratin fibres, collagen fibres, cell membranes and muscle fibres (Stettenheim, 2000, chapter 3; Fig. 4.1); and (2) these tissues are closely juxtaposed at a cellular level, in order to facilitate the growth, maintenance and manipulation of feathers (Homberger and DeSilva, 2000).

Samples of bird skin and muscle were retrieved from the pectoral region of ten zebra finches (*Taeniopygia guttata*) fresh and after one, two and four weeks of decay using the methods in Chapter 3 (section 2.1–2.2). Certain samples were imaged using a Nikon Eclipse LV100D-U stereomicroscope equipped with a photographic camera. Other samples were imaged using a Hitachi S3500N variable-pressure scanning electron microscope (SEM). These are the same samples as those analysed in chapter 4, details on preparation of tissues for light and electron microscopy can be found in chapter 4; section 2.2.

Samples of skin and muscle were also retrieved from the pectoral region of three additional zebra finches. Tissues from one of these were dissected and fixed immediately after death; the other two zebra finches were decayed for two and four weeks using the experimental setup described in Chapter 3 section 2.1–2.2. These additional tissue samples were fixed in 10% neutral buffered

formalin for 24 hours and then dehydrated using an ethanol series (30, 50, 70, 90 and 100%) according to standard histological technique (Bancroft and Gamble, 2002).

Tissues to be imaged through Micro-CT were prepared using different methods to those used to prepare tissues for SEM. Once prepared, small samples approximately 5mm in height and 1mm in width were tissues were critically point dried using carbon dioxide. Samples of critically point dried skin and muscle from each decay stage were fixed to brass stubs using nail varnish and imaged using synchrotron-based Micro-CT at the TOMCAT beam line of the Swiss Light Source, Paul-Scherrer Institut, Villigen, Switzerland. Images were taken using the 4 X objective, exposure times of 170–850 ms and energies of 10 Ke V. Approximately 2000 projections were produced for each sample. CT files were imported into Avizo 8.0 (Visualisation Sciences Group). 3D volume renderings were produced. Smaller volumes of adipose tissue ($160\mu m^3$), were manually segmented out to produce surface models of adipose tissue.

3. Results and discussion

3.1 Scanning Electron microscopy (SEM)

Scanning electron microscopy clearly revealed the impact of decay in specific surface features of bird skin and muscle. In particular, changes to the condition of individual cells in the epidermis (keratinocytes) (Fig. 5.1A, B), feather rachis, the arrangement of collagen fibres in the dermis and the diameter of muscle could be reliably recorded over time at all stages of decay (Fig. 5.1C). The 3D structure of tissues could be viewed only if they had become exposed on two sides or more. It was difficult to assess the effects of decay of the feather

follicle and muscles that support the feather in vivo (Fig. 5.1D). SEM images fail to resolve certain layers in the skin; in particular the germinative basal layer of the epidermis; more generally SEM was unable to single out collagenous layers of the dermis. It was not possible to identify subcellular details e.g. nuclei in this study; such structures have, however, been imaged previously using SEM by fracturing the sample using resin (Allen et al., 2007). SEM produces images of decayed tissues with an excellent level of resolution but integrating these images into a 3D framework was difficult.

The study of tissue decay at the ultra-structural level has been investigated traditionally using SEM (Briggs and Kear, 1993, 1994). This technique can produce high-resolution images of decayed non-biomineralized tissues in multiple orientations with minimal damage to the tissue (Fig. 5.1A–D). Additionally, depending on the study, electron microscopy can reveal visual evidence of mineralization, an important aspect of preservation (Briggs et al., 1993). Despite this versatility as concluded herein, others have indicated that, electron microscopy is a surface analysis technique (Betz et al., 2007). The interior of an object can be imaged only where exposed through dissection, which risks introducing artefacts. Alternatively, focused ion beam milling can be used to expose sub-surface features. The use of an ion beam to expose internal anatomy of a sample is a destructive technique and does not provide 3D images or volumetric information on the progress of decay (Zehbe et al., 2010). Despite these limitations, electron microscopy remains invaluable in that it allows rapid assessment of decay-related changes to tissue ultrastructure.

3.2 Histology

Analysis of histological sections using light microscopy revealed the progressive decay of the internal details of the same tissues in 2D with relatively high resolution. Individual tissue layers in the epidermis, e.g. the stratum corneum and stratum germinativum, and cellular details such as nuclei could be distinguished. Comparatively, individual layers in the dermis e.g. stratum superficiale and stratum compactum could not be distinguished, although individual collagen fibres in these layers could be traced along their length. The use of Fontana Masson stain improved the definition of certain tissue components such as melanin-pigmented barbules in developing feathers and keratin in fully developed feathers (Fig. 5.2A); these were easily distinguished from other tissues such as collagen and muscle by colour and noticeably reduced uptake of the stain respectively. Individual muscle fibres were harder to identify in extensively decayed tissue, but the separation of muscle fibres from one another could be easily interpreted (Fig. 5.2B–D). The 3D structure of these tissues can be inferred from the 2D sections, although this is more difficult in decayed tissues.

Standard histological techniques have conventionally been used to investigate the external and internal structure of tissues (Bancroft and Gamble, 2002), albeit at a lower resolution than SEM. Super resolution light microscopy, however, allows decayed tissues to be imaged at similar resolutions to those routinely used by electron microscopes (Huang, 2010). The primary advantage of conventional histology is that stains can be used to highlight specific tissues (Fig. 5.2A). The ability of histological stains to bind to certain tissues is altered by decay, and this has potential as an indirect guide as to the state of decay of the

tissues (Liu et al., 1994) (Fig. 5.2B, C). Staining usually improves the ease of identification of tissues in different decay stages once their structure has become altered. In sum, conventional histology fulfils all four conditions for optimum imaging of the effects of decay in non-biomineralized tissues.

However, observation of the structure of decayed tissues using histology has three disadvantages. (1) the production of histological thin sections is destructive; this prevents imaging of the same tissue sample of tissue in different orientations. Decay-related changes to the 3D tissue structure must be inferred by analysing multiple samples (Betz et al., 2007); (2) as discussed in chapter 3 - the decay process in non-biomineralized tissues is variable over short distances within the same animal (e.g. 100 μm), successive sections of tissue cannot be produced at sufficiently fine increments that variations in decay over small distances can be captured which makes inferring the 3D structure from a limited number of 2D slices problematic; and, (3) decayed tissues are less stable than fresh tissues, and are more likely to be damaged during preparation. Decay can alter the response of individual tissues to sectioning (Mohammed et al., 2012), so a range of sections produced through different methods may be required to understand the decay process in all tissue types.

3.3 Micro-computed tomography

The decay process in all tissue types could be resolved at relatively high resolution using micro-CT. Specifically, the decay-related changes to skin structure (Fig. 5.3), muscle fibres (Fig. 5.4) and adipocyte cell membranes (Fig. 5.5), were all easy to identify in 3D. However, it was difficult to distinguish

between different tissue types, e.g. collagen and muscle, using micro-CT datasets. For instance, individual cells in the outer and basal layers of the epidermis could not be identified even in fresh tissue, and instead appeared as a single layer in the data (Fig. 5.3) This was likely the result of insufficient density contrast.

The collagen layers in the dermis could not be traced along their length due to abrupt changes in orientation between individual slices. The orientation of adipocyte cell membranes was less variable between slices; therefore 3D models of adipose tissue could be produced. Their production required adipocyte cell membranes to be highlighted manually in each of 100 slices (Fig. 5.5). Pragmatically this meant models could only be produced on a smaller scale than the volume renderings ($\sim$160 μm^3).

Application of micro-CT, to resolve questions in palaeontology using both synchrotron and smaller lab-based x-ray sources has increased dramatically over the last decade (Donoghue et al., 2006; Sanchez et al., 2013; Keating et al., 2015). Previous studies have used micro-CT to investigate the taphonomy of biomineralized tissues, (Schwermann et al., 2012; Meyer et al., 2014) and to observe the expansion of putrefaction gas within the circulatory and digestive systems of moles (Mähler et al., 2015).

The resolution of micro-CT is similar to that of light and electron microscopy, but has other advantages. The primary advantage is that larger objects and entire organisms are imaged non-destructively, in some cases using lab-based x-ray sources it may be possible for the same tissue to be imaged multiple times in different stages of decay (Schwermann et al., 2012). However, micro-CT using lab-based x-ray sources use a polychromatic x-ray source, which increases the number of artefacts in the data relative to synchrotron x-ray

sources (Meganck et al., 2009). Further, in order to image non-biomineralized tissues using lab-based sources, the tissue must be infiltrated with a contrast stain, requiring the cessation of decay and destructive sampling (Pauwels et al., 2012). If destructive sampling is unavoidable, it is prudent to use monochromatic synchrotron x-ray sources when scanning small amounts of tissue, as they produce higher resolution images with fewer artefacts, and do not require contrast stains to be applied to image tissue ultrastructure (Holdsworth and Thornton, 2002; Betz et al., 2007). Synchrotron-based micro-CT scans are therefore an ideal method for investigating decay-related structural changes at the tissue and cellular level.

The obvious advantage of 3D CT scanning over histological thin sections is that it allows the same sample of tissue to be repeatedly sectioned in multiple orientations, allowing investigation of the complete volume of tissue, without requiring the internal structure of a sample to be exposed (Zehbe et al., 2010). This is critical to identification of representative tissue features: as discussed in Chapter 3, the level of decay in non-biomineralized tissues can vary over small distances. Further, the data produced via this method can be used to create 3D volume renderings that can be viewed in any plane to produce virtual thin sections so that the total volume may be investigated (Keating et al., 2015) (Figs. 5.3, 5.4).

3D digital models, of tissues or structures of particular interest, can be produced via segmentation of the dataset (Fig. 5.5). Segmentation involves manually highlighting a structure of interest in series of CT-slices; the volume of that structure is then interpolated between the slices in which it has been highlighted to produce a 3D model (Fig. 5.5). This process is not normally time-

consuming: it is possible to interpolate the margin / boundary of a structure by manually highlighting it in a small number of non-adjacent regions. However, as noted above the morphology of non-biomineralized tissues is complex such as the skin changes over a few μm. To provide enough information to accurately interpolate such a complicated structure, it must be highlighted in a series of adjacent slices, therefore segmentation becomes more time consuming. Clearly being able to highlight a particular type of tissue in multiple sections has applications for quantifying how specific structure or a certain tissue changes through the decay process.

Problematically, the main tissue components in bird skin – keratin fibres, collagen fibres, adipocytes and muscle fibres – are difficult to distinguish from one another based on their x-ray attenuation properties. Contrast-enhancing stains such as iodine (Lautenschlager et al., 2014) and osmium tetroxide (Betz et al., 2007) have been used to improve the contrast of non-biomineralized tissues in the past, but these are not tissue-specific (Metscher, 2009). The best approach to observing decay of non biomineralized tissues is to use histological sectioning and micro-CT in tandem, the former to understand the general arrangement, layering and appearance of a fresh or decayed non-biomineralized tissue and the latter to interpret the decayed tissue in 3D (Liu et al., 1994) (Fig. 5.2C).

3.4 Future applications of micro-CT

One area of taphonomy that would benefit greatly from the synchrotron-based micro-CT analysis is the study of the mineralization process in non-biomineralized tissues. Cellular details of non-biomineralized tissues are

commonly replicated in calcium phosphate (Briggs et al., 1993). The replication of tissues in calcium phosphate has been successfully induced in laboratory settings, but analysis of the products of such experiments have hitherto revealed little of the distribution of mineral precipitation through the 3D structure of non-biomineralized tissues (Briggs et al., 1993; Briggs and Kear, 1994). As micro-CT scans distinguish materials based upon their x-ray attenuation, it is theoretically possible to reveal the extent to which authigenic minerals replicate non-biomineralized tissues in 3D. For mineralization to occur some decay is necessary (Briggs, 2003). CT datasets may allow quantitative assessment of the extent and rate of tissue mineralisation and the extent of decay, allowing for more detailed interpretations of the relationship between decay and mineralisation in different tissue components (Jakob Vinther pers. comm. 2016).

4. Conclusion

Methods to be considered ideal for capturing the decay process in non-biomineralized tissues should show four properties. They should produce high-resolution images, image interior and exterior detail, image tissue in 3D and be able to track specific tissues through the decay process. None of the methods discussed here is ideally suited to all of these tasks, though all are capable of at least two. Though it does not fulfil all the requirements noted above, micro-CT is the best method available for studying the decay of non-biomineralized tissues because of the versatility of 3D datasets. Whereas rapid sample preparation, availability, and scanning times make SEM useful for initial or preliminary observations of tissue decay, micro-CT is the superior method as it allows investigation of the complete volume of a sample and facilitates quantitative

measurements of decay. Micro-CT scans also have some advantages over light microscopy, such as reduced sample preparation time and no need for manual interpretation of 3D structure. However, it is difficult to interpret Micro-CT images of decayed tissue without using histological sections of the same decayed tissue as a reference. Depending on the hypothesis being tested, we advise using all three methods in a holistic approach to capture the process of decay in complex non-biomineralized tissues. The opportunities for studying decay and preservation of non-biomineralized tissues in a palaeontological context using micro-CT have only just begun to be explored. It is hoped that as methods continue to develop and access to synchrotron facilities such as the Swiss Light Source becomes more widespread a renaissance in our ability to interpret the decay process in non-biomineralized tissues and their preservation in the fossil record will occur.

Acknowledgements

We thank Phil Donoghue for imaging samples at the Swiss Light Source,

Paul-Scherrer Institut, and John Cunningham and Joe Keating for help in

producing images using Avizo for this chapter.

CONCLUSIONS

The aims of this project were to improve our understanding of the taphonomic processes affecting the accumulation and preservation of birds and dinosaurs of the Early Cretaceous Jehol Biota Lagerstätte of NE China. Consequently, the results of this thesis are varied, with each chapter focussing upon a different topic or method of taphonomic research in relation to the taphonomy of birds and dinosaurs in the Jehol Biota.

Key Findings

Investigation of the deposits near to Lujiatun village reveals dinosaurs were buried in pyroclastic material that was remobilised into unchannelised sheet floods (chapter 2). The implication is that regional volcanic activity at the time was not directly responsible for the death and accumulation of all terrestrial vertebrates throughout the entire Jehol Group. Further, the distinct lithological differences between the fossiliferous beds of the Lujiatun Unit and the matrix of *Psittacosaurus* specimens reveals there were at least two, possibly three different types of burial events of dinosaurs and other components of the Jehol Biota in the Lujiatun Unit. Therefore the death and burial of animals in the Lujiatun Unit was not instantaneous and occurred over a longer period of time than has been previously been acknowledged.

Jiang *et al.* (2014) hypothesise the main cause of death transport and burial of the terrestrial component of the Jehol Biota was a series of pyroclastic density currents. However, patterns of skeletal articulation and completeness of key vertebrates *Confuciusornis* and microraptorines demonstrate no evidence of transport in a pyroclastic current or any other turbulent flow (chapter 3). Instead, their skeletal taphonomy reveals they underwent a rather unexceptional transport and burial process, with minimal floatation periods, the majority of disarticulation occurring at the bottom of the lake. In tandem with chapter 2, this evidence emphasises that regional volcanism cannot be invoked as the figurative 'smoking gun' for the death, transport and burial of all terrestrial components of the Jehol Biota. Rather the taphonomy of birds and dinosaurs of Jehol Biota is more complex and is not the result of a single factor in the present in the environment at the time.

In addition, the relationships between articulation and completeness of *Confuciusornis* and microraptorines indicate that the body plan and differences in the ecology of these two taxa does not affect the loss of completeness and articulation over the whole skeleton, but that the skeletal taphonomy of certain parts of the body may be impacted by functional anatomy.

I present the first predictive model for preservation of the skin in the fossil record; indicating what tissue components will be available for preservation at different stages of decay. The response of the skin to decay differs between birds and squamates, and this can be linked to the difference in relative decay resistance of its constituent tissues (Chapter 4). Generally, the

taphonomy of the skin of birds, squamates and by extrapolation all vertebrates is variable within and between different categories of tissue. Further, the decay and degradation of skin can vary over a short distance within one individual. During decay, the epidermis in bird skin is prone to fracture and fragment. Some fragments of epidermis once detached become entrapped within the feathers of the animal. Collagen is responsible for maintainance of skin cohesion post-mortem, particularly collagen in the uppermost portion of the dermis. Early in the decay process collagen fibres in the dermis of the pterylae and apterylae lose cohesiveness; this noticeably increases the thickness of the dermis of birds compared to that of geckos; which shows a smaller thickness increase relative to its condition whilst fresh. We hypothesise that this predisposition for fragmentation of the epidermis in combination with separation of collagen fibres in the dermis reduces the chances of large contiguous sheets of bird skin entering the fossil record and may explain why fossils of reptile skin, that does not share these attributes are more commonly identified.

The variability of the extent of decay within a single tissue category highlights the need for the complete volume of decaying tissues to be imaged in high resolution. The potential for micro-CT to image decayed non-biomineralized tissues is discussed here for the first time. While scanning electron microscopy and optical microscopy both possess analytical features that micro-CT does not, we reveal that using micro-CT in conjunction with the other two methods improved the overall ability to resolve decay related changes to non-biomineralized tissues in three dimensions.

Adachi, E., Hayashi, T., 1986. In vitro formation of hybrid fibrils of type v collagen and type 1 collagen limited growth of type 1 collagen into thick fibrils by type v collagen. Connective Tissue Research 14, 257–266.

Albardi, L., 2003. Adaptation to the land: The skin of reptiles in comparison to that of amphibians and endotherm amniotes. Journal of Experimental Zoology 298, 12–41.

Alexander, D.E., Gong, E., Martin, L.D., Burnham, D.A., Falk, A.R., 2009. Model tests of gliding with different hindwing configurations in the four-winged dromaeosaurid *Microraptor gui*. Proceedings of the National Academy of Sciences, USA 107, 2972–2976.

Allison, P.A., 1986. Soft-bodied animals in the fossil record: The role of decay in fragmentation during transport. Geology 14, 979–981.

Allison, P.A., 1988. The role of anoxia in the decay and mineralization of proteinaceous macro- fossils. Paleobiology 14, 139–154.

Amiot, R., Wang, X., Zhou, Z., Wang, W., Lécuyer, C., Buffetaut, E., Fluteau, F., Ding, Z., Kusuhashi, N., Mo, J., Philippe, M., Suteethorn, V., Wang, Y., Xu, X., 2015. Environment and ecology of East Asian dinosaurs during the Early Cretaceous inferred from stable oxygen and carbon isotopes in apatite. Journal of Asian Earth Sciences 98, 358–370.

Ando, M., Toyohara H., Sakaguchi, M., 1992. Post-mortem tenderization of rainbow trout muscle caused by the disintegration of collagen fibers in the pericellular connective tissue. Nippon Suisan Galkkaishi 58, 567–570.

Antoine, P.-O., Orliac, M.J., Atici, G., Ulusoy, I., Sen, E., Cubukcu, H.E., Albayrak, E., Oyal, N., Aydar, E., Sen, S., 2012. A rhinocerotid skull cooked-to-death in a 9.2 Ma-old ignimbrite flow of Turkey. PLoS One 7, e49997.

Asara, J.M., Schweitzer, M.H., Freimark, L.M., Phillips, M., Cantley, L.C., 2007. Protein sequences from Mastodon and *Tyrannosaurus rex* revealed by mass spectrometry. Science 316, 280–285.

Bancroft, J.D., Gamble, M., 2002. Theory and practice of histopathological techniques, fifth ed. Churchill Livingstone, New York.

Bandyopadhyay, S., RoyChowdhury, T.K., Sengupta, D.P., 2002.Taphonomy of some Gondwana vertebrate assemblages of India. Sedimentary Geology 147, 219–245.

Baxter, P.J., 1990. Medical effects of volcanic eruptions. Bulletin of Volcanology 52, 532–544.

Beardmore, S.R., Orr, P.J., Manzocchi, T., 2012a. Float or sink: modelling the taphonomic pathway of marine crocodiles (Mesoeucrocodylia, Thalattosuchia) during the death–burial interval. Palaeobiodiversity and Palaeoenvironments 92, 83–98.

Beardmore, S.R., Orr, P.J., Manzocchi, T., Furrer, H., Johnson, C., 2012b. Death decay and disarticulation: Modelling the skeletal taphonomy of marine reptiles demonstrated using *Serpianosaurus* (Reptilia; Sauropterygia). Palaeogeography, Palaeoclimatology, Palaeoecology 337–338, 1–13.

Behrensmeyer, A.K., Kidwell,S.M., Gastaldo, R.A., 2000. Taphonomy and palaeobiology. Paleobiology 26, 103–147.

Bellairs, A., 1969. The skin In: *The life of reptiles. Vol. 2.* Widenfeld and Nicholson, London. 283p.

Benjimini, Y., Hochberg, Y., 1995. Controlling the false discovery rate: a practical and powerful approach to multiple testing. Journal of the Royal Statistical Society. Series B 57, 289–300.

Benecke, M., 2001. A brief history of forensic entomology. Forensic Science International 120, 2–14.

Bertazzo, S., Maidment, S.C.R., Kallepitis, C., Fearn, S., Stevens, M., Xie, H.-N., 2015. Fibres and cellular structures preserved in 75-million–year-old dinosaur specimens. Nature Communications 6, 7352.

Benton, M.J., 2008. How to find a dinosaur, and the role of synonymy in biodiversity studies. Paleobiology 34, 516–533.

Benton, M.J., Zhou, Z., Orr, P.J., Zhang, F., Kearns, S.L., 2008. The remarkable fossils from the Early Cretaceous Jehol Biota of China and how they have changed our knowledge of Mesozoic life. Proceedings of the Geologists' Association 119, 209–228.

Bertazzo, S., Maidment, S.C.R., Kallepitis, C., Fearn, S., Stevens, M., Xie, H.-N., 2015. Fibres and cellular structures preserved in 75-million–year-old dinosaur specimens. Nature Communications 6, 7352.

Betz, O., Wegst, U., Weide, D., Heethoff, M., Helfen, L., Lee, W.-K., Cloetens, P., 2007. Imaging applications of synchrotron X-ray phase-contrast microtomography in biological morphology and biomaterials science. I. General aspects of the technique and its advantages in the analysis of millimetre-sized arthropod structure. Journal of Microscopy 227, 51–71.

Bickart, K.J., 1984. A field experiment in avian taphonomy. Journal of vertebrate palaeontology 4, 525–535.

Blair, T.C., McPherson, J.G., 1999. Grain-size and textural classification of coarse sedimentary particles. Journal of Sedimentary Research 69, 6–19.

Brand, L.R., Hussey, M., Taylor, J., 2003. Decay and disarticulation of small vertebrates in controlled experiments. Journal of Taphonomy 1, 69–95.

Branny, M.J., Sparks, R.S.J., 1990. Fiammé formed by diagenesis and burial-
compaction in soils and subaqueous sediments. Journal of the Geological Society
147, 919–922.

Brantly, S.R., Waitt, R.B., 1988. Interrelations among pyroclastic surge, pyroclastic
flow and lahars in Smith Creek valley during first minutes of 18 May 1980
eruption of Mount St. Helens, USA. Bulletin of Volcanology 50, 304–326.

Brenchley, P.J., Newell, G., 1970. Flume experiments on the orientation and transport of
models and shell valves. Palaeogeography, Palaeoclimatology, Palaeoecology 7, 185–
220.

Briggs, D.E.G., 1995. Experimental taphonomy. Palaios 10, 539–550.

Briggs, D.E.G., 2003. The role of decay and mineralization in the preservation of soft-
bodied fossils. Annual review of Earth and Planetary Sciences 31, 275–301.

Briggs, D.E.G., Kear, A.J., 1993a. Decay and preservation of polychaetes: taphonomic
thresholds in soft-bodied organisms. Paleobiology 19, 107–135.

Briggs, D.E.G., Kear, A.J., 1993b. Fossilisation of soft tissue in the laboratory. Science
259, 1439–1442.

Briggs, D.E.G., Kear, A.J., 1994. Decay of *Branchiostoma*: implications for soft-tissue
preservation in conodonts and other primitive chordates. Lethaia 26, 275–287.

Briggs, D.E.G., Kear, A.J., Martill, D.M., Wilby, P.R., 1993. Phosphatization of soft-
tissue in experiments and fossils. Journal of the Geological Society, London 150,
1035–1038.

Briggs, D.E.G., McMahon, S., 2016. The role of experiments in investigating the
taphonomy of exceptional preservation. Palaeontology 59, 1–11.

Briggs, D.E.G., Williams, S.H., 1981. The restoration of flattened fossils. Lethaia 14,
157–164.

Brocklehurst, N., Upchurch, P., Mannion, P.D., O'Connor, J., 2012. The completeness of the fossil record of Mesozoic Birds: Implications for Early Avian Evolution. PLoS ONE 7, e39056.

Buhr, R. J., Cason, J.A., Rowland, G.N., 1996. Feather retention force in broilers ante-, peri-, and post-mortem influenced by carcasss orientation, angle of extraction and slaughter method. Poultry Science 76, 1591–1601.

Casal, G.A., Martínez, R.D., Ibiricu, L.M., González, R., Foix, N., 2013. Taphonomy of the threopod dinosaur *Aniksosaurus darwini*, Bajo Barreal Formation, Late Cretaceous of Patagonia (Argentina). Ameghiniana 50, 571–592.

Castruccio, A., Clavero, J., Rivera, A., 2010. Comparative study of lahars generated by the 1961 and 1971 eruptions of Calbuco and Vilarrica volcanoes, Southern Andes of Chile. Journal of Volcanology and Geothermal Research 3–4, 297–311.

Chang, M.C., Tanaka, J. 2002. FT-IR study for hydroxyapatite/collagen nano compesite cross-linked by gluteraldehyde. Biomaterials 23, 4811–4818.

Chen, W.-M., Lee, T., Lee, P.V.-S., Lee, J.W., Lee, S.-J., 2010. Effects of internal stress concentrations in plantar soft-tissue –A preliminary three-dimensional finite element analysis. Medical Engineering and Physics 32, 324–331.

Chen, P.-J., Li, J., Matsukawa, M., Zhang, H., Wang, Q., Lockley, M.G. 2006. Geological ages of dinosaur-track-bearing formations in China. Cretaceous Research 27, 22–32.

Chiappe, L.M., Marugán-Lobón, J., Shu'an, J., Zhou, Z., 2008. Life history of a basal bird: morphometrics of the Early Cretaceous *Confuciusornis*. Biology Letters 4, 719–723.

Chinsamy, A., Chiappe, L.M., Marugán-Lobón, J., Gao, C., Zhang, F., 2012. Gender identification of the Mesozoic bird *Confuciusornis sanctus*. Nature Communications 4, 1381.

Clements, T., Dolocan, A., Martin, P., Purnell, M.A., Vinther, J. Gabbot, S.E., 2016. The eyes of Tullimonstrum reveal a vertebrate affinity. Nature 532, 500–503.

Coria, R.A., Chiappe, L.M. 2007. Embryonic skin from Late Cretaceous Sauropods (Dinosauria) of Auca Mahuevo, Argentina. Journal of Paleontology 81, 1528–1532.

Colleary, C., Dolocan, A., Gardner, J., Singh, S., Wuttke, M., Rabenstein, R., Habersetzer, J., Schaal, S., Feseha, M., Clemens, M., Jacobs, B.F., Currano, E.D., Jacobs, L.L., Sylvestersen, R.L., Gabbot, S.E.,Vinther, J., 2015. Chemical, experimental, and morphological evidence for diagenetically altered melanin in exceptionally preserved fossils. PNAS 112, 12592–12597.

Craik, J.E., McNeil, I.R.R., 1964. 14. Histological studies of stressed skin. In: Kenedi, R.M. (Ed.) *Biomechanics and related bioengineering topics: Proceedings of a symposium held in Glasgow*. Oxford, Pergamon Press.

Darwin, C., 1859. *On the Origin of Species by Means of Natural Selection or the Preservation of Favoured Races in the Struggle for Life* (John Murray, London, 1859).

Davis, P.G., 1994. The taphonomy of birds. Unpublished PhD thesis, University of Bristol.

Davis, P.G., Briggs, D.E.G., 1998. The impact of decay and disarticulation on the preservation of fossil birds. Palaios 13, 3–13.

Ding, Q., Tian, N., Wang, Y., Jiang, Z., Chen, S., Dong, W., Zhang, W., Zheng, S., Xie, A., Zhang, G., Liu, Z., 2016. Fossil coniferous wood from the Early Cretaceous Jehol Biota in western Liaoning, NE China: New material and palaeoclimate implications. Cretaceous Research 61, 57–70.

Dhouailly, D., 2004. A new scenario for the evolutionary origin of hair, feather, and avian scales. Journal of Anatomy 214, 587–606.

Dodson, P., Behrensmeyer, A.K., Bakker, R.T., Smith, J., 1980. Taphonomy and paleoecology of the dinosaur beds of the Jurassic Morrison Formation. Paleobiology 6, 208–232.

Dong, L., Rocek, Z. Wang, Y., Jones, M.E.H., 2013. Anurans from the Lower Cretaceous Jehol Group of western Liaoning, China. PLoS ONE 8, e69723.

Donoghue, P.C.J., Bengston, S., Dong, Xi-.P., Gostling, N.J., Huldtgren, T., Cunningham, J.A., Yin, C., Yue, Z., Peng, F., Stampanoni, M., 2006. Synchrotron X-ray tomographic microscopy of fossil embryos. Nature 442, 680–683.

Dornbos, S.Q., 2010. Phosphatization through the Phanerozoic. In: (eds Allison, P.A., and Bottjer, D.J.) *Taphonomy, Second Edition: Process and Bias Through Time. Topics in Geobiology*Springer, New York, 435–456.

Du, L., 2004. Scientists warn of threats to fossil-rich Chinese site. Science 305, 172–173.

Dufek, J., 2016. The fluid mechanics of pyroclastic density currents. The Annual Review of Fluid Mechanics 48, 495–485.

Dyke, G., de Kat, R., Palmer, C., van der Kindere, J., Naish, D., Ganapathisubramani, B., 2013. Aerodynamic performance of the feathered dinosaur *Microraptor* and the evolution of feathered flight. Nature Communications 4, 2489.

Edwards, N.P. Barden, H.E., van Dongen, B.E., Manning, P.L. Larson, P.L. Bergman, U. Sellers, W.I., Wogelius, R.A., 2011. Infared mapping resolves soft tissue preservation in 50 million year-old reptile skin. Proceedings of the Royal Society B 278, 3209–3218.

Efremov,I.A. 1940. Taphonomy: a new branch of paleontology. Pan-American Geologist 74, 81–93.

Erickson, G.M., Mackovicy, P.J., Inouye,B.D., Zhou, C.-F., Gao, K.-Q. 2009. A life table for *Psittacosaurus lujiatunensis*: Initial insights into ornithischian dinosaur population biology. The Anatomical Record 292, 1514–1521.

Evans, S.E., Wang, Y. 2007. A juvenile lizard specimen with well-preserved skin impressions from the Upper Jurassic/Lower Cretaceous of Daohugou, Inner Mongolia, China. Naturwissenschaften 94, 431–439.

Evans, S.E., Wang, Y., Jones, M.E.H. 2007. An aggregation of lizard skeletons from the Lower Cretaceous of China. Senckenbergiana lethaea 87, 109–118.

Faux, C.M., Padian, K., 2007. The opisthotonic posture of vertebrate skeletons: post-mortem contraction or death throes? Paleobiology 33, 201–226.

Fiedler, S., Graw. M., 2003. Decomposition of buried corpses, with special reference to the formation of adipocere. Naturwissenschaften 90, 291–300.

Fisher, R.V., Schmincke, H.-U., 1984. Pyroclastic Rocks. Springer-Verlag, Berlin.

Foster, J.R., Hunt-Foster, R.K., 2011. New occurrences of dinosaur skin of two types (Sauropoda? and Dinosauria indet.) from the Late Jurassic of North America (Mygatt-Moore Quarry, Morrison Formation). Journal of Vertebrate Paleontology 31, 717–721.

Freutel, M., Schmidt, H., Dürseken, L., Ignatius, A., Galbusera, F., 2014. Finite element modelling of soft tissues: Material models, tissue interaction and challenges. Clinical Biomechanics 29, 363–372.

Fürsich, F.T., Sha, J., Jiang, B., Pan, Y., 2007. High resolution palaeoecological and taphonomic analaysis of Early Cretaceous lake biota, western Liaoning (NE-China). Palaeogeography, Palaeoclimatology, Palaeoecology 253, 434–457.

Gaines, R.R., Hammarlund, E.U., Hou, X., Qi, C., Gabbott, S.E., Zhao, Y., Peng, J., Canfield, D.E. 2012. Mechanism for Burgess Shale-type preservation. PNAS 109, 5180–5184.

Gao, C., Morschhauser, E.M., Varricchio, D.J., Liu, J. and Zhao, B., 2012. A second soundly sleeping dragon: new anatomical details of the Chinese troodontid *Mei long* with implications for phylogeny and taphonomy. PLoS ONE 7, (e) 45203.

Gatesy, S.M., Dial, K.P., 1996. Locomotor modules and the evolution of avian flight. Evolution 50, 331–340.

Gernon, T.M., Field, M., Sparks, R.S.J., 2009. Depositional processes in a kimberlite crater: the Upper Cretaceous Orapa South Pipe (Botswana). Sedimentology 56, 623–643.

Gill-King, H., 1997. Chemical and ultrastructural aspects of decomposition. In: Hayland, W.D. and Sorg, M., (eds.) *Forensic taphonomy: the post-mortem fate of human remains.* Boca Raton: CDC Press, 93-103.

Godefroit, P., Sinista, S.M. Dhouailly, D., Bolotsky, Y.L., Sizov, A.V., McNamara, M.E., Benton, M.J., Spagna, P., 2014. A Jurassic ornithischian dinosaur from Siberia with both feathers and scales. Science 345, 451–455.

Goff, M.L., 2009. Early post-mortem changes and stages of decomposition in exposed cadavers. Experimental and Applied Acarology 49, 21–36.

Gong, E.-P., Martin, L.D., Burnham, D.A., Falk, A.R., Hou, L.-H., 2012. A new species of *Microraptor* from the Jehol Biota of northeastern China. Palaeoworld 21, 81–91

Grimes, S.T., Brock, F., Rickard, D., Davies, K.L., Edwards, D., Briggs, D.E.G., Parkes, R.J. 2000. Understanding fossilization: experimental pyritization of plants. Geology 29, 123–126.

Groenewald, G.H., Welman, J., MacEachern, J.A., 2001. Vertebrate burrow complexes from the Early Triassic *Cynognathus* Zone (Driekoppen Formation, Beaufort Group) of the Karoo Basin, South Africa. Palaios 16, 148–160.

Guo, Z., Liu, J., Wang, X., 2003. Effect of Mesozoic volcanic eruptions in the western Liaoning Province, China on paleoclimate and paleoenvironment. Science in China, Series D 46, 1261–1272.

Hallsworth, C.R., Knox, R.W.O.B., 1999. BGS rock classification scheme. Volume 3. Classification of sediments and sedimentary rocks. British Geological Survey Research Report, RR 99–03.

Hammer, Ø., Harper, D.A.T., Ryan, P.D., 2001. PAST: Paleontological statistics software package for education and data analysis. Palaeotologica Electronica 4, 9pp.

Han, G., Chiappe, L.M., Ji, S.-A., Habib, M., Turner, A.H., Chinsamy, A., Liu, X.,Han, L., 2014. A new raptorial dinosaur with exceptionally long feathering provides insight into dromaeosaurid flight performance. Nature Communications 5, 4382.

Hansell, A., Oppenheimer, C., 2004. Health hazards from volcanic gasses: a systematic literature review. Archives of environmental health. 59, 628–639.

He, H.Y., Wang, X.L., Zhou, Z.H., Jin, F., Wang, F., Yang, L.K., Ding, X., Boven, A., Zhu, R.X., 2006. 40Ar/39Ar dating of Lujiatun Bed (Jehol Group) in Liaoning, northeastern China. Geophysical Research Letters. 33, L04303.

Heiken, G., 1974. An atlas of volcanic ash. Smithsonian Contributions to the Earth Sciences. 12, 1–101.

Hedrick, B.P., Gao, C., Omar, G.I., Fengjiao, S.C., Dodson, P., 2014. The osteology and taphonomy of a *Psittacosaurus* bonebed assemblage of the Yixian Formation (Lower Cretaceous), Liaoning, China. Cretaceous Research 51, 321–340.

Hethke, M., Fürsich, F.T., Jiang, B., Klaus, R., 2013. Oxygen deficiency in Lake Sihetun; formation of the Lower Cretaceous Liaoning Fossillagerstätte (China). Journal of the Geological Society 170, 817–831.

Hof, C.H.J., Briggs, D.E.G., 2008. Decay and mineralization of mantis shrimps (Stomatopods; Crustacea); a key to their fossil record. Palaios 12, 420–438.

Hogg, S.E.,1982. Sheet floods, sheetwash, sheetflow, or...? Earth-Science Reviews 18, 59–76.

Holdsworth, D.W., Thornton, M.M., 2002. Micro-CT in small animal and specimen imaging. Trends in Biotechnology 20, S34–S39.

Homberger, D.G., DeSilva, K.N., 2000. Functional microanatomy of the feather-bearing integument: implications for the evolution of birds and avian flight. American Zoologist 40, 533–574.

Horner, J.R., 1984. A 'segmented' epidermal tail frill in a species of hadrosaurian dinosaur. Journal of Paleontology 58, 270–271.

Hu, Y., Meng, J., Wang, Y., Li, C., 2005. Large Mesozoic mammals fed on young dinosaurs. Nature 433, 149–152.

Huang, B., 2010. Super-resolution optical microscopy: multiple choices. Current Opinion in Chemical Biology 14, 10–14.

Hubert, J.F., Hyde, M.G., 1982. Sheet-flow deposits of graded beds and mudstones on an alluvial sandflat-playa system: Upper Triassic Blomidon redbeds, St Mary's Bay, Nova Scotia. Sedimentology 29, 457–474.

Janko, M., Zink, A., Gigler, A.M., Heckl, W.M., Stark, R.W., 2010. Nanostructure and mechanics of mummified type 1 collagen from the 5300-year-old Tyrolean Iceman. Proceedings of the Royal Society B 277, 2301–2309.

Jiang, B.Y., Fürsich, F.T., Hethke, M., 2012. Depositional evolution of the Early Cretaceous Sihetun Lake and implications for regional climatic and volcanic history in western Liaoning, NE China. Sedimentary Geology 257–260, 31–44.

Jiang, B.Y., Fürsich, F.T., Sha, J.G., Wang, B., Niu, Y.Z., 2011. Early Cretaceous volcanism and its impact on fossil preservation in Western Liaoning, NE China. Palaeogeography, Palaeoclimatology, Palaeoecology 302, 255–269.

Jiang, B., Harlow, G.E., Wohletz, K., Zhou, Z., Meng, J., 2014. New evidence suggests pyroclastic flows are responsible for the remarkable preservation of the Jehol Biota. Nature Communications 5, 3151.

Jiang, B., and Sha, J., 2007. Preliminary analysis of the depositional environments of the Lower Cretaceous Yixian Formation in the Sihetun area, western Liaoning, China. Cretaceous Research 28, 183–193.

Keating, J.N., Marquart, C.L., Donoghue, C.J., 2015. Histology of the heterostracan dermal skeleton: Insight into the origin of the vertebrate mineralized skeleton. Journal of Morphology 276, 657–680.

Kemp, R.A., Unwin, D.M., 1999. The skeletal taphonomy of *Archaeopteryx*: a quantitative approach. Lethaia 30, 229–238.

Kellner, A.W.A., Wang, X., Tischlinger, D.A.C., Hone, D.W.E., Meng, X., 2010. The soft tissue of *Jeholopterus* (Pterosauria, Anurognathidae, Batrachognathinae) and the structure of the pterosaur wing membrane. Proceedings of the Royal Society B 277, 321–329.

Kidwell, S.M., Behrensmeyer, A.K., 1988. Overview: ecological and evolutionary implications of taphonomic processes. Palaeogeography, Palaeoclimatology, Palaeoecology 63, 1–13.

Kim, J.Y., Kim, K.S., Lockley, M.G., Seo, S.J., 2010. Dinosaur skin impressions from the Cretaceous of Korea: New insights into modes of preservation. Palaeogeography, Palaeoclimatology, Palaeoecology 293, 167–174.

Kling, G.W., Clark, M.A., Wagner, G.N., Compton, H.R., Humphrey, A.M., Devine, J.D., Evans, W.C., Lockwood, J.P., Tuttle, M.L., Koenigsberg, E.J. 1987. The 1986 Lake Nyos gas disaster in Cameroon, West Africa. Science 236, 169–175.

Krapovickas, V., Mancuso, A.C., Mariscano, C.A., Domnanovich, N.S., Schultz, C.L., 2013. Large tetrapod burrows from the Middle Triassic of Argentina: a behavioural adaptation to seasonal semi-arid climate? Lethaia 46, 154–169.

Lange, L., Huang, Y., Busk, P.K. 2016. Microbial decomposition of keratin in nature—a new hypothesis of industrial relevance. Applied Microbial Biotechnology 100, 2083–2096.

Lautenschlager, S., Bright, J.A., Rayfield, E.J., 2014. Digital dissection – using contrast-enhanced computed tomography scanning to elucidate hard- and soft-tissue anatomy in the common buzzard *Buteo buteo*. Journal of Anatomy 224, 412–431.

Li, Q., Clarke, J.A., Gao, K-.Q., Meng, Q., Li, D., D'Alba, L., Shawkey, M.D., 2014. Melanosome evolution indicates a key physiological shift within feathered dinosaurs. Nature 507, 350–353

Liu, A., Nishimura, T., and Takahashi, K., 1994. Structural changes in endomysium and perimysium during post-mortem aging of chicken *Semitendinosus* muscle–contribution of structural weakening of intramuscular connective tissue to meat tenderisation. Meat Science 38, 315–328.

Lillywhite, H.B., Maderson, P.F.A., 1982. Skin structure and permeability. In: Gans, C., and Pough, H.F. (eds.) *Biology of the Reptilia, vol 12.* Academic Press, London.

Lindgren, J., Alwmark, C., Caldwell, M.W., Fiorillo, A.R. 2009. Skin of the Cretaceous mosasaur *Plotosaurus*: implications for aquatic adaptations in giant marine reptiles. Biology Letters 5, 528–531.

Lindgren, J., Uvdal, P., Sjövall, P., Nilsson, D.E., Engdahl, A., Schultz, B.P., Thiel, V., 2012. Molecular preservation of the pigment melanin in fossil melanosomes. Nature Communications 3, 824.

Lloyd, G.T., Davis, K.E., Pisani, D., Tarver, J.E., Ruta, M., Sakamoto, M., Hone, D.W.E., Jennings, R., Benton, M.J., 2008. Dinosaurs and the Cretaceous terrestrial revolution. Proceedings of the Royal Society B 275, 2483–2490.

Loughlin, S.C., Baxter, P.J., Aspinall, W.P., Darroux, B., Harford, C.L., Miller, D., 2002. Eyewitness accounts of the 25 June 1997 pyroclastic flows and surges at Soufriére Hills Volcano, Montserrat, and implications for disaster mitigation. In: Druitt, T.H., and Kokelaar, B.P., (eds) 2002. *The Eruption of Soufriére Hills Volcano, Montserrat from 1995 to 1999.* Geological Society, London, Memoirs 21, 211–262.

Lucas, A.M., and P.R. Stettenheim. 1972. Avian anatomy. Integument, volume II. Washington, D.C. : U.S. Government Printing Office.

MacNaughton, A.F., 1978. A histological study of post mortem changes in the skeletal muscle of the fowl (*Gallus domestus*). 1. The muscle fibres. Journal of Anatomy 125, 461–476.

Mähler, B., Schwermann, A., H., Wuttke, M., Schultz, J.A., Martin, T., 2015. Four-dimensional virtopsy and the taphonomy of a mole from the Oligocene of Lake Enspel (Germany). Palaeobiology, Palaeoenvironments 95, 115–131.

Major, J.J., 2003. Post-eruption hydrology and sediment transport in volcanic river systems. Water Resources Impact 5, 10–15.

Major, J.J., Pierson, T.C., Dinehart, R.L., Costa, J.E., 2000. Sediment yield following severe volcanic disturbance - A two decade perspective from Mount St. Helens. Geology 28, 819–822.

Manning, P.L., Morris, P.M., McMahon, A., Jones, E., Gize, A., Macquaker, J.H.S., Wolff, G., Thompson, A., Marshall, J., Taylor, K.G., Lyson, T., Gaskell, S., Reamtong, O., Sellers, W.I. van Dongen, B.E., Buckley, M., Wogelius. R.A., 2009. Mineralized soft-tissue structure and chemistry in a mummified hadrosaur from the Hell Creek Formation, North Dakota (USA). Proceedings of the Royal Society B 276, 3429–3437.

Mannion, P.D., Upchurch, P., 2010. Completeness metrics and the quality of the sauropodomorph fossil record through geological and historical time. Paleobiology 36, 283–302.

Martill, D.M., 1990. Macromolecular resolution of fossilised muscle tissue from an elopomorph fish. Nature 346, 171–172.

Martill, D.M., Unwin, D.M., 1989. Exceptionally well preserved pterosaur wing membrane from the Cretaceous of Brazil. Nature 340, 138–140.

Matikeviciene, V., Masiliuniene, D., Grigskis, S., 2009. Degradation of keratin containing wastes by bacteria with keratinolytic activity. Environment Technology Resources. Proceedings of the 7th International Scientific and Practical Conference 1, 284–289.

Mayr, G., Peters, S.D., Plodowski, G., Vogel, O., 2002. Bristle-like integumentary structures at the tail of the horned dinosaur *Psittacosaurus*. Naturwissenschaften 89, 361–365.

McBride, E.F., 1974. Significance of colour in red, green, purple, olive, brown, and grey beds of Difunta Group, Northeastern Mexico. Journal of Sedimentary Petrology 44, 760–773.

McKenna, M.C., Wyss, A.R., Flynn, J.J., 2006. Paleogene pseudoglyptodont xenarthrans from central Chile and Argentine Patagonia. American Museum Novitates 3536 1–18.

McNamara, M.E., Orr, P.J., Alcalá, L., Anadón, P., Peñalver, E., 2012. What controls the taphonomy of exceptionally preserved taxa–environment or biology? A case study using frogs from the Miocene Libros konservat-lagerstätte (Teruel, Spain). Palaios 27, 63–77.

McNamara, M.E., Orr, P.J., Kearns, S.L., Alcala, L., Anadon, P., Penalver Molla, E., 2009. Soft-tissue preservation in Miocene frogs from Libros, Spain: insights into the genesis of decay microenvironments. Palaios 24, 104–117.

McNamara, M.E., Orr, P.J., Kearns, S.L., Alcalá, L., Anadón, P., Peñalver-Mollá, E., 2010. Exeptionally preserved tadpoles fromt the Miocene of Libros, Spain: ecomorphological reconstruction and the impact of ontogeny upon taphonomy. Lethaia 43, 290–306.

McNamara, M.E., Orr, P.J., Kearns, S.L., Alcalá, L., Anadón, P., Peñalver, E., 2016a. Reconstructing carotenoid-based and structural coloration in fossil skin. Current Biology 8, 1075–1082.

McNamara, M.E., Orr, P.J., Manzoochi, T., Alcalá, L., Anadón, P., Peñalver, E., 2011. Biological controls upon the physical taphonomy of exceptionally preserved salamanders from the Miocene of Rubielos de Mora, northeast Spain. Lethaia 45, 210–226.

McNamara, M.E., van Dongen, B.E., Lockyear, N.P., Bull, I.D., Orr, P.J., 2016b. Fossilisation of melanosomes via sulfurization. Palaeontology 59, 337–350.

Meganck, J.A., Kozloff, K.M., Thornton, M.M., Broski, S.M., Goldstein, S.A., 2009. Beam hardening artifacts in micro-computed tomography scanning can be reduced by X-ray beam filtration and the resulting images can be used to accurately measure BMD. Bone 45, 1104–1116.

Menard, H.W., Boucot, A.J., 1951. Experiments on the movement of shells by water. American Journal of Science 249, 131–151.

Meng, J., Hu, Y., Li, C., Wang, Y., 2006. The mammal fauna in the Early Cretaceous Jehol Biota: implications for diversity and biology of Mesozoic mammals. Geological Journal 41, 439–463.

Meng, Q., Liu, J.,Varricchio, D.J., Huang, T., Gao, C., 2004. Parental care in an ornithischian dinosaur. Nature, 431, 145–146.

Menon, G.K., Menon, J., 2000. Avian epidermal lipids, functional considerations and relationships to feathering. American Zoologist 40, 540–552.

Metscher, B.D., 2009. Micro CT for developmental biology a versatile tool for high-contrast at histological resolutions. Developmental Dynamics 238, 632–640.

Meyer, M., Elliott, D., Wood, A.D., Polys, N.F., Colbert, M., Maisano, J.A., Vickers-Rich, P., Hall, M., Hoffman, K.H., Schneider, G., Xiao, S., 2014. Three-dimensional micro CT analysis of the Ediacara fossil *Pteridinium simplex* sheds light on its ecology and phylogenetic affinity. Precambrian Research 249, 79–87.

Micali, G., F. Lacarrubba, A. Bongu, D.P., West. 2001. 14. The skin barrier. Freinkel, R.K., Voodley, D.T. (eds.) *The biology of the skin.* Carnforth, UK: Parthenon.

Mohammed, F., Arishiya, T.F., Mohamed, S., 2012. Microtomes and microtome knives – a review and proposed classification. Annals of Dentistry, University of Malaya 19, 43–50.

Murdock, D.J.E., Gabbott, S.E., Mayer, G., Purnell, M.A., 2014. Decay of velvet worms (Onychophora), and bias in the fossil record of lobopodians. BMC Evolutionary Biology 14, 222

Navalón, G., Marugán-Lobón, Chiappe, L.M., Sanz, J.L., Buscalioni, A.D., 2015. Soft-tissue and dermal arrangement in the wing of an Early Cretaceous bird: Implications for the evolution of avian flight. Scientific Reports 5, 14864

Norell, M.A., Clark, J.M., Chiappe, L.M., Dashzeveg, D., 1995. A nesting dinosaur. Nature 378, 774–776.

Norell, M.A., Makovicky, P.J., 1999. Important features of the dromaeosaur skeleton II: Information from newly collected specimens of *Velociraptor mongoliensis*. American Museum Novitates 3282, 1–27.

Nudds, R.L., and Dyke, G.J., 2010. Narrow primary feather rachises in *Confuciusornis* and *Archaeopteryx* suggests poor flight ability. Science 328, 887–889.

O'Connor, J., Chang, H., 2013. Hindlimb feathers in Paravians: Primarily "wings" or ornaments? Biology Bulletin 42, 616–621.

O'Connor, J., Wang, X., Sullivan, C., Zheng, X., Tubaro, P., Zhang, X., Zhou, Z., 2013. Unique caudal plumage of *Jeholornis* and complex tail evolution in early birds. Proceedings of the National Academy of Sciences, USA 110, 17404–17408.

O'Connor, J.K., and Zhou, Z.Z., 2012. A redescription of Chaoyangia beishanensis (Aves) and a comprehensive phylogeny of Mesozoic birds. Journal of Systematic Palaeontology 11, 889–906.

O'Connor, J., Zhou, Z., Xu, X., 2011. Additional specimen of *Microraptor* provides evidence of dinosaurs preying on birds. Proceedings of the National Academy of Sciences, USA 108, 19662–19665.

Oliver, J.S., Graham, R.W., 1994. A catastrophic kill of ice-trapped coots: time averaged versus scavenger-specific disarticulation patterns. Paleobiology 20, 229–244.

Olsen, E.C., 1952. The evolution of a Permian vertebrate chronofauna. Evolution 6, 181–196.

Orr, P.J., Briggs, D.E.G., Kearns, S.L., 1998. Cambrian Burgess Shale animals replicated in clay minerals. Science 281, 1173–1175.

Orr, P.J., Briggs, D.E.G., 1999. Exceptionally preserved conchostracans and other crustaceans from the Upper Carboniferous of Ireland. Special Papers in Palaeontology 62, 1–68.

Paik, I.S., Kim, H.J., 2006. Playa lake and sheetflood deposits of the Upper Cretaceous Jinlong Formation Korea: occurrences and palaeoenvironments. Sedimentary Geology 187, 83–103.

Pan, Y., Fürsich, F.T., Zhang, J., Wang, Y., Zheng, X., 2015. Biostratinomic analysis of *Lycoptera* beds from the Early Cretaceous Yixian Formation, western Liaoning, China. Palaeontology 58, 537–561.

Pan, Y., Sha, J., Fürsich, F.T., Wang, Y., Zhang, X., Yao, X., 2011. Dynamics of the lacustrine fauna from the Early Cretaceous Yixian Formation, China: implications of volcanic and climatic factors. Lethaia 45, 299–314.

Pan, Y., Sha, J., Zhou, Z., Fürsich, F.T., 2013. The Jehol Biota: Definition and distribution of exceptionally preserved relicts of a continental Early Cretaceous ecosystem. Cretaceous Research. 44, 30–38.

Parfitt, E.A., Wilson, L., 2008. 8. Pyroclastic falls and pyroclastic density currents, in: *Fundamentals of Physical Volcanology*. Blackwell Science Ltd., Oxford, pp. 105–125.

Parry, L.A., Wilson, P., Sykes, D., Edgecombe, G.D., Vinther, J., 2015. A new fireworm (Amphinomidae) from the Cretaceous of Lebanon identified from three dimensionally preserved myoanatomy. BMC Evolutionary Biology 15, 256.

Paul, G.S., 2010. Comment on "Narrow primary feather rachises in *Confuciusornis* and *Archaeopteryx* suggest poor flight ability". Science 330, 320.

Pauwels, E., Van Loo, D., Cornillie, P., Brabant, L., Van Hoorebeke, L. 2012. An explanatory study of contrast agents for soft tissue visualization by means of high resolution X-ray computed tomography imaging. Journal of Microscopy 250, 21–31.

Pearce, K.L., K. Rosenvold, H.J. Anderson, D.L., Hopkins. 2011. Water distribution and mobility in meat during the conversion of muscle to meat and ageing and the impacts on fresh meat quality attributes- a review. Meat Science 89, 111–124.

Pei,R., Li,Q., Meng,Q., Gao,K.-Q., Norrel,M.A., 2014. A new specimen of *Microraptor* (Theropoda: Dromaeosauridae) from the Lower Cretaceous of western Liaoning, China. American Museum Novitates 3821, 1-29

Peters, R.H. 1983. *The ecological implications of body size*. Cambridge, MA, Cambridge University Press.

Prum, R.O., 1999. Development and evolutionary origin of feathers. Journal of Experimental Zoology (Molecular Developmentary Evolution) 285, 291–306.

Ramshaw, J.A.M., Rigby, B.J., Mitchell, T.W., Nieass, A., 1986. Changes in the physical and chemical properties of skin collagen from broiler chickens exhibiting oily bird syndrome. Poultry 65, 43–50.

Raup, D.M., 1976. Species diversity in the Phanerozoic: an interpretation. Paleobiology 2, 289–297.

Redelstorff, R., P.J. Orr. 2015. The anatomy of nonbiomineralized chordate fossils: insights from experimental decay of *Xenopus laevis* tadpoles. Palaios 30, 355–351.

Reisdorf, A.G., Wuttke, M., 2012. Re-evaluating Moodie's opisthotonic-posture hypothesis in fossil vertebrates Part 1: Reptiles- the taphonomy of bipedal dinosaurs *Compsognathus longipes* and *Juravenator* from the Solnhofen Archipelago (Jurassic, Germany). Palaeobiology, Palaeoenvironments 92, 119–168.

Riffel, A., Lucas, F., Heeb, P., Brandelli, A., 2003. Characterization of a new keratinolytic bacterium that completely degrades native feather keratin. Archives of Microbiology 179, 258–265.

Rogers, C.S., Hone, D.W.E., McNamara, M.E., Zhao, Q., Kearns, S.L., Benton, M.J., 2015. The Chinese Pompeii? Death and destruction of dinosaurs in the Early

Cretaceous of Lujiatun, NE China. Palaeogeography, Palaeoclimatology, Palaeoecology 427, 89–99

Ryu, Y.C., B.C. Kim., 2005. The relationship between muscle fiber characteristics, post mortem rate, and meat quality of pig longissimus dorsi muscle. Meat Science 71, 351–357.

Sagemann, J., Bale, S.J., Briggs, D.E.G., Parkes, R.J., 1999. Controls on the formation of authigenic minerals in association with decaying organic matter: an experimental approach. Geochemica et Cosmochimica Acta 63, 1083–1095.

Sanchez, S., Dupret, V., Tafforeau, P., Trinajstic, K.M., Ryll, B., Gouttenoire, L.W., Zylberberg, L., Peyrin, F., Ahlberg, P.E. 2013. 3D Microstructural architecture of muscle attachments in extant and fossil vertebrates revealed by synchrotron microtomography. PLOS ONE 8, e56992.

Sansom, R.S., Gabbott, S.E., Purnell, M.A., 2010. Non-random decay of chordate characters causes bias in fossil interpretation. Nature 463, 797-800

Sansom, R.S., Gabbott, S.E., Purnell, M.A., 2011. Decay of vertebrate characters in hagfish and lamprey (Cyclostomata) and the implications for the vertebrate fossil record. Proceedings of the Royal Society B 278, 1150-1157.

Sansom, R.S., Gabbot, S.E., Purnell, M.A., 2013. Atlas of vertebrate decay: a visual and taphonomic guide to fossil interpretation. Palaeontology 56, 457–474.

Schäfer, W., 1972. Ecology and Palaeoecology of marine environments: Chicago University Press, Chicago, 568p.

Schroger, A.W., 1944. Avian adipocere. The Wilson Bulletin 56, 216–217.

Schweitzer, M.H., 2011. Soft tissue preservation in terrestrial Mesozoic vertebrates. Annual Review of Earth and Planetary Sciences 39, 187–216.

Schwermann, A.H., Wuttke, M., Schultz, J.A., 2012. Virtopsy of the controlled decomposition of a dormouse *Eliomys quercinus* as a tool to analyse the taphonomy

of *Heterohyus nanus* from Messel (Eocene, Germany). Palaeobiodiversity and
Palaeoenvironments 92, 29–43

Seilacher, A., Reif, W.-E., Westphal, F., 1985. Sedimentological, ecological and temporal
patterns of fossil Lagerstätten. Philosophical Transactions of the Royal Society of
London Series, B 311, 5–23.

Siebe, C., Scaaf, P., Urrutia-Fucugauchi, J., 1999. Mammoth bones embedded in a late
Pleistocene lahar from Popocatépetl volcano, near Tocuila, central Mexico.
Geological Society of America Bulletin 111, 1550–1562.

Smith, R.M.H., 1993. Vertebrate taphonomy of the late Permian floodplain deposits in the
southwestern Karoo Basin of South Africa. Palaios 8, 45–67.

Soares, M.B., 2003. A taphonomic model for the Mesosauridae assemblage of the Irati
Formation (Paraná Basin, Brazil). Geologica Acta 1, 349–361

Sparks, R.S.J., 1976. Grain size variations in ignimbrites and implications for the
transport of pyroclastic flows. Sedimentology 23, 147–188.

Stettenheim, P.R., 2000. Integumentary morphology of modern birds- an overview.
American Zoologist 40, 461–477.

Sulpizio, R., Dellino, P., Doronzo, D.M., Sarocchi, D., 2014 Pyroclastic density currents:
state of the art and perspectives. Journal of Volcanology and Geothermal Research
283, 36–65.

Sun, G., Dilcher, D.L., Zheng, S., Zhou, Z., 1998. In search of the first flower: A Jurassic
Angiosperm, *Archaeofructus*, from Northeast China. Science 27, 1692–1695.

Suzuki, Y., Tsujimoto, Y., Matsui, H., Watanabe, K., 2006. Decomposition of extremely
hard-to-degrade animal proteins by thermophilic bacteria. Journal of bioscience and
bioengineering 102, 73–81.

Syme, C.E., Salisbury, S.W., 2014. Patterns of aquatic decay and disarticulation in
juvenile Indo-Pacific crocodiles (*Crocodylus porosus*), and implications for the

taphonomic interpretation of fossil crocodyliform material. Palaeogeography
Palaeoclimatology Palaeoecology 412, 108–123

Tucker, M.E., 2001. *Sedimentary Petrology, 3rd edn*. Blackwell Science Ltd., Oxford.

Tzu,S., 1924. The His Yüan Lu or Instructions to coroners (Version from 1843, compiled
by Tung Lien). Proceedings of the Royal Society of Medicine 17, 59–107.

Vallance, J.W., 2000. Lahars, in: Sigurdsson, H. (ed) *Encyclopedia of Volcanoes*.
Academic Press, New York, pp. 601–616.

Varricchio, D. J., Martin, A. J., Katsura, Y., 2007. First trace and body fossil evidence of
a burrowing, denning dinosaur. Proceedings of the Royal Society B 274, 1361–
1368.

Vinther, J., Nicholls, R., Lautenschlager, S., Pittman, M., Kaye, T.G., Rayfield, E., Mayr,
G., Cuthill, I.C., 2016. Current Biology 26, 2456–2462.

Vinther, J., Briggs, D.E.G., Prum, R.O., Saranathan, V., 2008. The colour of fossil
feathers. Biology Letters 4, 522–525.

Wang, Y.-Q., Hu, Y.-M., Li, C.-K., 2006. Review of recent advances on study of Mesozoic
mammals in China. Vertebrata PalAsiatica 44, 193–204.

Wang, Y., Dong, L., Evans, S.E., 2010. Jurassic-Cretaceous herpetofaunas from the Jehol
associated strata in NE China: evolutionary and ecological implications. Bulletin of
the Chinese Academy of Sciences 24, 76–79.

Wang, X., McGowan, A.J., Dyke, G.J., 2011. Avian wing proportions and flight styles :
first step towards predicting the flight modes of Mesozoic birds. PLoS ONE 8,
e28672.

Wang, X.-L., Zhou, Z.-H., 2003. Mesozoic Pompeii, in: Chang,M.-M., Chen,P.-J., Wang,Y.-
Q., Wang, Y.(eds). *The Jehol Biota: the Emergence of Feathered Dinosaurs, Beaked
Birds and Flowering Plants.* Shanghai Scientific and Technical Publishers,
Shanghai, pp. 19–35.

Wiese, F.K., 2003. Sinking rates of dead birds: improving estimates of seabird mortality due to oiling. Marine Ornithology 31, 65–70.

Wilby, P.R., 1993. The role of organic matrices in post-mortem phosphatisation of soft-tissues. Kaupia 2, 99–113.

Wilby, P.R., D.E.G., Briggs. 1997. Taxonomic trends in the resolution of detail preserved in fossil phosphatised soft tissues. Geobios 20: 493–502.

Williams, C.M., Richter, C.S., MacKenzie Jr., J.M., Shih, C.H., 1990. Isolation, identification and characterization of a feather-degrading bacterium. Applied and environmental microbiology 56, 1509–1515.

Wilson, P., Parry, L.A., Vinther, J., and Edgecomb, G.D., 2016. Unveiling biases in soft-tissue phosphatisation: extensive preservation of musculature in the Cretaceous (Cenomanian) Polychaete *Rollinschaeta myoplena* (Annelida: Amphinomidae). Palaeontology 59, 463–479.

Xu, X., Norell, M.A., 2004. A new troodontid dinosaur from China with avian-like sleeping posture. Nature 431, 838–841.

Xu, X., Norell, M.A., 2006. Non-avian dinosaur fossils from the Lower Cretaceous Jehol Group of western Liaoning, China. Geological Journal 41, 419–437.

Xu, X., Wang, X.-L., Wu, X.-C., 1999. A dromaeosaurid dinosaur with filamentous integument from the Yixian Formation of China. Nature 401, 262–266.

Xu, X., Zhou, Z., Wang, X., Kuang. X., Zhang, F., Du, X., 2003. Four-winged dinosaurs from China. Nature 421, 335–340.

Yang, W., Li, S., Jiang, B., 2007. New evidence for Cretaceous age of the feathered dinosaurs of Liaoning: zircon U-Pb SHRIMP dating of the Yixian Formation in Sihetun, northeast China. Cretaceous Research 28, 177–182.

Zehbe, R., Haibel, A., Riesemeier, H., Gross, U., Kirkpatrick, J., Schubert, H., Brochhausen, C., 2009. Going beyond histology. Synchrotron micro-computed

tomography as a methodology for biological tissue characterization: from tissue morphology to individual cells. Journal of the Royal Society Interface 7, 49–59.

Zhang, F., Kearns. S.L., Orr, P.J., Benton, M.J., Zhou, Z., Johnson, D., Xu, X., Wang, X., 2010a. Fossilized melanosomes and the colour of Cretaceous dinosaurs and birds. Nature 463, 1075–1078.

Zhang, H., Wang, B., Fang, Y., 2010b. Evolution of insect diversity in the Jehol Biota. Science China (Earth Sciences) 53, 1908–1917.

Zhang, F., Zhou, Z., Benton, M.J., 2008. A primitive confusciusornithid bird from China and its implications for early avian flight. Science in China Series D: Earth Sciences 51, 625–639

Zhang, Z., Gao, C., Meng, Q., Liu, J., Hou, L., Zeng, G. 2009. Diversification in an Early Cretaceous avian genus: evidence from a new species of *Confuciusornis* from China. Journal of Ornithology 150, 783–790.

Zhao, Q., Barret, P.M., Eberth, D.A., 2007. Social behaviour and mass mortality in the basal ceratopsian dinosaur *Psittacosaurus* (Early Cretaceous, Peoples Republic of China). Paleontology 50, 1023–1029.

Zhao, Q., Benton, M.J., Sullivan, C., Sander, P.M., Xu, X., 2013. Histology and postural change during growth of the ceratopsian dinosaur *Psittacosaurus lujiatunensis*. Nature Communications 4, 2079 doi:10.1038/ncomms3079.

Zhao,Q., Benton, M.J., Xu, X., Sander, P.M., 2014. Juvenile-only clusters and behaviour of the Early Cretaceous dinosaur *Psittacosaurus*. Acta Palaeontologica Polonica 59, 827–833.

Zheng, S.L., Zhang, W., Ding, Q.H., 2001. Discovery of fossil plants from the middle-upper Jurassic Tuchengzi Formation in western Liaoning, China. Acta Palaeontologica Sinica 40, 67–85.

Zheng, X., Zhou, Z., Wang, X., Zhang, F., Zhang, X., Wang, Y., Wei, G., Wang, S., Xu. X., 2013. Hind wings in basal birds and the evolution of leg feathers. Science 339:

1309–1312.

Zhou, Z. 2014a. Dinosaur evolution: feathers up for selection. Current Biology 24, R751–R753.

Zhou, Z., 2014b. The Jehol Biota, an Early Cretaceous terrestrial Lagerstätte: new discoveries and implications. National Science Review 1, 543–559.

Zhou, L., Alego, T.J., Feng, L., Zhu, R., Pan, Y., Gao, S., Zhao, L., Wu, Y., 2016. Relationship of pyroclastic volcanism and lake-water acidification to Jehol Biota mass mortality events (Early Cretaceous, northeastern China). Chemical Geology 428, 59–76.

Zhou, Z., Barrett, P.M., Hilton, J., 2003. An exceptionally preserved Lower Cretaceous ecosystem. Nature 421, 808–814.

Zhou, Z. and Zhang, F. 2003. *Jeholornis* compared to *Archaeopteryx*, with a new understanding of the earliest avian evolution. Naturwissenschaften 90, 220–225.

Zhou, Z., and Zhang, F., 2006. Mesozoic birds of China–a synoptic review. Vertebrata PalAsiatica 44, 74–98.

FIGURES

Figure 2.1.

The Lujiatun Unit, part of the Jehol Group, in NE China. A. Stratigraphic context of the Lujiatun Unit. B. Location maps for of sites logged (A–D) around Lujiatun and position of Lujiatun in Liaoning Province (highlighted), NE China.
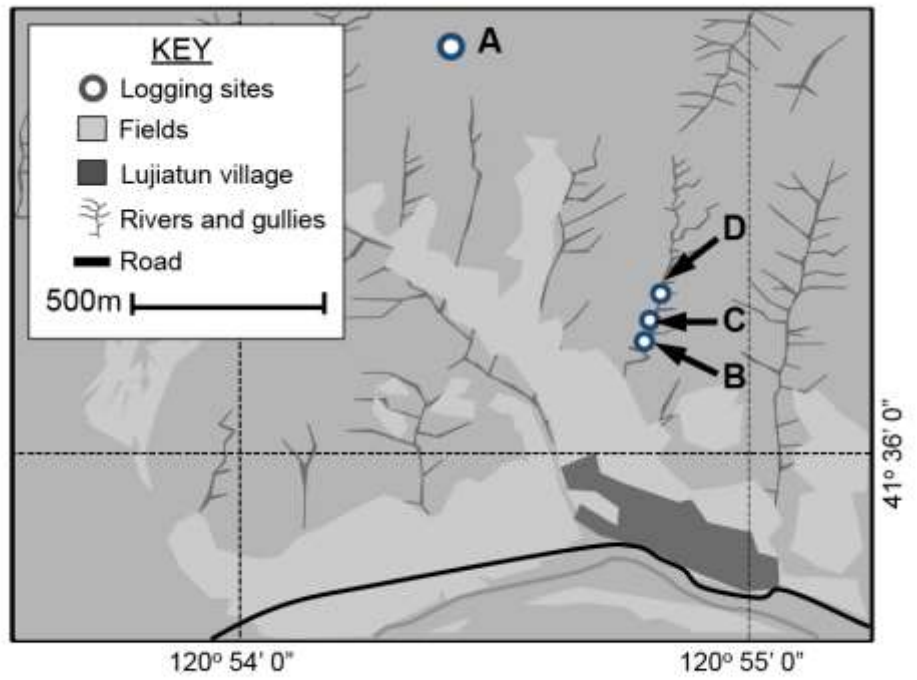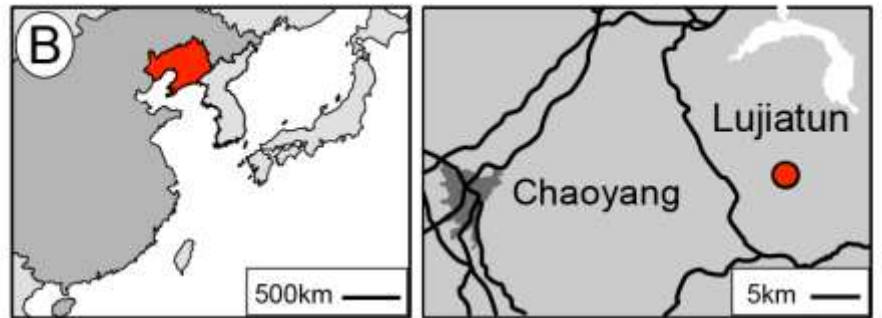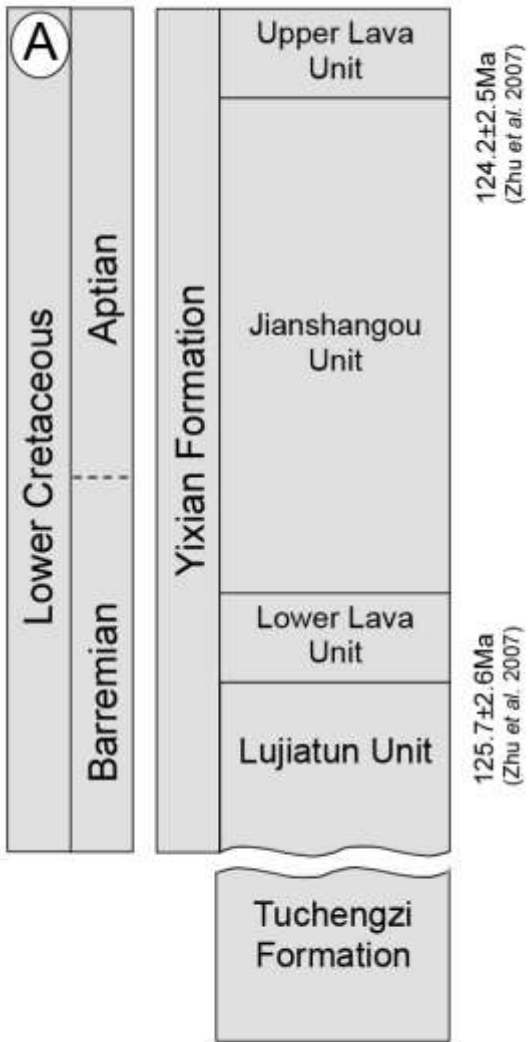
Figure 2.2.

Field sedimentology at the Lujiatun locality. A. Photograph of the site of log B showing the Lower Lava Unit capping the hills and the Upper Grey Siltstone at its base. B. Excavation into the Upper Grey Siltstone near to the site of log B. C. Several ~10 cm thick beds within the Pink Tuffaceous Sandstone at the base of Log A, and at the bottom of the photograph the top bed of the Lower Tuffaceous Siltstones, the horizon to which excavations have been dug to (grain size card for scale 10 cm long). D. Photograph showing the site for Log A and the extent of the Upper Grey Siltstones. E. The Lower Tuffaceous Siltstones at the base of Log A.

Figure 2.3.

Stratigraphic logs of the Lujiatun Unit. Logs A–D are capped by the andesitic lava of the Lower Lava Unit. Log A; articulated remains were found within the bed at the base of the Upper Grey Siltstones (UGS) as it grades into the Pink Tuffaceous Sandstones (PTS). Extensive excavations occur in both the Upper Grey Siltstones and Lower Tuffaceous Siltstones (LTS). Scales are in meters, and grain sizes follow Bair and McPherson (1999). Solid lines represent horizons traced between sections; dashed lines represent hypothesised relationships between horizons.
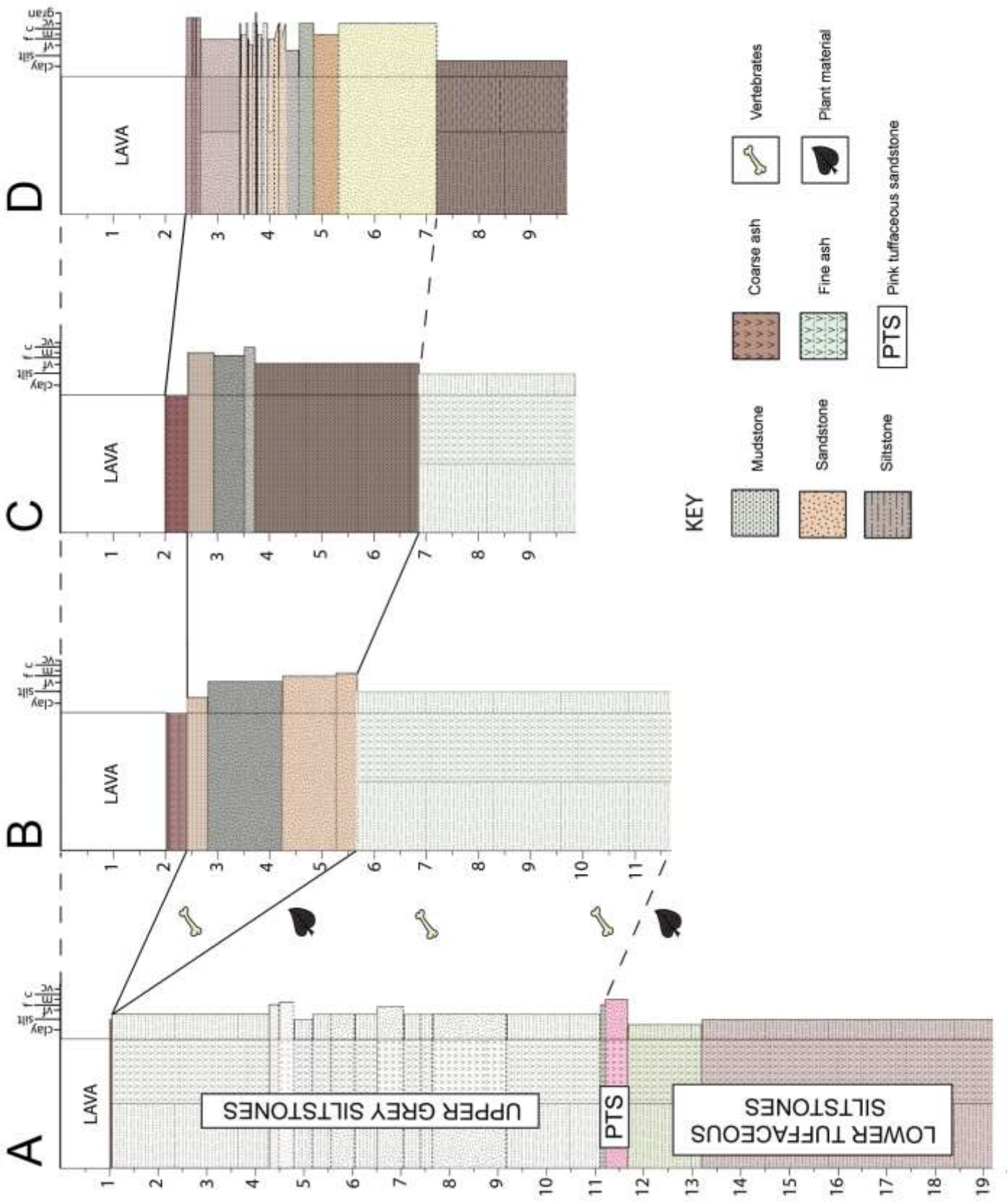
Figure 2.4.

The fossiliferous sediments and matrices of the Lujiatun Unit. A. Photomicrograph of upper grey siltstone containing a partial tooth row in lower part of image and a biotite-rich volcanic rock fragment in top right of image; pseudo-fiammé, the result of alteration of vitric shard are visible on the left hand margin of the image. Scale bar equals1000μm. B. Close-up of articulated ribs within the Pink Tuffaceous Sandstone. Weathered orange vitric ash particles are visible in hand sample. Scale bar equals 2mm. C. Photomicrograph of the Pink Tuffaceous Sandstone with orange coloured vitric ash, detailing large rounded vesicles and delicate vesicle walls. Scale bar equals 500μm. D. Photomicrograph of sample from the Lower Tuffaceous Siltstone, showing several pseudo-fiammé. Scale bar equals 500 μm E. Photomicrograph of the matrix of IVPP V14748. Scale bar equals 500 μm. F. Photomicrograph of the lahar matrix from IVPP V14341 (Zhao et al. 2007) showing volcanic rock fragment in the lower left hand corner of the image. Scale bar equals 500 μm.
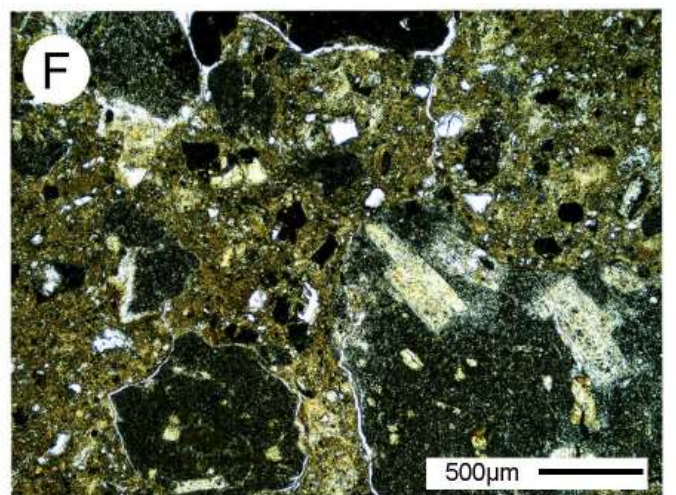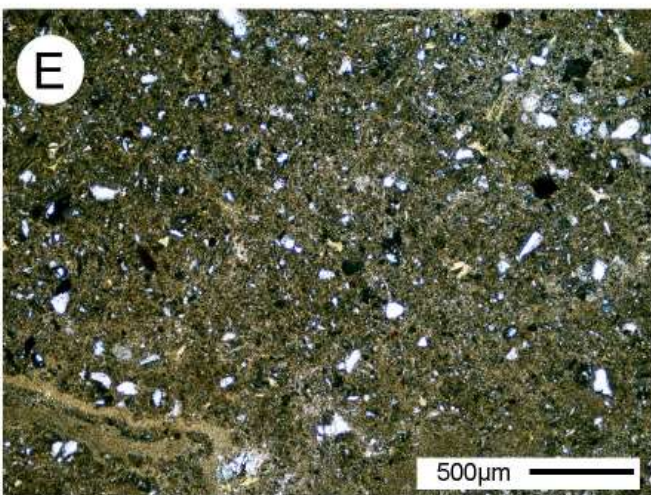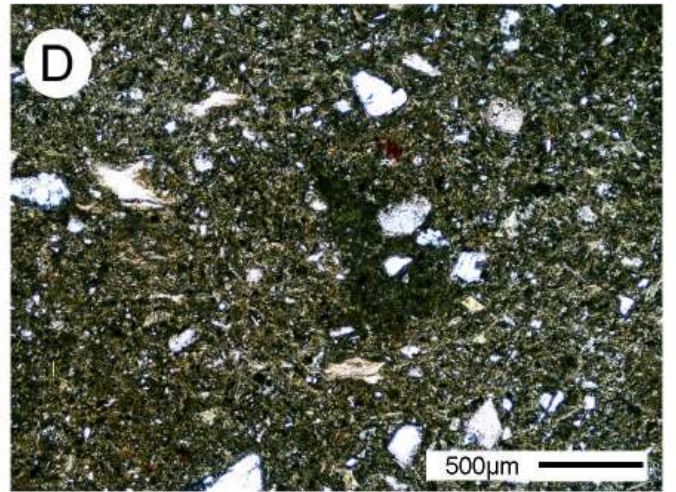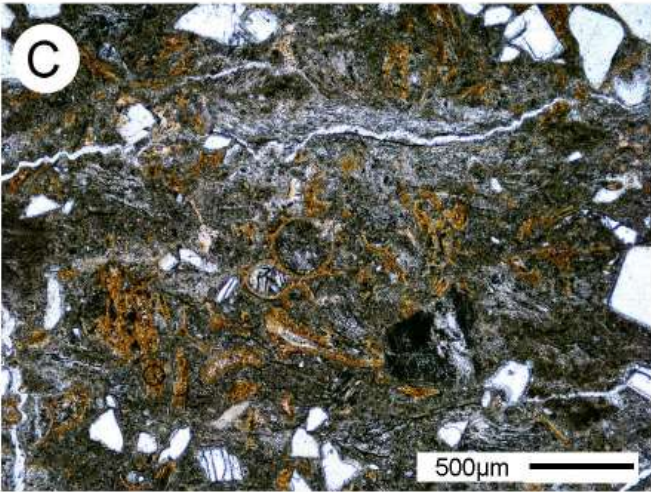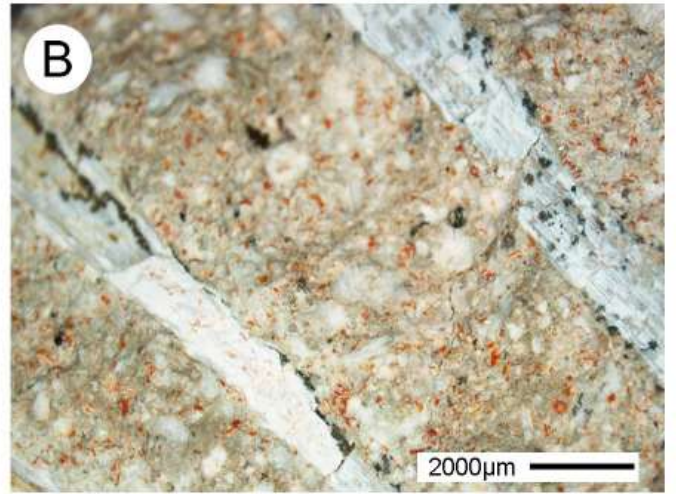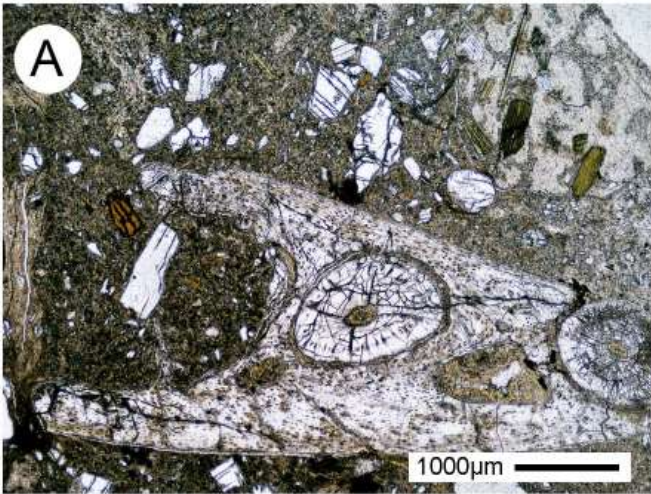
Figure 2.5.

Reconstruction of the depositional setting along the northern edge of a basin, based on this study and that by Jiang & Sha (2007). Light grey represents pyroclastic deposits, remobilised as sheetfloods; arrows indicate sense of motion. Dark grey clouds represent pyroclastic flows and ash clouds. Scale refers only to position of sites and volcanic centre, size and position of highlands at basin edge not to scale. Inset shows a *Psittacosaurus* being overwhelmed by a mass movement deposit.
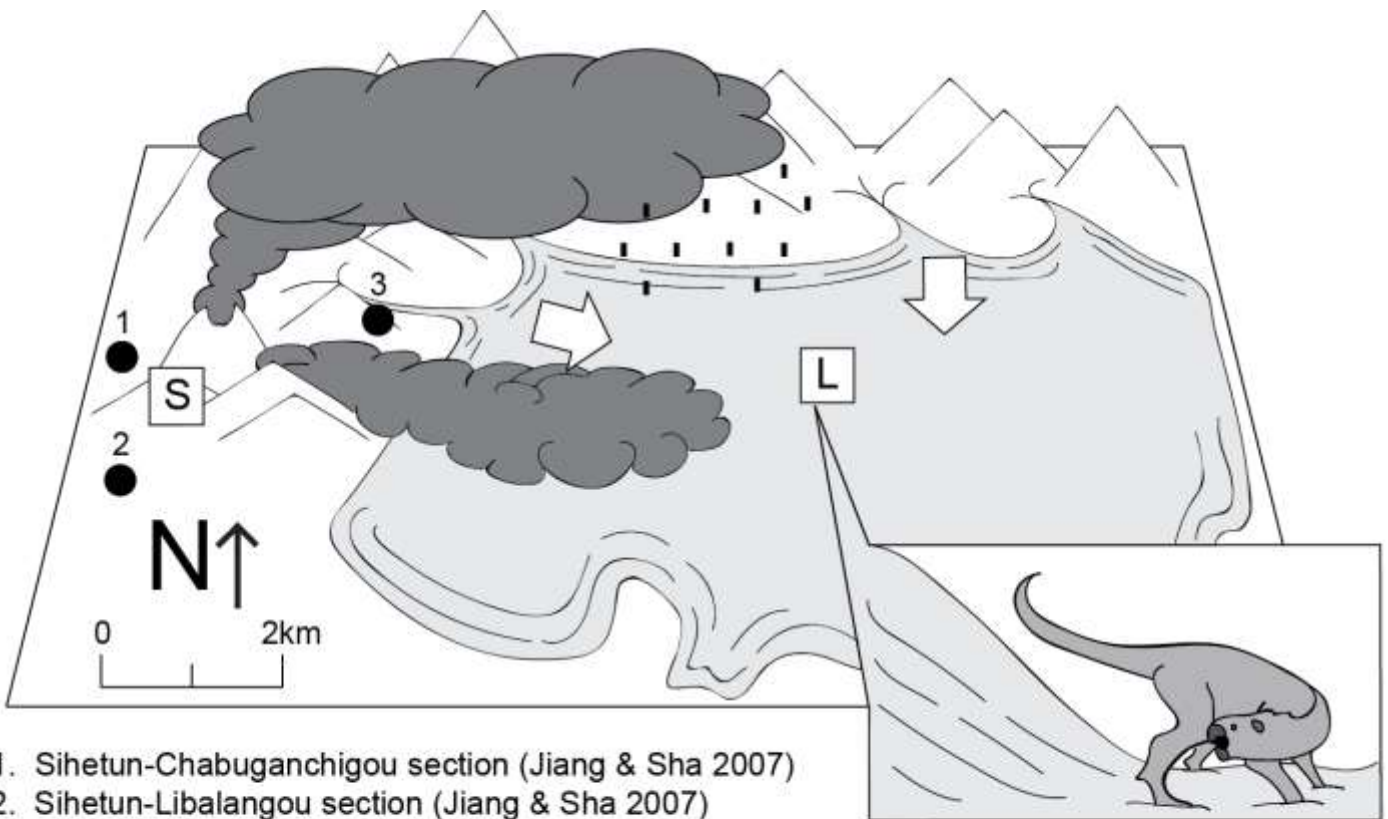
1. Sihetun-Chabuganchigou section (Jiang & Sha 2007)
2. Sihetun-Libalangou section (Jiang & Sha 2007)
3. Huanbanjigou-Jianshangou section (Jiang & Sha 2007)
S. Sihetun village
L. Lujiatun village & section (This study)

Figure 3.1.

Diagram of *Confuciusornis* sp. skeleton subdivided into the nine skeletal units used when assessing skeletal completeness and articulation (right forelimb; left forelimb; right hindlimb; left hindlimb; skull; cervical vertebrae; dorsal vertebrae; caudal vertebrae; ribs) and the seven points of inter unit articulation: 1. Skull-cervical vertebrae (s-cv); 2. Cervical vertebrae-dorsal vertebrae (cv-d); 3. Left forelimb-axial skeleton (rfl-a); 4. Right forelimb-axial skeleton (lfl-a); 5. Left hindlimb-axial skeleton (rhl-a); 6. Right hindlimb-axial skeleton (lhl-a) and 7. Dorsal vertebrae-caudal vertebrae (d-cu).

Skull

Cervical
vertebrae

Ribs

Left
forelimb

Dorsal
vertebrae

Right
forelimb

1

2

3

4

5

6

7

Left
hindlimb

Right
hindlimb
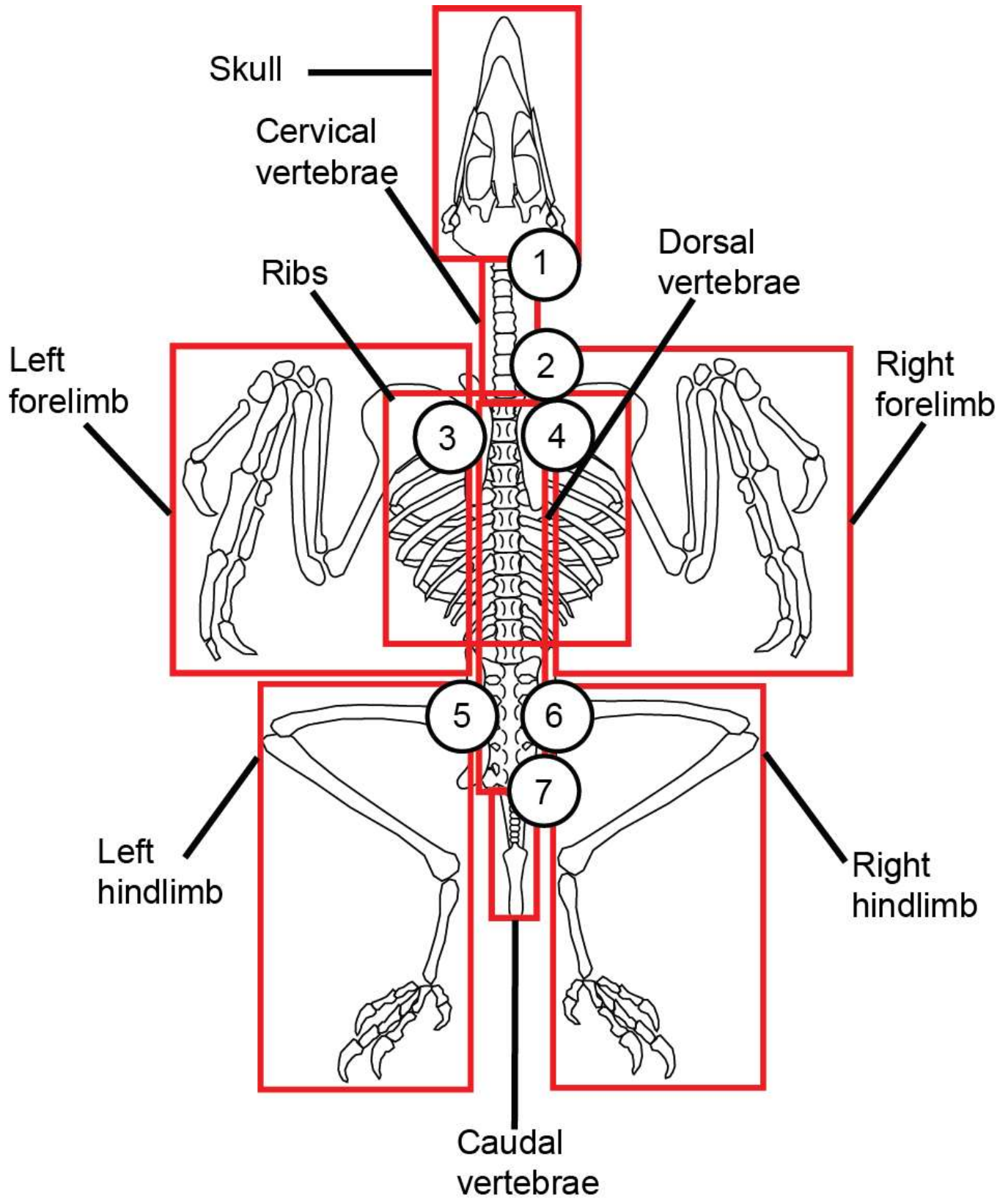
Caudal
vertebrae

Figure 3.2.

Photographs and diagrams of *Confuciusornis sp.* demonstrating all states of completeness and articulation of the forelimbs (A), hindlimbs (B), cervical vertebrae (C), dorsal vertebrae (D), caudal vertebrae (E), ribs (F) and skull (G). "No examples" represents a particular state of articulation and completeness for an anatomical unit that was not identified.
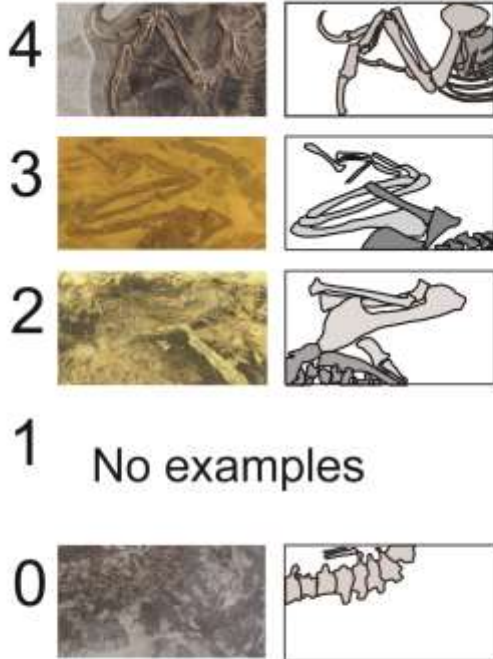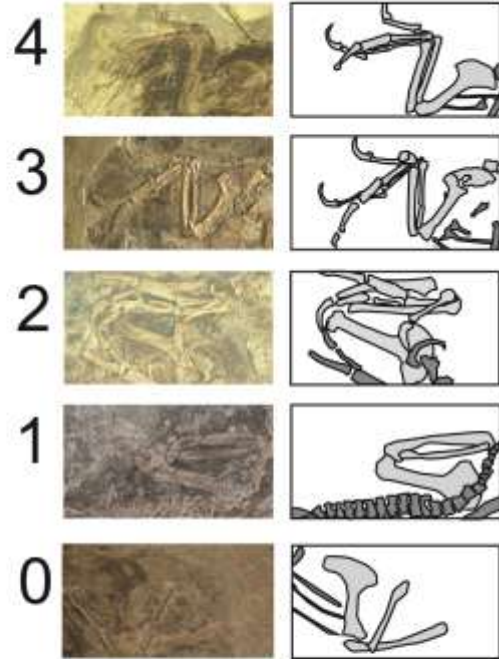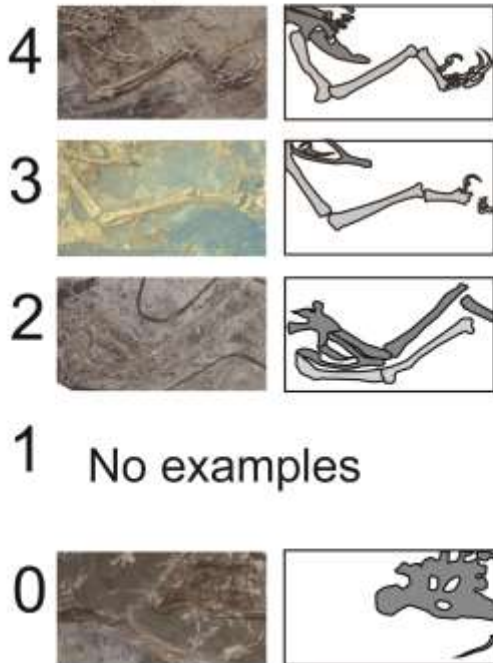
C

Completeness

4
3
2
1
0 No examples

Articulation

4
3
2
1
0

D
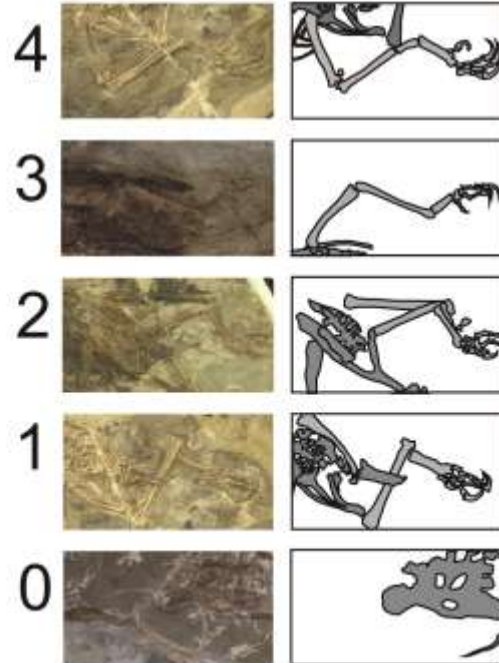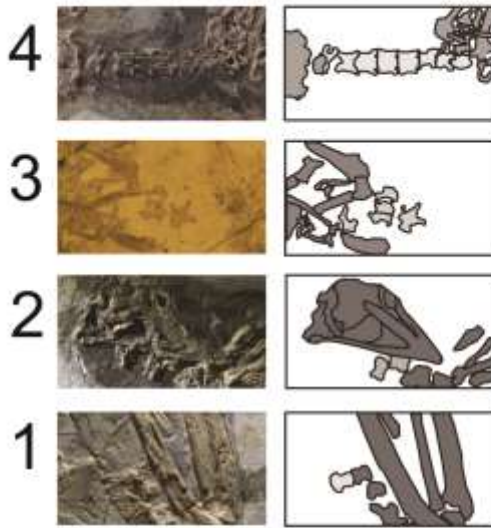
Completeness

4
3
2
1 No examples
0 No examples

Articulation
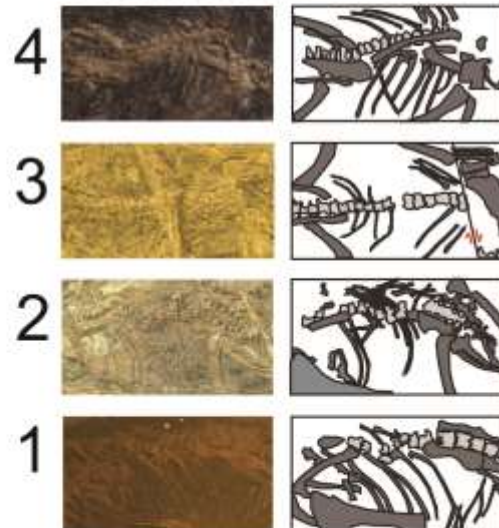
4
3
2
1
0 No examples
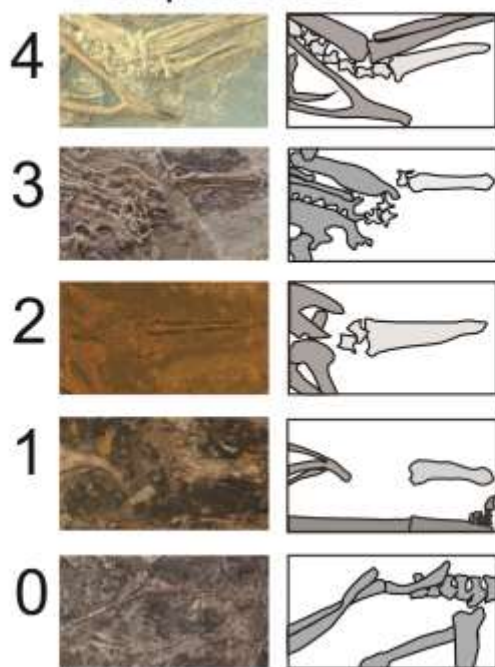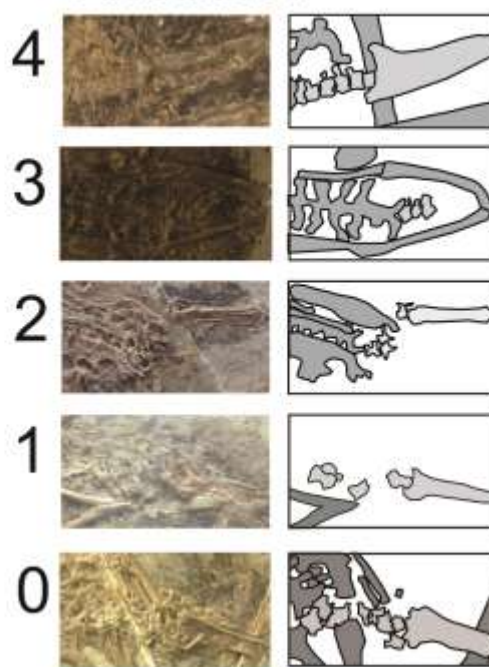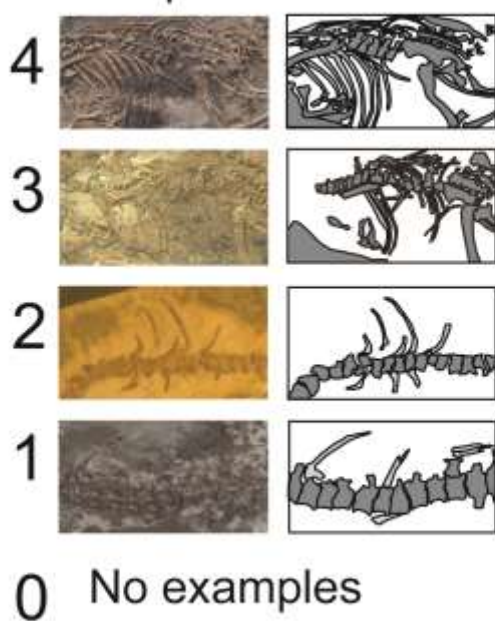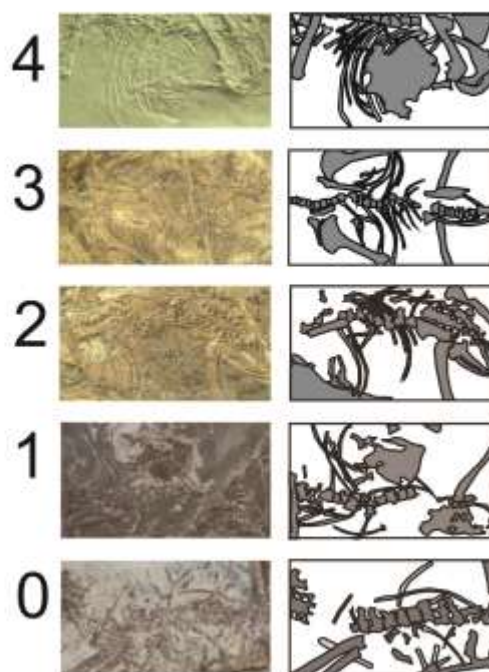
G Completeness   Articulation

4

3

2

1

0 No examples
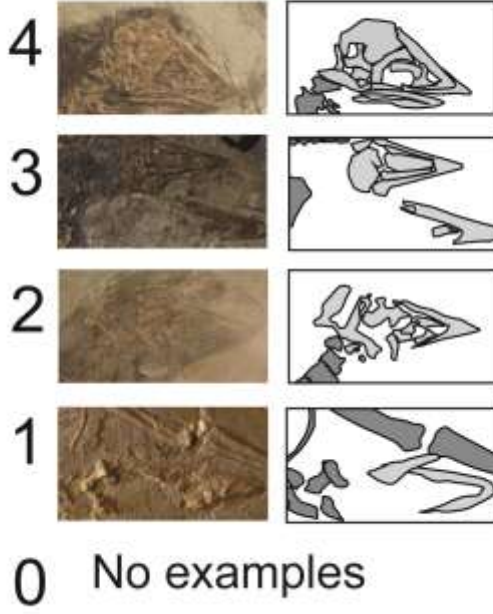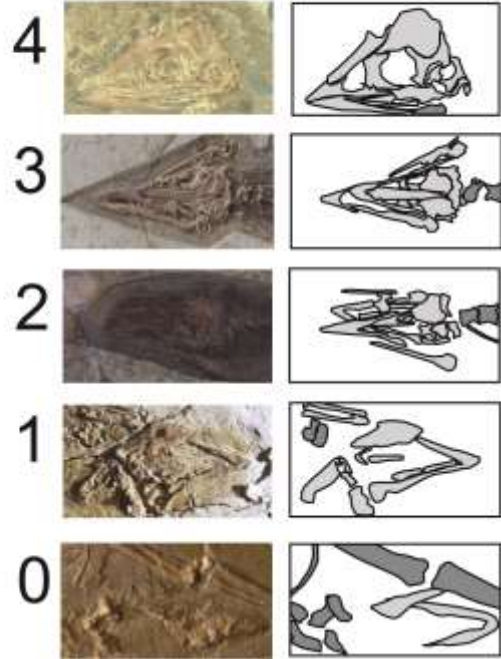
Figure 3.3

Scatterplot of completeness versus articulation for *Confuciusornis* (red) and

microraptorines (blue) and boundaries between each taphonomic trend indicated;

boxplots show the distribution of articulation and completeness scores.
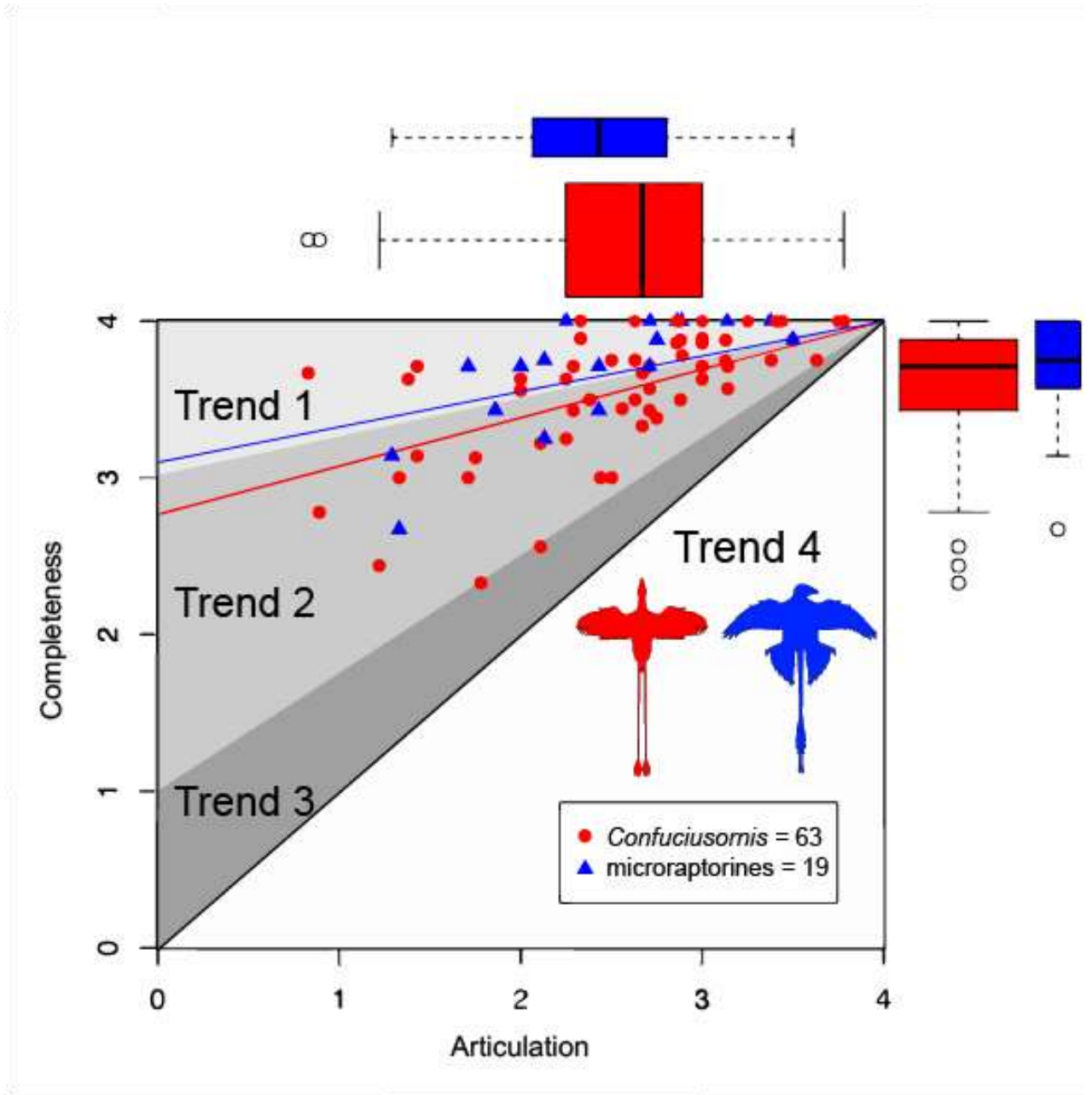
Figure 3.4

Outline drawing of the limbs of *Confuciusornis* and microraptorines, Each limb is divided into four sub-units, proximally to distally for the forelimb these are; the humerus, tibia and fibula, metacarples and the phalanges. For the hindlimb; the femur, tibia and fibula, metatarsals and the phalanges. There are also four points of articulation, for the forelimb; the shoulder, elbow, wrist and phalanges. For the hindlimb; the hip, knee, ankle and phalanges. Numbers of specimens in which each element is present and each joint is articulated are given.

Confusciusornis

Right forelimb n=57

Phalanges complete: 46
Metacarples complete: 52
Radius and ulna complete: 55
Humerus complete: 55
Wrist articulated: 41
Elbow articulated: 44
Shoulder articulated: 40
Phalanges articulated: 39

Left forelimb n=59

Humerus complete: 57
Radius and ulna complete: 57
Metacarples complete: 54
Phalanges complete: 44
Shoulder articulated: 40
Elbow articulated: 40
Wrist articulated: 41
Phalanges articulated: 39

Right hindlimb n=63

Phalanges complete: 61
Metatarsals complete: 63
Tibiia and fibula complete: 63
Femur complete: 61
Knee articulated: 36
Ankle articulated: 46
Phalanges articulated: 54
Hip articulated: 38

Left hindlimb n=62

Femur complete: 61
Tibiia and fibula complete: 58
Metatarsals complete: 57
Phalanges complete: 53
Knee articulated: 38
Hip articulated: 36
Ankle articulated: 43
Phalanges articulated: 48

microraptorines

Right forelimb n=20

Phalanges complete: 17
Metacarples complete: 17
Radius and ulna complete: 18
Humerus complete: 18
Wrist articulated: 13
Phalanges articulated: 15
Elbow articulated: 10
Shoulder articulated: 7

Left forelimb n=20

Metacarples complete: 13
Phalanges complete: 13
Humerus complete: 17
Radius and ulna complete: 16
Wrist articulated: 12
Shoulder articulated: 5
Elbow articulated: 12
Phalanges articulated: 14

Right hindlimb n=19

Phalanges complete: 18
Tibiia and fibula complete: 19
Femur complete: 19
Metatarsals complete: 18
Knee articulated: 12
Phalanges complete: 17
Hip articulated: 10
Ankle articulated: 14

Left hindlimb n=19

Femur complete: 18
Tibiia and fibula complete: 18
Phalanges complete: 17
Knee articulated: 13
Metatarsals complete: 18
Hip articulated: 8
Phalanges complete: 17
Ankle articulated: 15

Figure 3.5

Bubbleplots of articulation versus completeness in each of the nine skeletal units of *Confuciusornis*. Both articulation and completeness are scored from 0 to 4. The size of each circle is proportional to the number of specimens for that combination of articulation and completeness. Fit of the data to a linear (solid line) and non-linear (dashed line) trend line. Values beneath each plot are: Pearsons r-squared (R^2), accompanying p value, and intercept of the trend line with the y-axis (T), Spearman rank-order (rs) and Spearman rank p-value)

Right forelimb

Articulation

r^2 0.40; p 7.7x10⁻⁸; T 2.59
rs 0.68; p 1.4x10⁻⁸

Left forelimb

Articulation

r^2 0.42; p 1.3x10⁻⁸; T 2.50
rs 0.67; p 6.85x10⁻⁹

Right hindlimb

Articulation

r^2 0.08; 1.6x10⁻²; T 3.76
rs 0.28; p 2.48x10⁻²

Left hindlimb

Articulation

r^2 0.42; 8.3x10⁻⁵; T 2.64
rs 0.60; p 2.85x10⁻⁷

Cervical vertebrae

Articulation

r^2 0.22; 8.5x10⁻⁵; T 3.34
rs 0.38; p 2.45x10⁻³

Dorsal vertebrae

Articulation
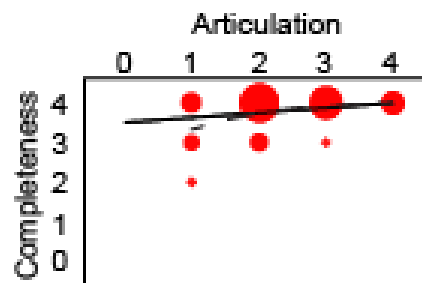
r^2 0.12; 8.4x10⁻³; T 3.49
rs 0.35; p 1.29x10⁻²

Caudal vertebrae
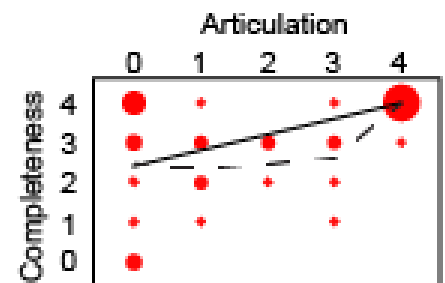
Articulation

r^2 0.19; 1.2x10⁻³; T 2.42
rs 0.48; p 5.73x10⁻⁴

Skull

Articulation

r^2 0.33; 1.1x10⁻⁷; T 2.82
rs 0.50; p 6.04x10⁻⁴

Ribs
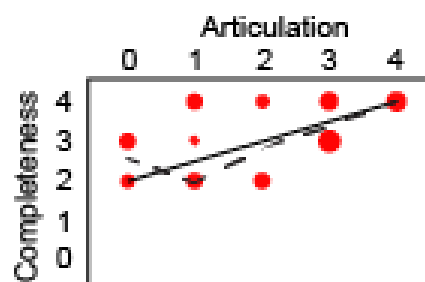
Articulation

r^2 0.36; 9.6x10⁻⁵; T 1.96
rs 0.67; p 1.68x10⁻⁵

Key

5   10   15   20   30

200

Figure 3.6

Bubbleplots of articulation versus completeness in each of the nine skeletal units of microraptorines. Both articulation and completeness are scored from 0 to 4. The size of each circle is proportional to the number of specimens for that combination of articulation and completeness. Fit of the data to a linear (solid line) and non-linear (dashed line) trend line. Values beneath each plot are: Pearsons r-squared (R^2) accompanying p value, and intercept of the trend line with the y-axis (T), Spearman rank-order (rs) and Spearman rank p-value.

Right forelimb

r² 0.35; p 3.3x10⁻³; T 2.49
rs 0.65; p 2.03x10⁻³

Left forelimb

r² 0.65; p 1.2x10⁻⁵; T 1.60
rs 0.78; p 4.78x10⁻⁵

Right hindlimb

r² 0.35; 1.6x10⁻²; T 3.34
rs 0.41; p 8.32x10⁻²

Left hindlimb

r² 0.58; p 8.3x10⁻⁵; T 2.46
rs 0.53; 1.93x10⁻²

Cervical vertebrae

r² 0.23; p 2.2x10⁻²; T 3.75
rs 0.40; p 8.71x10⁻²

Dorsal vertebrae

r² 0.08; p 1.00; T 3.63
rs 0.00; p 1.00

Caudal vertebrae

r² — ; p 2.0x10⁻²; T 4.00
rs — ; p 5.73x10⁻⁴

Skull

r² 0.22; p 1.6x10⁻²; T 3.06
rs 0.40; p 6.04x10⁻⁵

Ribs

r² 0.21; p 8.8x10⁻²; T 2.22
rs 0.54; p 1.68x10⁻⁵

Key

5   10   15   20   30

202
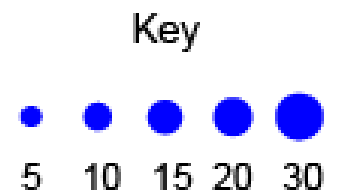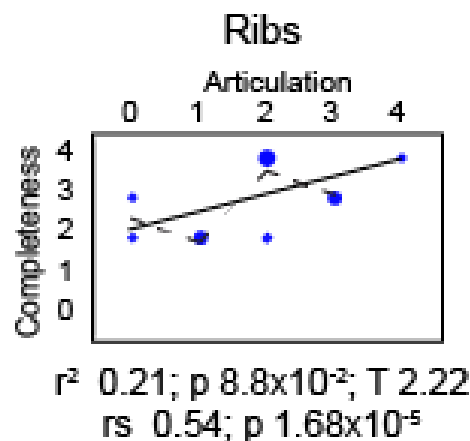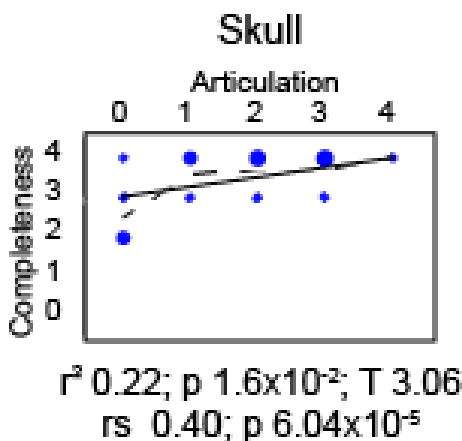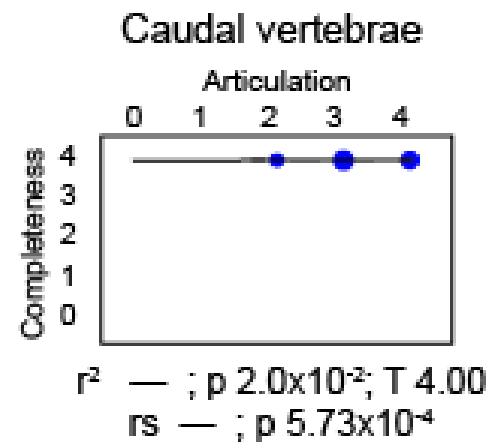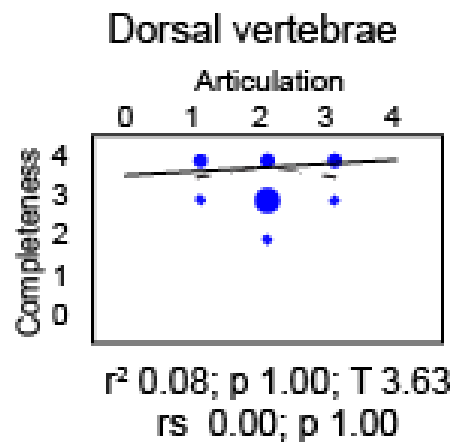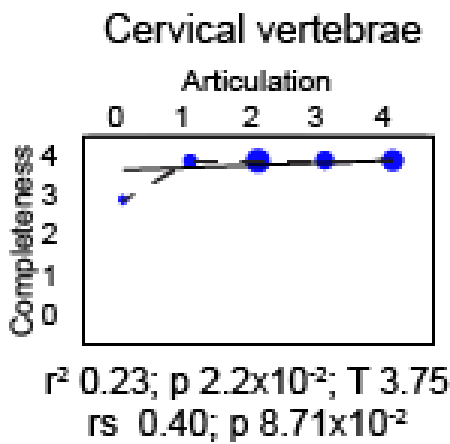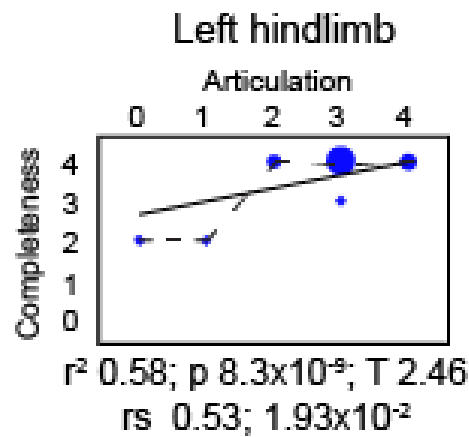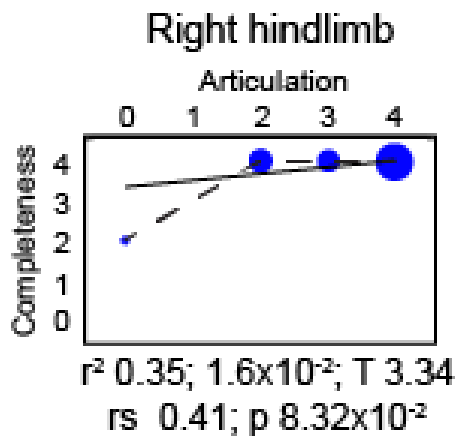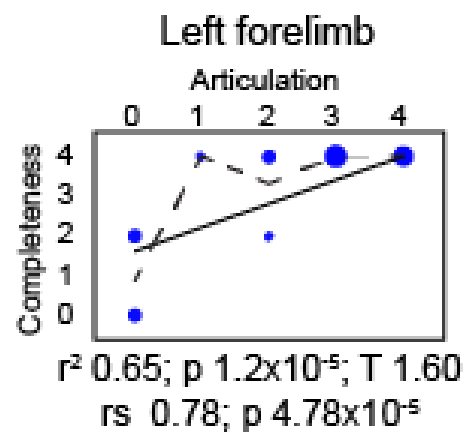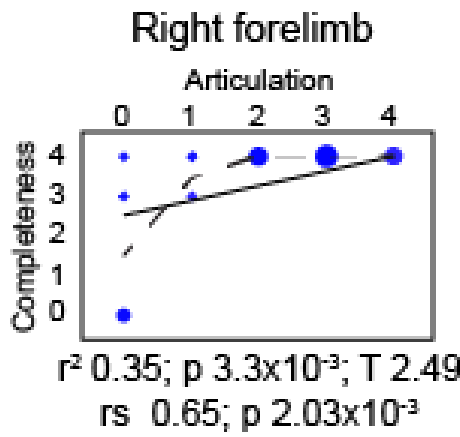
Figure 3.7

Limb tables for loss of completeness and disarticulation in*Confuciusornis* and microraptorines.. Each value represents the number of elements absent or points of articulation disarticulated in each of the five levels of completeness/articulation. Elements/articulations more commonly found present/articulated are highlighted in yellow, those more commonly found absent/disarticulated are highlighted in red. Abbreviations: ph—phalanges; met—metacarples/metatarsals; wr—wrist; ank—ankle; elb—elbow; kne—knee; sh—shoulder; hip—hip; r/u—radius/ulna; t/f—tibia/fibula; hu—humerus; fe—femur

Confuciusornis

COMPLETENESS

front right

	ph	met	r/u	hu	TOT
4	0	0	0	0	46
3	6	0	0	0	6
2	3	3	0	0	3
1	-	-	-	-	0
0	2	2	2	2	2

front left

	ph	met	r/u	hu	TOT
4	0	0	0	0	44
3	10	0	0	0	10
2	3	3	0	0	3
1	-	-	-	-	0
0	-	-	-	-	0

back right

	ph	met	t/f	fe	TOT
4	0	0	0	0	59
3	2	0	0	2	4
2	-	-	-	-	0
1	-	-	-	-	0
0	-	-	-	-	0

back left

	ph	met	t/f	fe	TOT
4	0	0	0	0	52
3	4	0	1	0	5
2	2	2	0	0	2
1	2	2	2	0	2
0	1	1	1	1	1

ARTICULATION

front right

	ph	wr	elb	sh	TOT
4	0	0	0	0	28
3	4	4	2	6	10
2	5	5	2	2	7
1	4	2	3	3	4
0	7	7	7	7	7

front left

	ph	wr	elb	sh	TOT
4	0	0	0	0	23
3	3	2	3	5	13
2	6	5	4	5	10
1	5	4	3	3	5
0	7	7	7	7	7

back right

	ph	ank	kne	hip	TOT
4	0	0	0	0	18
3	1	1	11	9	22
2	2	7	6	7	12
1	3	6	6	6	7
0	2	2	2	2	2

back left

	ph	ank	kne	hip	TOT
4	0	0	0	0	21
3	2	3	7	6	17
2	4	4	6	8	11
1	2	6	6	7	8
0	5	5	5	5	5

microraptorines

COMPLETENESS

front right

	ph	met	r/u	hu	TOT
4	0	0	0	0	16
3	1	1	0	0	2
2	-	-	-	-	0
1	-	-	-	-	0
0	2	2	2	2	2

front left

	ph	met	r/u	hu	TOT
4	0	0	0	0	13
3	-	-	-	-	0
2	3	3	0	0	3
1	1	1	1	0	1
0	3	3	3	3	3

back right

	ph	met	t/f	fe	TOT
4	0	0	0	0	18
3	-	-	-	-	0
2	1	1	0	0	1
1	-	-	-	-	0
0	-	-	-	-	0

back left

	ph	met	t/f	fe	TOT
4	0	0	0	0	16
3	1	0	0	0	1
2	1	1	1	1	2
1	-	-	-	-	0
0	-	-	-	-	0

ARTICULATION

front right

	ph	wr	elb	sh	TOT
4	0	0	0	0	4
3	1	1	3	5	7
2	0	1	4	3	4
1	1	2	1	2	2
0	4	4	4	4	4

front left

	ph	wr	elb	sh	TOT
4	0	0	4	0	4
3	0	0	0	6	6
2	1	2	1	2	4
1	1	0	0	0	1
0	5	5	5	5	5

back right

	ph	ank	kne	hip	TOT
4	0	0	0	0	6
3	0	0	0	4	4
2	1	4	5	4	7
1	-	-	-	-	0
0	1	1	1	1	1

back left

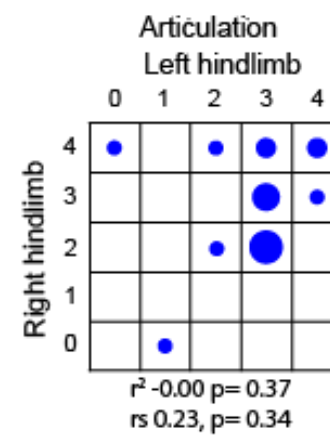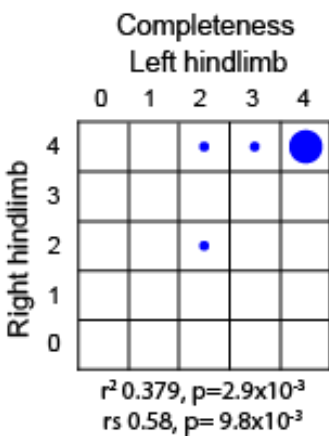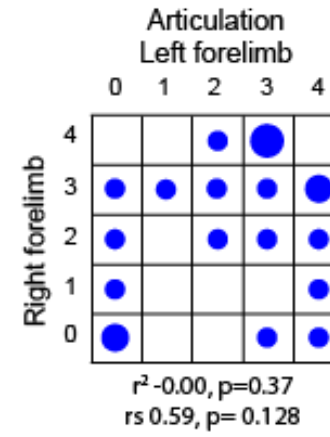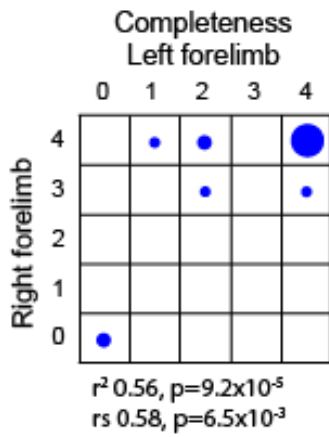|	ph	ank	kne	hip	TOT
4	0	0	0	0	2
3	1	1	4	7	13
2	0	1	1	2	2
1	0	1	1	1	1
0	1	1	1	1	1

Figure 3.8

Paired appendage bubble plots for *Confuciusornis* (red), and microraptorines (blue).

Confuciusornis

Completeness
Left forelimb

r² 0.45, p=8x10⁻⁸
rs 0.45, p=0.001

Articulation
Left forelimb

r² 0.22, p=0.11
rs 0.08, p= 2.5x10⁻²

Completeness
Left hindlimb

r² 0.02, p=0.79
rs 0.04, p= 0.73

Articulation
Left hindlimb

r² 0.15, p=0.001
rs 0.436, p= 6.1x10⁻⁴

microraptorines

Completeness
Left forelimb

r² 0.56, p=9.2x10⁻⁵
rs 0.58, p=6.5x10⁻³

Articulation
Left forelimb

r² -0.00, p=0.37
rs 0.59, p= 0.128

Completeness
Left hindlimb

r² 0.379, p=2.9x10⁻³
rs 0.58, p= 9.8x10⁻³

Articulation
Left hindlimb

r² -0.00 p= 0.37
rs 0.23, p= 0.34

206

Figure 3.9

Scatterplot of completeness versus articulation for specimens of *Confuciusornis* (A) and microraptorines (B) in different orientations, with corresponding linear trend lines forced through the taphonomic origin. Non-linear trend lines are fitted to each taxon in each orientation (C), from left to right: *Confuciusornis* dorsoventral, *Confuciusornis* oblique, *Confuciusornis* lateral, microraptorines dorsoventral, microraptorines oblique, microraptorines lateral. Orientations: dorsoventral—sagittal plane perpendicular to bedding plane; oblique—sagittal plane perpendicular to bedding plane with slight tilt to the right or left; lateral —sagittal plane parallel to the bedding plane.

A

B

C

Confuciusornis   microraptorines
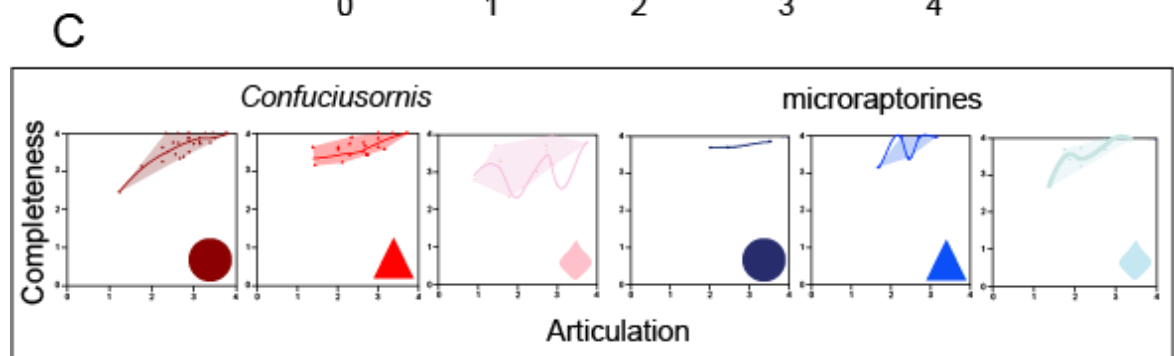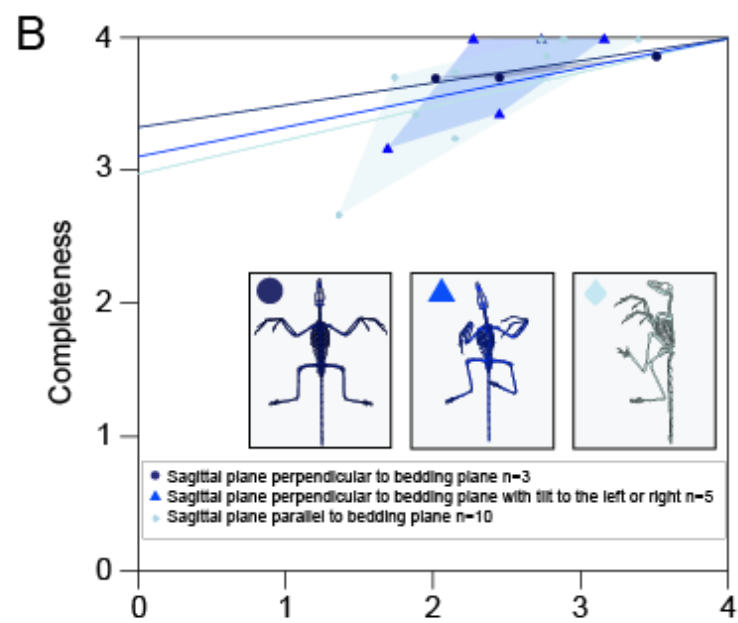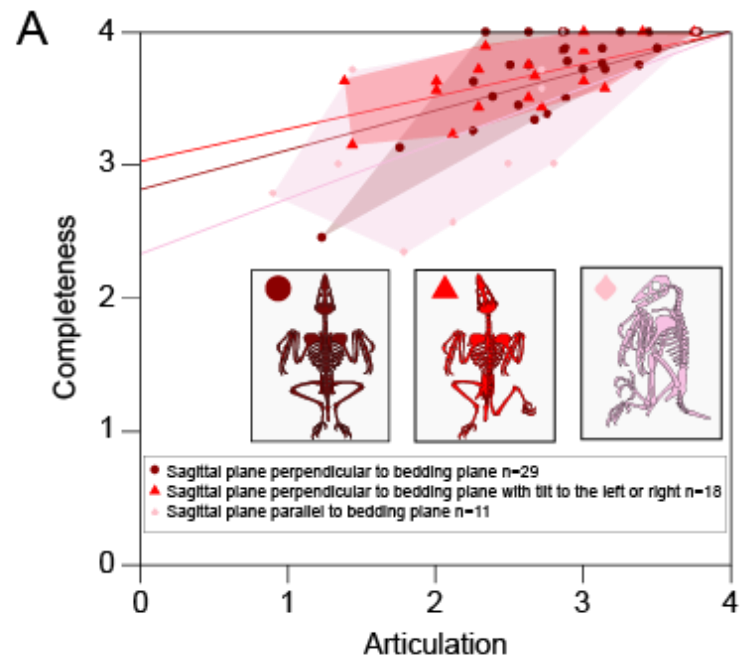
Figure 3.10

(A) Scatterplot of intra-unit articulation versus inter unit articulation (IUA) for specimens of *Confuciusornis* (red) and microraptorines (blue). Values beneath each plot are: Pearsons r-squared (R^2), intercept of the trend line forced through taphonomic origin at (1,4) with the y-axis (T), Spearman rank-order (rs) and Spearman rank p-value (p).

(B and C) Bar plots representing the frequency of each IUA score for each IUA point for *Confuciusornis* (B) and microraptorines (C). Abbreviations: rfl-a—right forelimb-axial skeleton; lfl-a—left forelimb axial skeleton; rhl-a—right hindlimb-axial skeleton; lhl-a—left hindlimb-axial skeleton; s-cv—skull-cervical vertebrae; cv-d—cervical vertebrae-dorsal vertebrae; d-cu—dorsal vertebrae-caudal vertebrae.

A
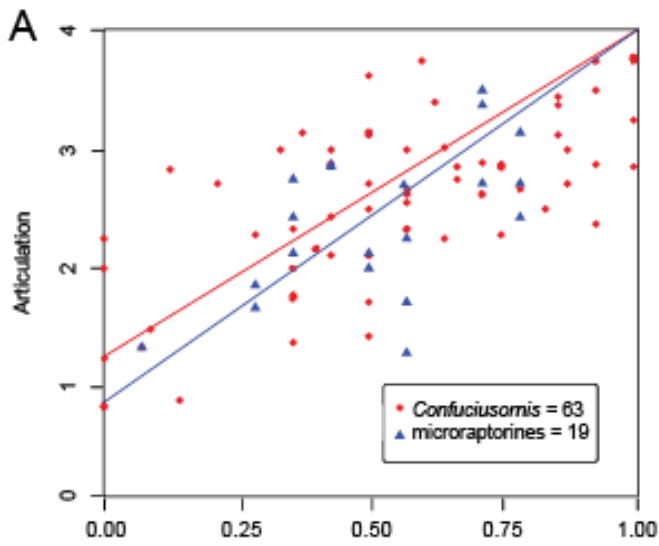
Confusciusornis: r² 0.43; p 3.2x10-9; T 1.14; rs 0.61; p 1.22x10⁻⁷
microraptorines: r² 0.29; p 8.4x10-3; T 0.74; rs 0.48; p 6.91x10⁻²

B

C
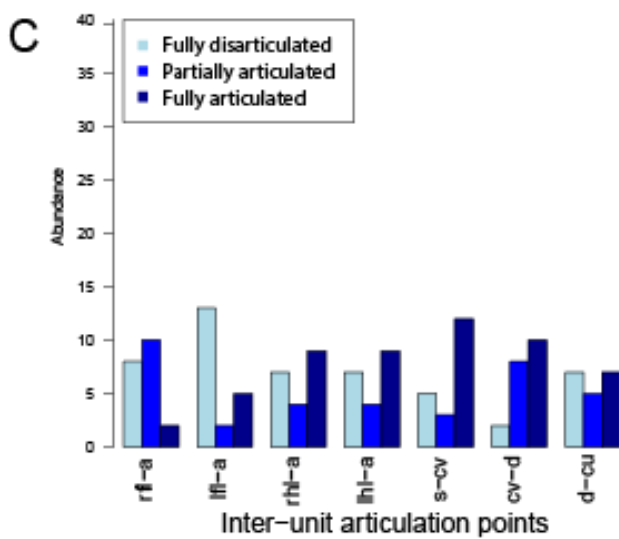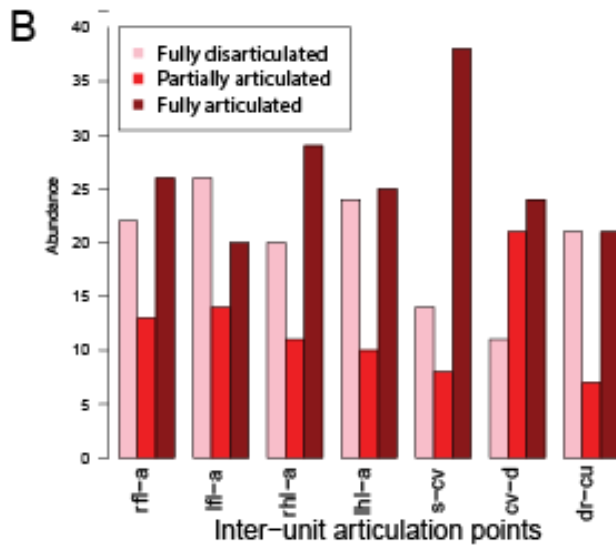
Figure 3.11

Representative diagram of the analysis of inter unit articulation scores (IUA) (A).

Example inter-unit articulation data set is separated into two groups. Each specimen is

represented by a box; (1) specimens with disarticulated rfl-a and (2) specimens with

disarticulated s-cv. The units that have become disarticulated are highlighted in red.

Boxes highlighted in blue are specimens shared between both groups. The percentage

of each group that have both IUA disarticulated is expressed underneath the

highlighted specimens. A Venn-diagram demonstrates how specimens with both units

disarticulated are shared between both groups and the different proportions they

contribute to those groups. Bubble plots (B–E) representing the co-occurrence of two

points of articulation between units scored the same in a single specimen;

Confuciusornis inter-unit disarticulation (B), *Confuciusornis* inter-unit articulation (C)

microraptorines inter-unit disarticulation (D) and microraptorines inter-unit

disarticulation (E). The radius of each circle represents the percentage of $1°$ found

alongside $2°$ in the same specimen. Abbreviations: rfl-a—right forelimb-axial

skeleton; lfl-a—left forelimb axial skeleton; rhl-a—right hindlimb-axial skeleton; lhl-

a—left hindlimb-axial skeleton; s-cv—skull-cervical vertebrae; cv-d—cervical

vertebrae-dorsal vertebrae; d-cu—dorsal vertebrae-caudal vertebrae.
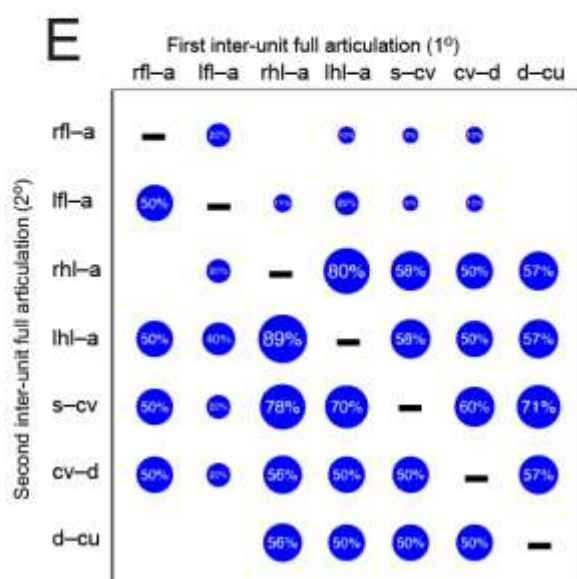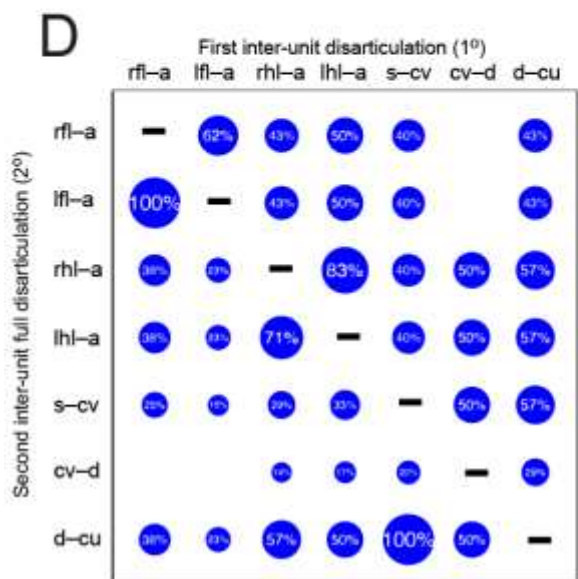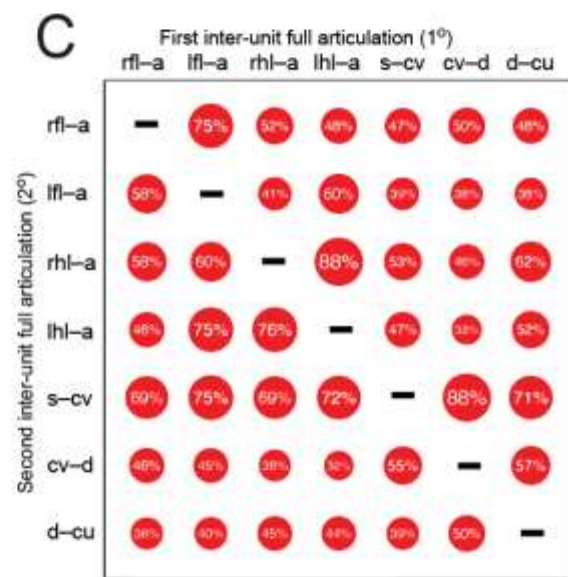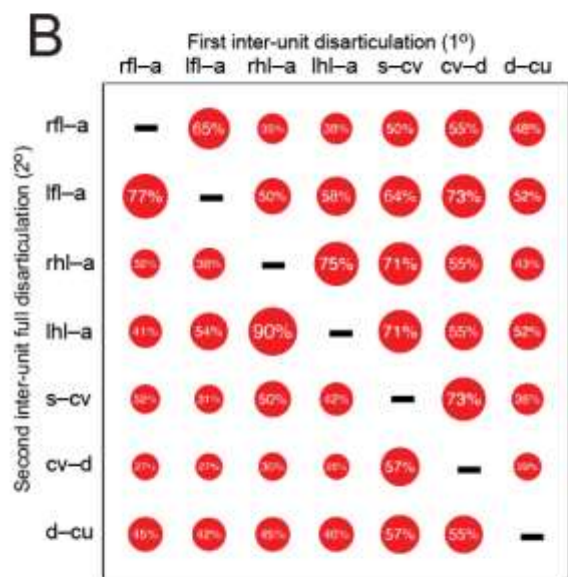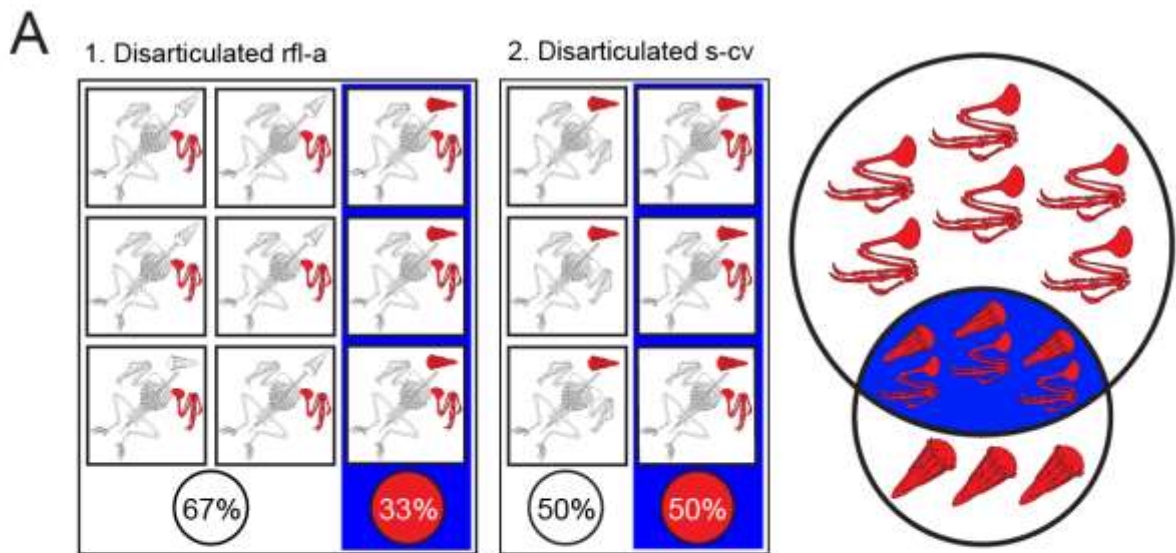
Figure 4.1

Schematic illustrations of the structure of the integument and underlying muscle in reptilians and avians and the underlying musculature. A; Graphic cross section through the integument of A; a gecko showing the outer scale surface and hinge region of the scale, B; a zebra finch showing feather support structures. e; epidermis, d; dermis, s; subcutis, m; muscle, C; branching indicating how the four tissue categories are composed of a variety of tissue components. Colour of each component relates to the colours in A and B.
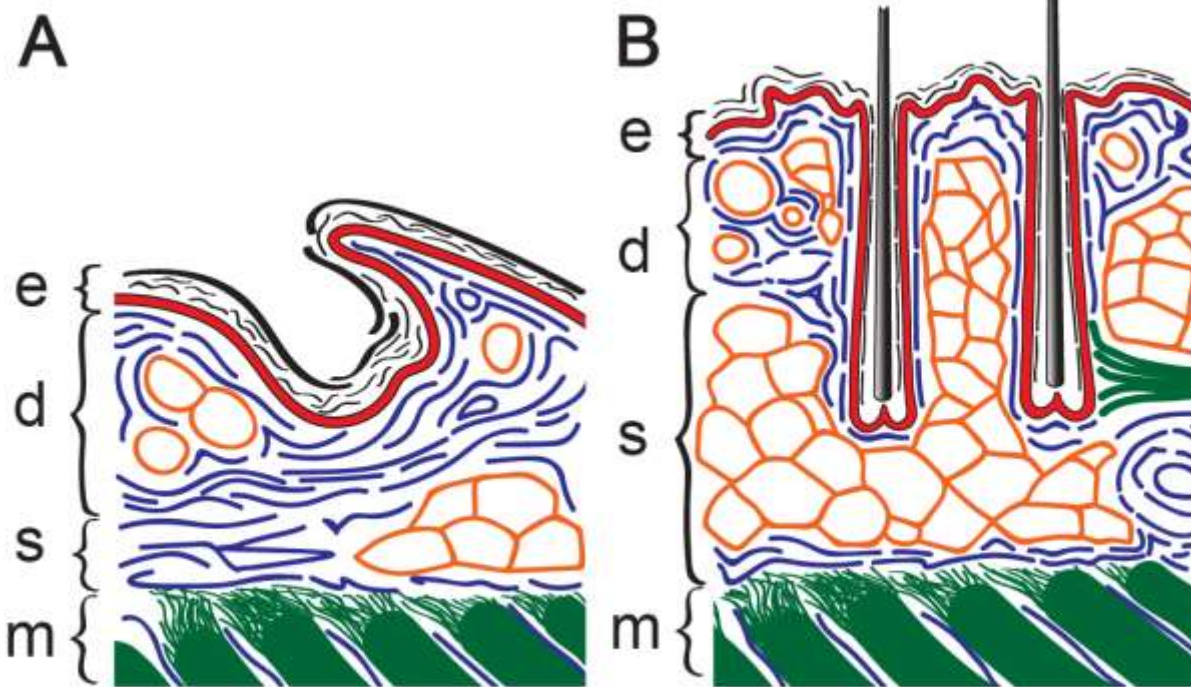
Figure 4.2

Light microscope images of fresh and decayed epidermis and dermis of zebra finches (A–D), feathers (E–H), adipose tissue (I–M), muscle (N–Q) and gecko epidermis, dermis (R–U). Decay stage of tissue in each image indicated. Scale bars equal 100.

A	Fresh	B	Stage one	C	Stage two	D	Stage three
E	Fresh	F	Stage one	G	Stage two	H	Stage three
I	Fresh	J	Stage one	K	Stage two	L	Stage three	M	Stage four
N	Fresh	O	Stage one	P	Stage two	Q	Stage three
R	Fresh	S	Stage one	T	Stage two	U	Stage three
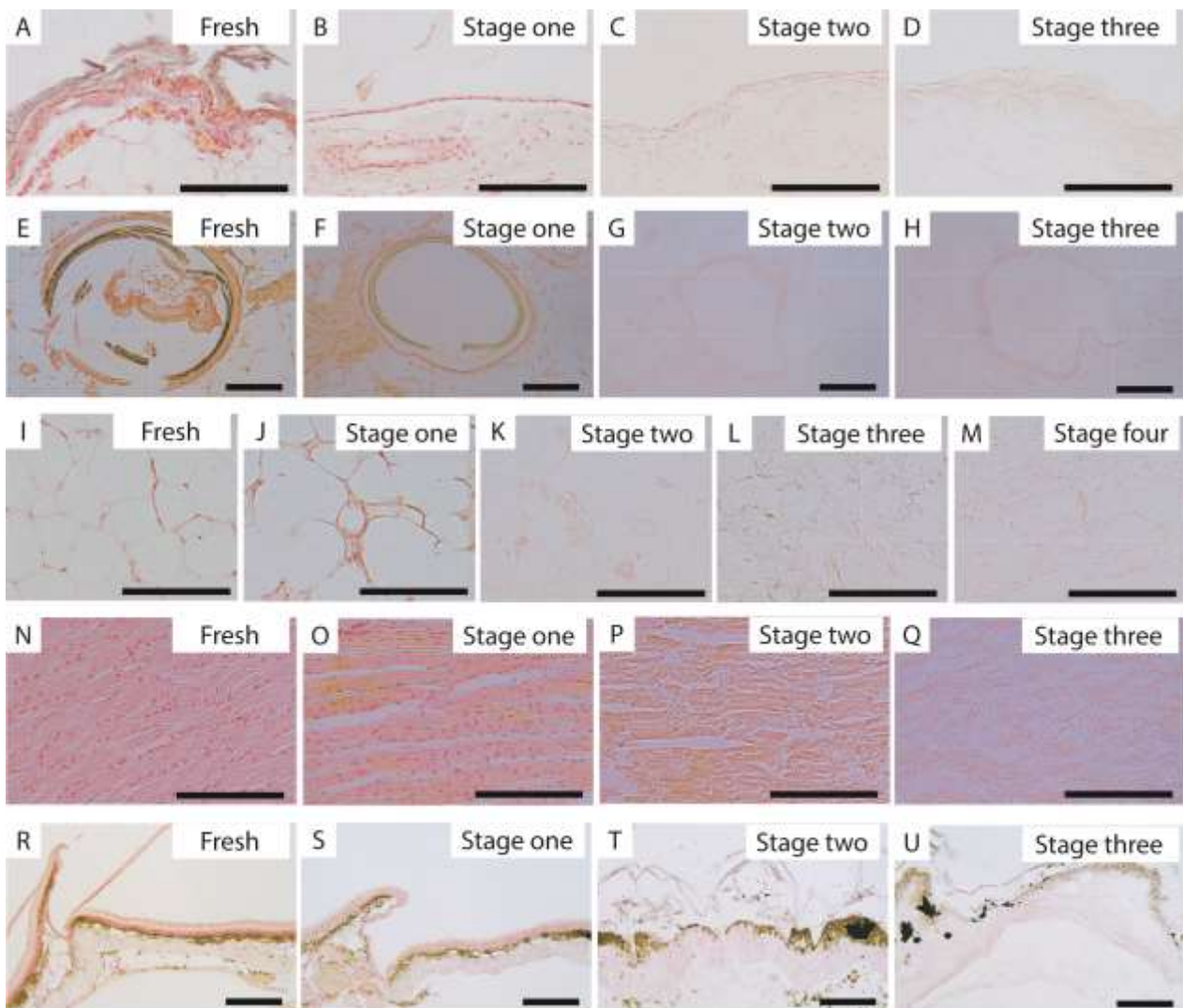
Figure 4.3

SEM images of keratinocytes *in situ* (A–C), fractures in the surface of epidermis at

lower magnifications in later stages of decay (D–F) and keratinocytes trapped within

the barbs and barbules of feathers (G–J).
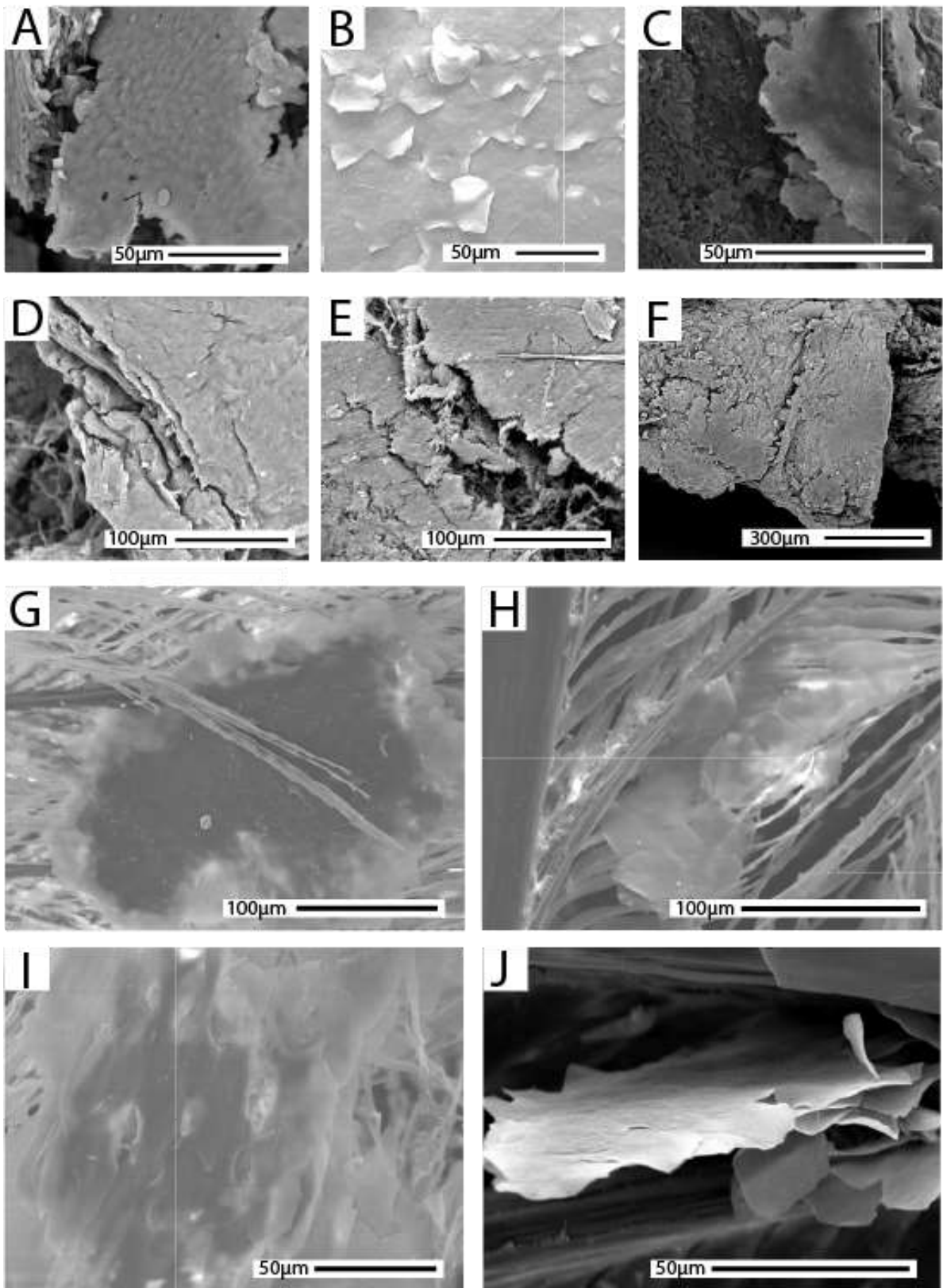
Figure 4.4

Diagrammatic representations of the observed decay stages of the different tissue categories in avian and reptilian integument. Examples of fresh tissue are at the top from left to right; (A) zebra finch epidermis and dermis in cross section, (B) feather in transverse section, (C) transverse view of muscle fibres and (D) gecko integument. (E–L) Successive decay stages (vertically arranged) for left to right; zebra finch epidermis and dermis in cross section (E), fully developed (F) and undeveloped (G) zebra finch feathers and support structures, zebra finch adipocytes bound with (H) and without collagen fibers (I), zebra finch muscle in transverse (J) and longitudinal views (K) and gecko epidermis and dermis in cross section (L). The decay sequence for zebra finch feathers is shown with the presence of developed feathers and with undeveloped feathers and from decay stage one to three with the removal of the feather. Tissue componen abbreviations; A: adipocytes; C: collagen fibers; Ch: chromatophores; En: endomysium; Ep: epimysium; Fm: dermal feather muscle fibers; Fr: feather rachis; Me: Melanophores; Mf: muscle fiber; My: myofibrils; Sc: stratum corneum; Sg; stratum germinativum.

A

Sc Sg C

B

C Sg Sc Fr Fm

C

Mf My En Ep

D

Sc A Ch Me Sg C

E

F

G

H

I

J

K

L
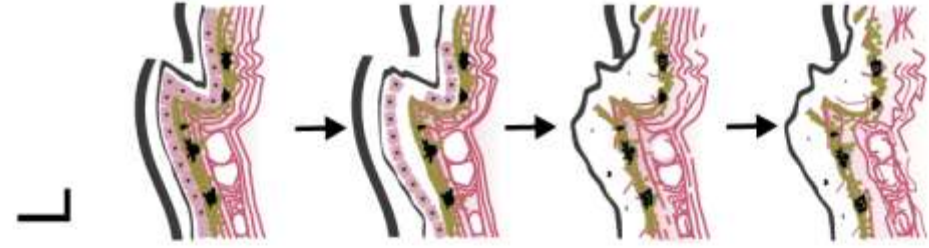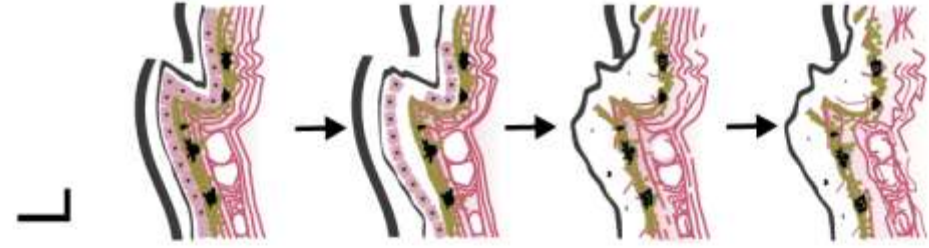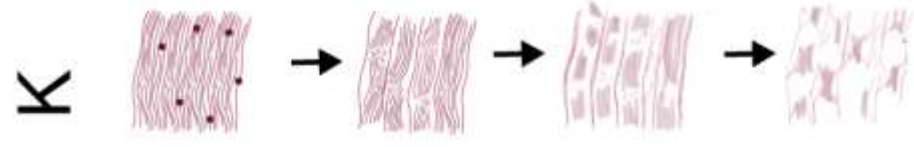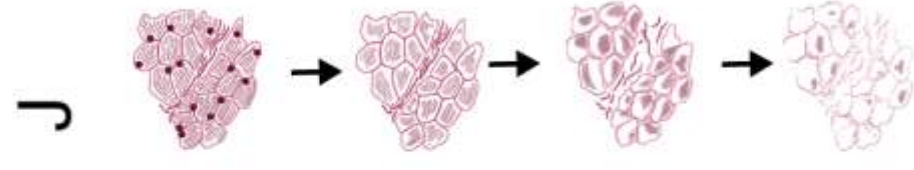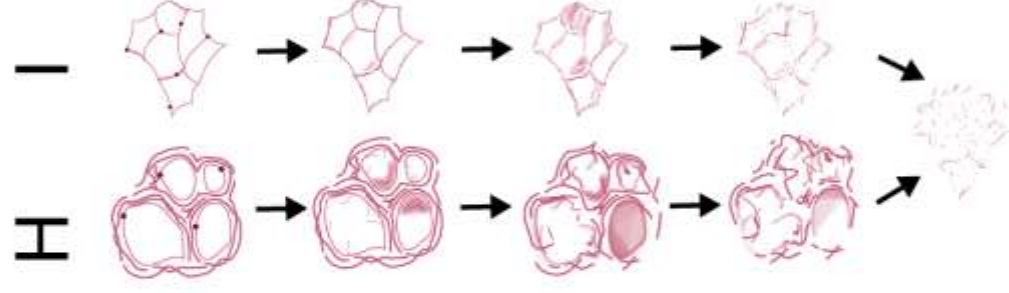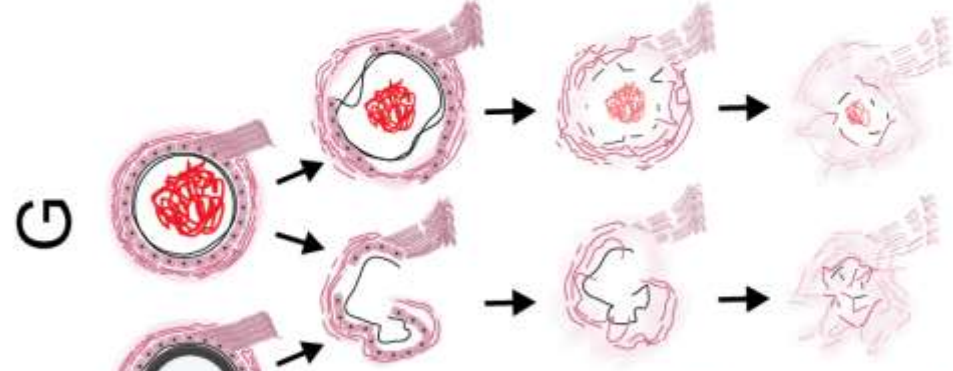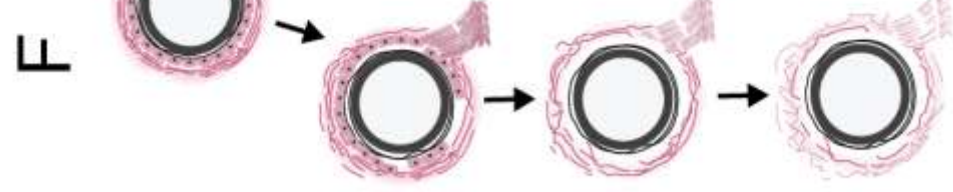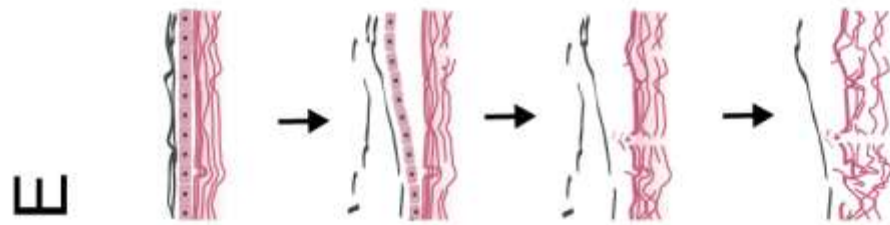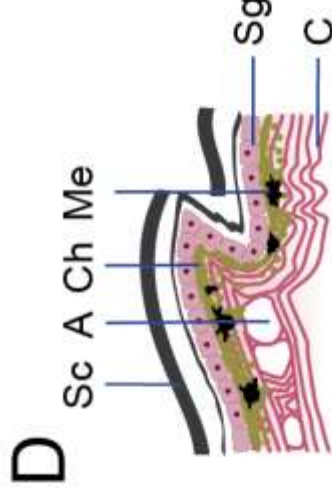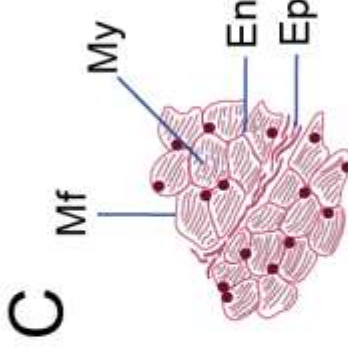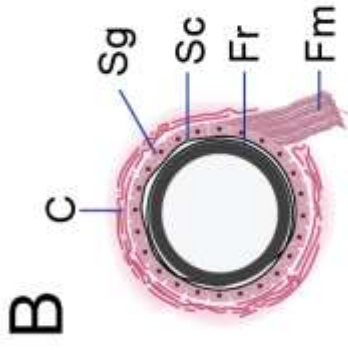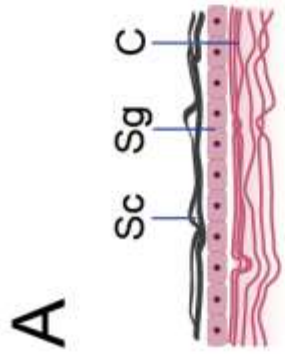
Figure 4.5

(A) Plot of decay stage versus sampling point for four tissue categories of finch skin; epidermis and dermis, adipose tissue, skeletal muscle, feathers and also for gecko skin. Each cell represents a sample of tissue. Each cell is color coded with the average value for the replicates indicated. Numbers in cell indicates decay stage for each replicate, letters in parentheses refer to the individual finch (F–N) or gecko (B–J) the sample was taken from. The number of replicates can vary between tissues and sampling point.

(B) Stacked histograms demonstrating the distribution of decay stages among total sampling points for individual finches (F–N) and geckos (B–J).
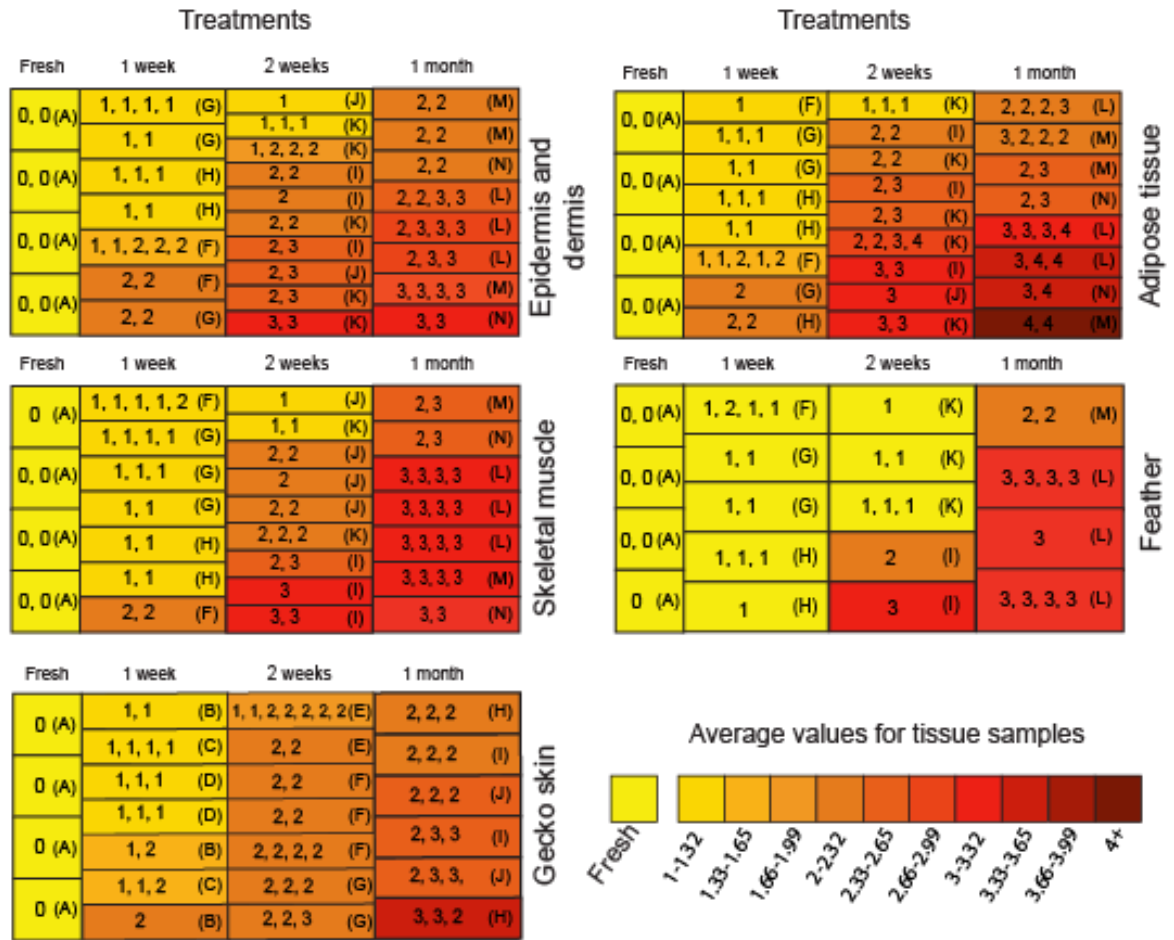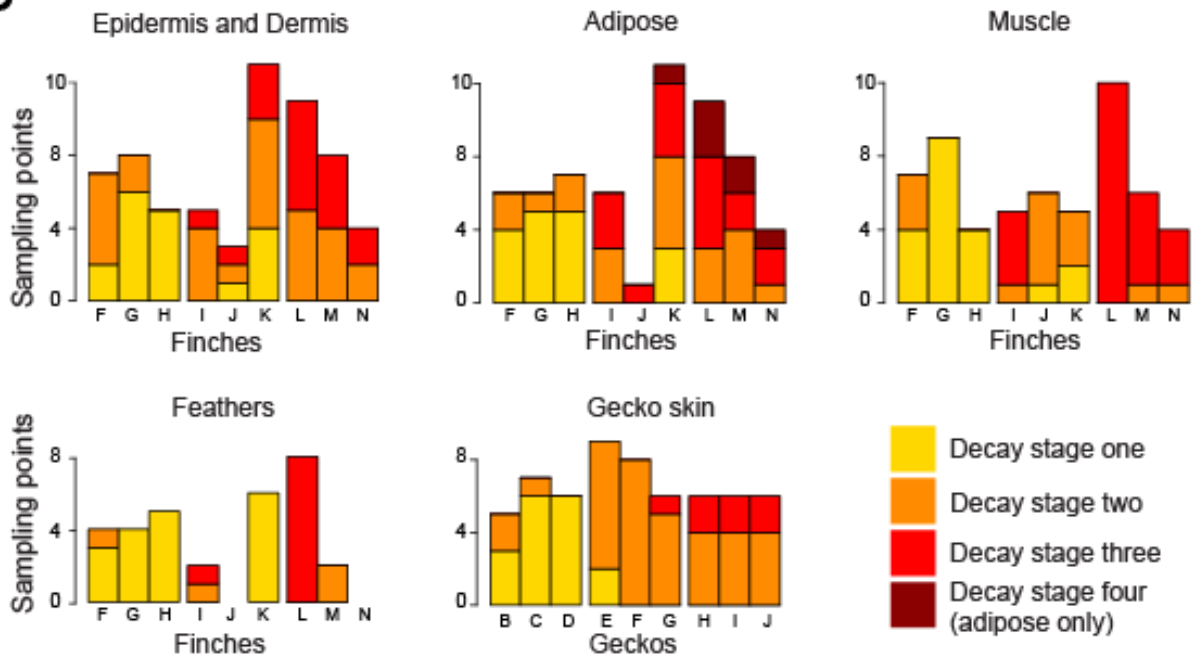
Figure 4.6

Boxplots demonstrating changes in the dimensions of tissue categories and components, revealing the general trend of the data. Change in thickness of dermis in zebra finch pterylae (A), change in thickness of dermis in zebra finch apterylae (B), change in muscle fiber diameter (C), change in area occupied by muscle tissue (D), change in thickness of dermis in gecko skin (E), change in thickness of pigmented layer in gecko dermis (F). Colored data points indicate the contribution of each individual finch (Q, F–N) and gecko (A–J) to each decay stage demonstrating how the range of measurements for each individual in each decay stage overlap with ranges of other individuals.

A

B

C

D

E

F

Finch Q

Finch F
Finch G
Finch H

Finch I
Finch J
Finch K

Finch L
Finch M
Finch N

Gecko A
Gecko B
Gecko C
Gecko D

Gecko E
Gecko F
Gecko G

Gecko H
Gecko I
Gecko J

224
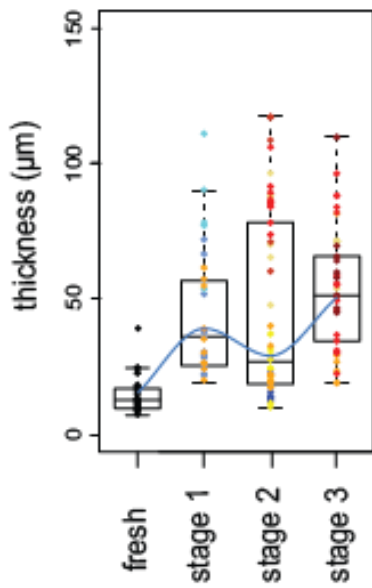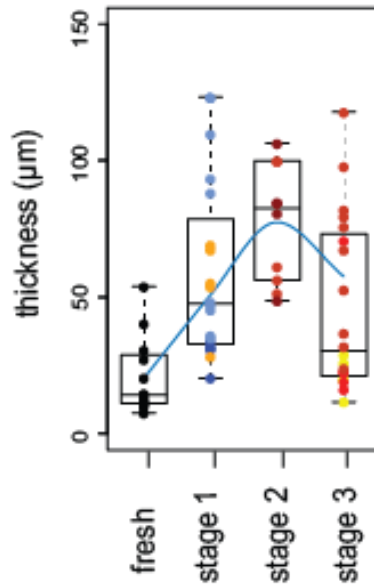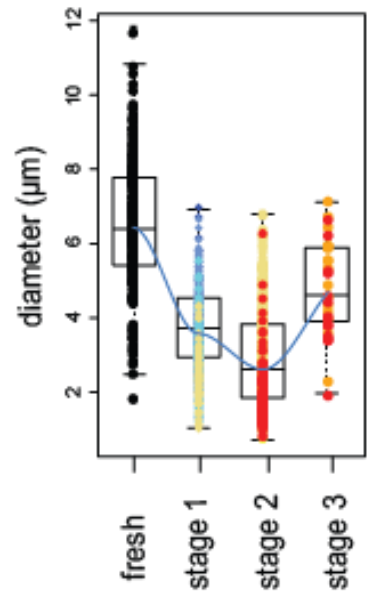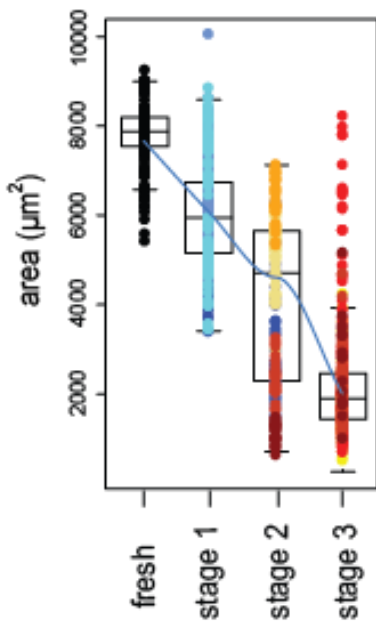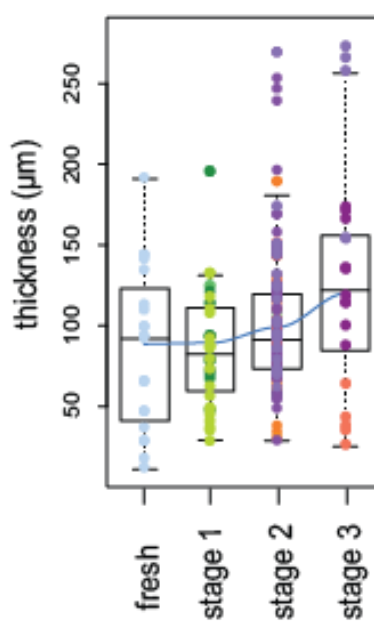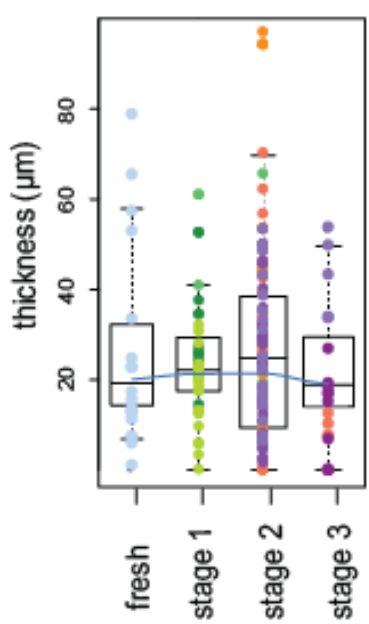
Figure 4.7

Schematic representation of the tissue components in bird skin available for preservation when relative tissue categories are fresh (A), at decay stage one (B), at decay stage two (C) and at decay stage three (D). Dashed stratum corneum represents its absence locally.

A Fresh tissue
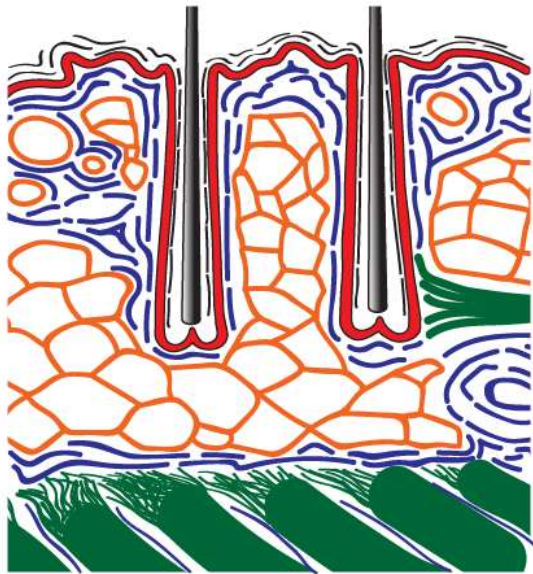
B Decay stage one
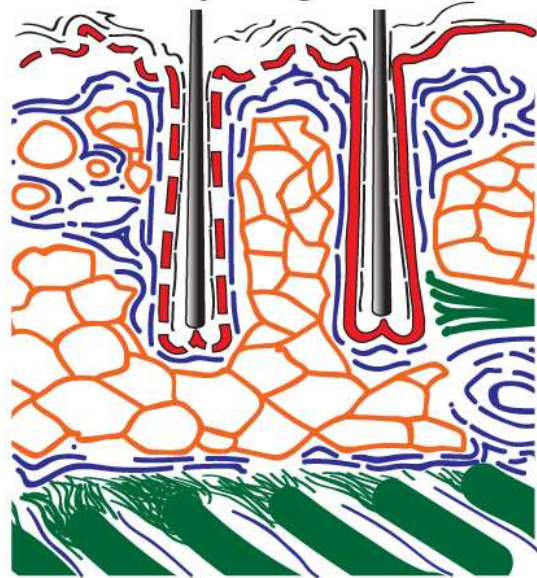
C Decay stage two

D Decay stage
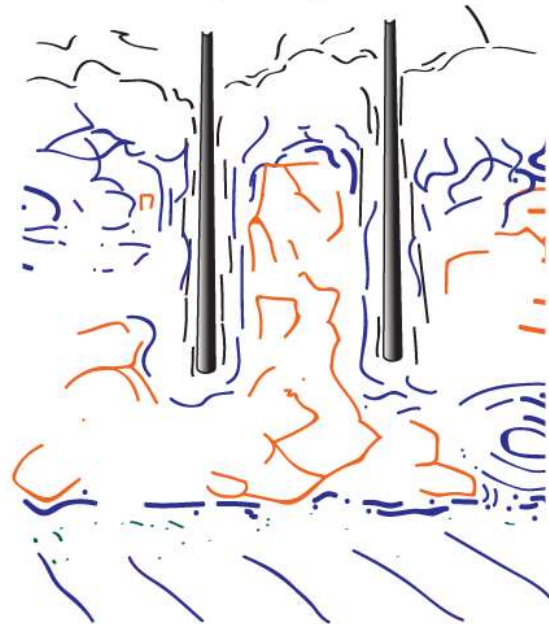
KERATIN FIBERS

FEATHERS

STRATUM GERMINATIVUM

COLLAGEN FIBERS

ADIPOCYTES

MUSCLE FIBERS

Figure 5.1

Selection of SEM images of fresh and decayed zebra finch integument. (A) Fresh

epidermis, (B) keratinocytes in a four week decayed epidermis, (C) one week decayed

muscle tissue, (D) four weeks decayed feather projecting from epidermis and dermis.

Scale bars equal to 200 µm.
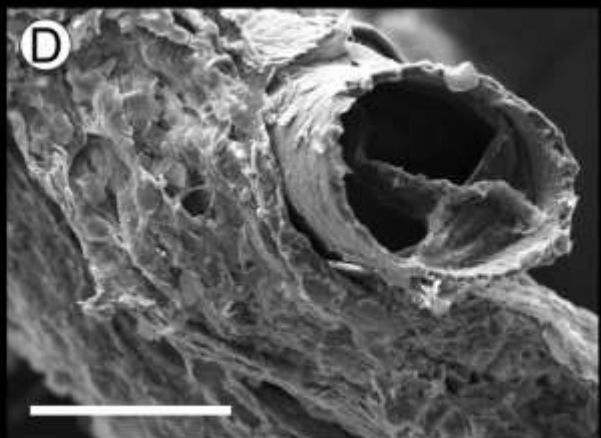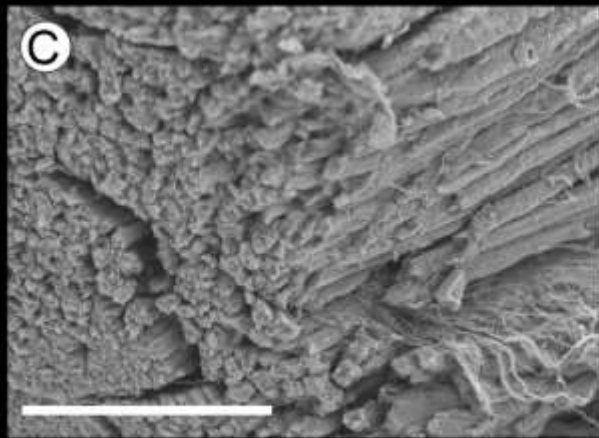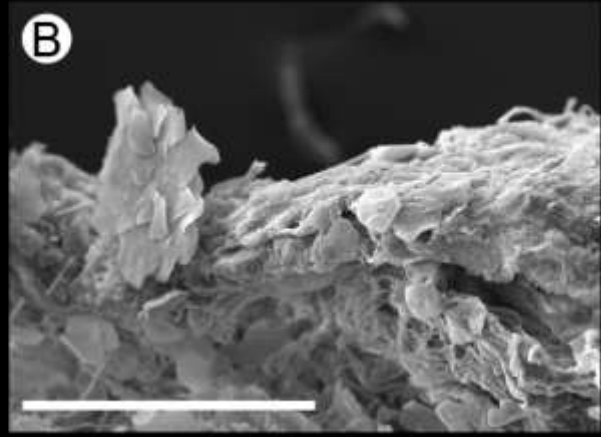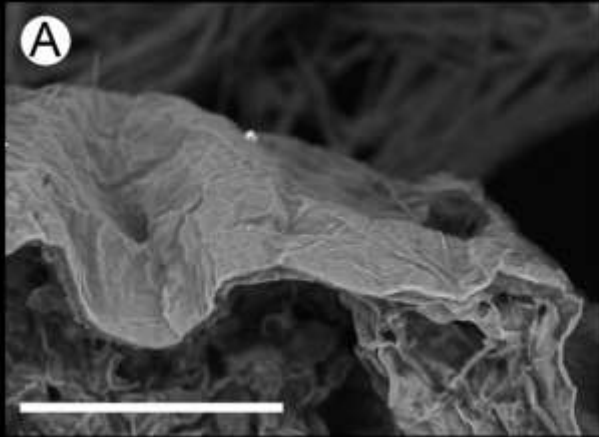
Figure 5.2

Photomicrographs of fresh and decayed zebra finch tissues stained using fontanna masson. (A) Transverse view of developing feather demonstrating tissue specific staining of melanin rich tissues in feather barbs and barbules (black) and adipose, collagen and muscle (red). (B) Transverse view of muscle fibres. (C) Longitudinal view of decayed muscle fibres demonstrating reduced effectiveness of histological stains compared to (D) longitudinal view of fresh muscle fibres. Scale bars equal to 100 µm.
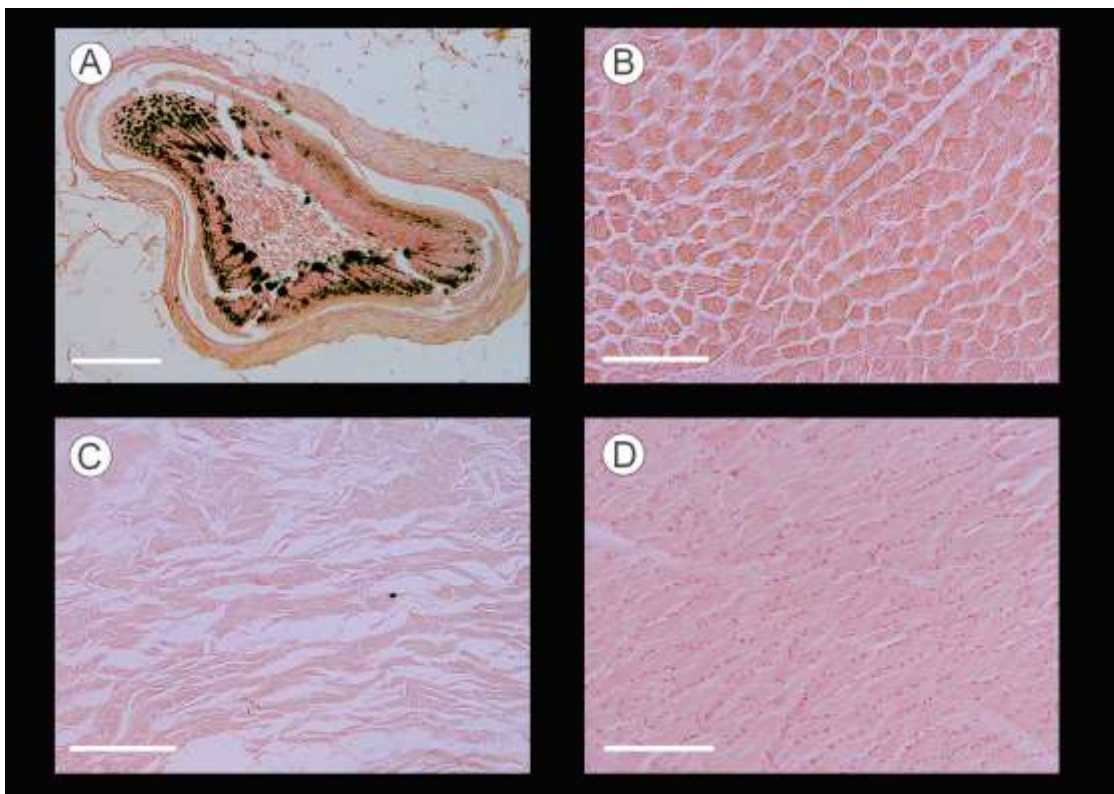
Figure 5.3

Micro-CT produced thin sections of muscle tissue sampled at different points in the

decay process; fresh (A, B), two weeks of decay (C, D) and four weeks of decay (E,

F) superimposed over exposed internal surfaces of volume renderings in different

orientations; lateral (A, C, E) and transverse (B, D, F). Scale bars equal to 1 mm.
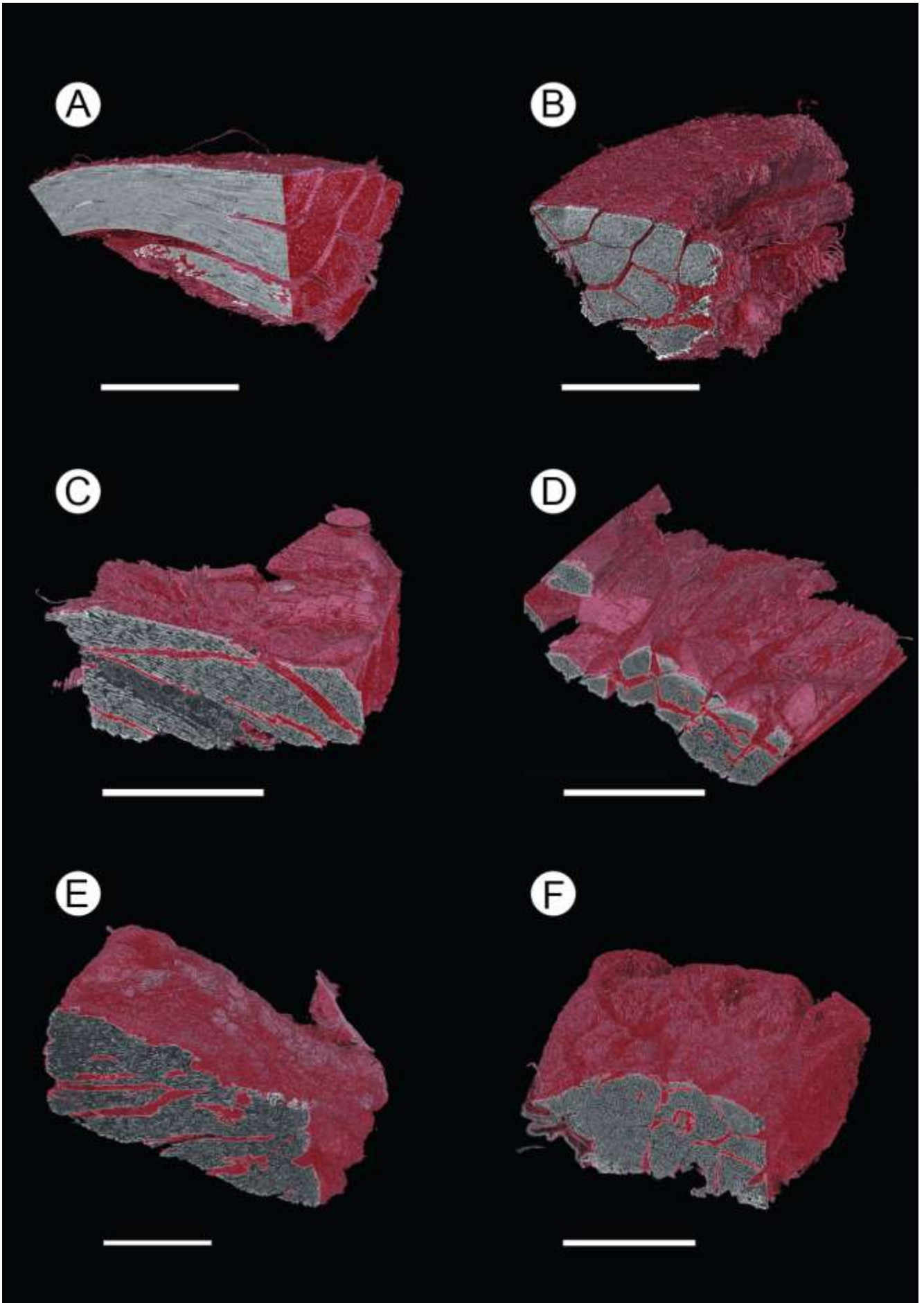
Figure 5.4

Slices of micro-CT data (A, C, E), and volume renderings (B, D, F) of zebra finch

skin at different points in the decay process; fresh (A, B), two weeks of decay (C, D)

and four weeks of decay (E, F). Key a; adipose, e; epidermis, f; feather, m; feather

muscle. Scale bars equal to 1 mm.
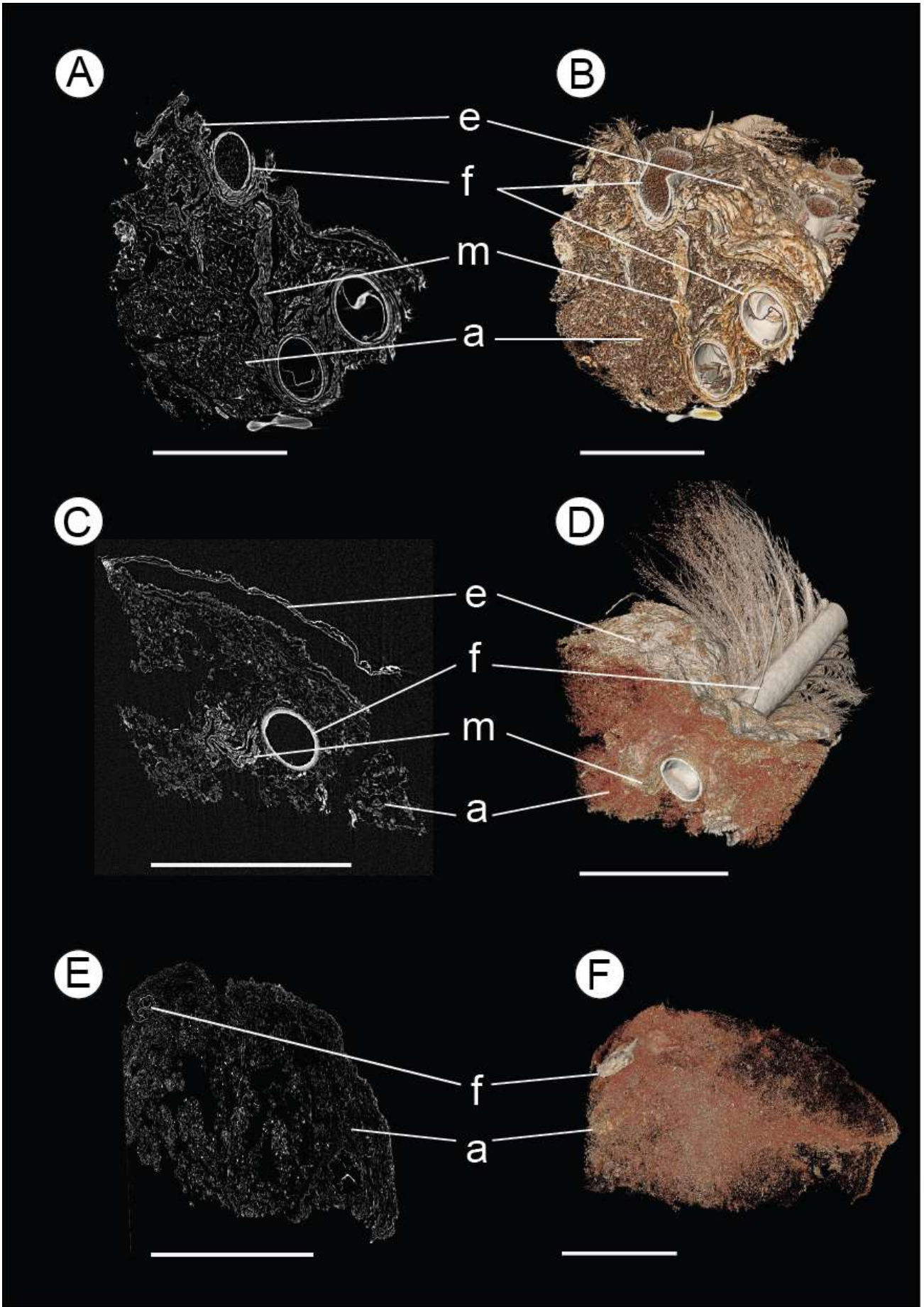
Figure 5.5

Cubes of segmented adipose tissue at different points in the decay process; (A) Fresh, (B) two weeks of decay and (C) four weeks of decay. Purple; exterior 2D surface. Pink; interior 3D surface. Scale bars equal to 100 µm.

A Undecayed adipose tissue

3D data

2D data
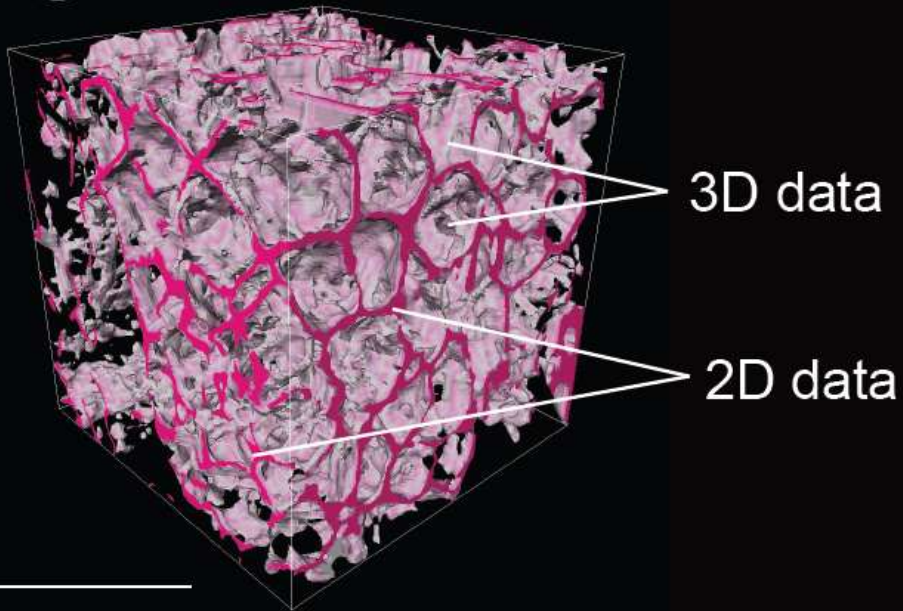
B 2 weeks decayed

C 4 weeks decayed

236
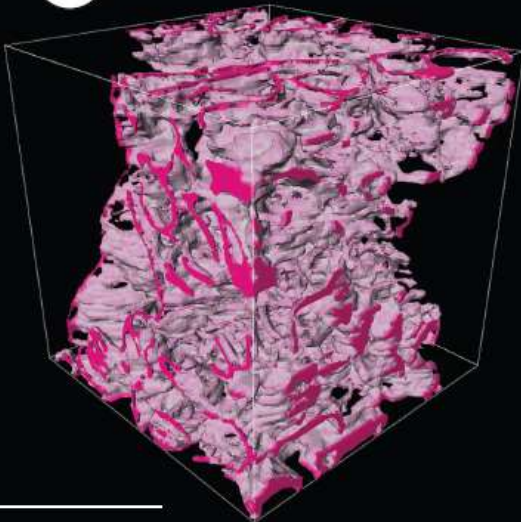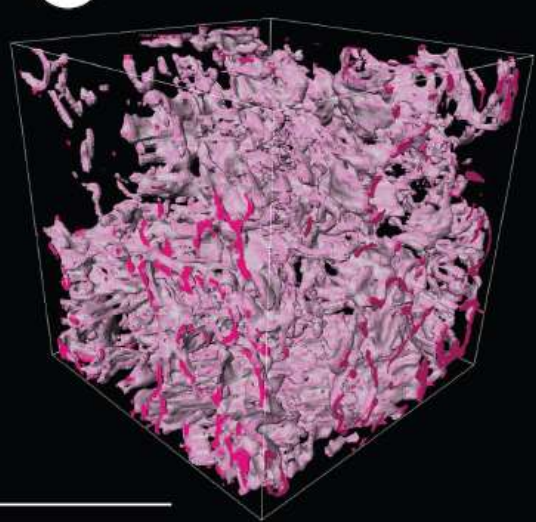
TABLES FOR CHAPTER 3

Tables 3.1–3.6:

Scheme for the assessment of skeletal articulation and completeness in the nine

skeletal units of *Confuciusornis* and microraptorines. Each variable can be scored

from 0 (least complete/articulated) to 4 (most complete/articulated).

Requirements/examples for each score are given.

Table 3.1	Limbs; right and left forelimbs, right and left hindlimbs	
	Confuciusornis and Microraptorines	
	Completeness	Articulation
4	All sub units present	All articulated
3	3 sub units present	1–2 breaks
2	2 sub units present	3–10 breaks
1	1 sub units present	>11 breaks
0	No sub units present	No articulation

Table 3.2	Cervical vertebrae			
	Confuciusornis (8 vertebrae)		Microraptorines (10 vertebrae)	
	Completeness	Articulation	Completeness	Articulation
4	6+ vertebrae, 76–100%	All articulated	9+ vertebrae, 76–100%	All articulated
3	4–5 vertebrae, 51–75%	1–2 breaks	6–8 vertebrae, 51–75%	1–2 breaks
2	2–3 vertebrae, 26–50%	3–4 breaks	3–5 vertebrae, 26–50%	3–5 breaks
1	Single vertebrae, 11–25%	>5 breaks	1–2 vertebrae, 11–25%	>6 breaks
0	No vertebrae, 0–10%	No articulation	No vertebrae, 0–10%	No articulation

Table 3.3	Dorsal vertebrae			
	Confuciusornis (19 vertebrae)		Microraptorines (18 vertebrae)	
	Completeness	Articulation	Completeness	Articulation
4	14+ vertebrae, 76–100%	All articulated	15+ vertebrae, 76–100%	All articulated
3	9–13 vertebrae, 51–75%	1–2 breaks	10–14 vertebrae, 51–75%	1–2 breaks
2	5–8 vertebrae, 26–50%	3–10 breaks	5–9 vertebrae, 26–50%	3–9 breaks
1	3–4 vertebrae, 11–25%	>11 breaks	2–4 vertebrae, 11–25%	>10 breaks
0	0–2 vertebrae, 0–10%	No articulation	0–1 vertebrae, 0–10%	No articulation

Table 3.4		Caudal vertebrae		
	Confuciusornis (8 vertebrae)		Microraptorines (26 vertebrae)	
	Completeness	Articulation	Completeness	Articulation
4	6+ vertebrae, 76–100%	All articulated	15+ vertebrae, 76–100%	All articulated
3	4–5 vertebrae, 51–75%	1–2 breaks	10–14 vertebrae, 51–75%	1–2 breaks
2	2–3 vertebrae, 26–50%	3–4 breaks	5–9 vertebrae, 26–50%	3–10 breaks
1	1 vertebrae, 11–25%	>5 breaks	2–4 vertebrae, 11–25%	>11 breaks
0	No vertebrae, 0–10%	No articulation	0–1 vertebrae, 0–10%	No articulation

Table 3.5		Ribs		
	Confuciusornis (22 ribs)		Microraptor (20 ribs)	
	Completeness	Articulation	Completeness	Articulation
4	18+ ribs, 76–100%	All articulated	16+ ribs, 76–100%	All articulated
3	12–17 ribs, 51–75%	1–2 breaks	11–15 ribs, 51–75%	1–2 breaks
2	6–11 ribs, 26–50% c	3–10 breaks	6–10 ribs, 26–50%	3–10 breaks
1	3–5 ribs, 11–25%	>11 breaks	2–5 ribs, 11–25%	>11 breaks
0	0–2 ribs, 0–10%	No articulation	0–1 ribs, 0–10%	No articulation

Table 3.6		Skull		
	Confuciusornis		microraptorines	
	Completeness	Articulation	Completeness	Articulation
4	All skull elements present	All skull elements articulated	All skull elements complete	All articulated
3	Moderately complete; cranium often present, occipital/ 1 or 2 lower jaws often absent.	One to two disarticulated elements; usually the lower jaw is displaced from cranium.	Moderately complete; often missing some combination of maxilla and jugal bones.	One to two disarticulated elements, usually maxilla disarticulated from the premaxilla.
2	Three or more skull elements present; typically frontal, maxilla, parietal.	More than two disarticulations; Typically posterior cranium remains articulated; premaxilla and lower jaws disarticulated	Three or more skull elements absent; typically jugal and parts of the post orbital.	More than two disarticulations; typically the jaws and maxilla.
1	Single example; fragment of premaxilla	Near total disarticulations; area of skull around the jugal may remain articulated but also fragmented.	No examples.	Near total disarticulations; typically the frontal and maxilla remain articulated.
0	Head entirely absent	No articulation.	Head entirely absent	No articulation.

Table 3.7:

Descriptive statistics of taphonomic trends for total specimens and individual skeletal

units for *Confuciusornis* and microraptorines.

Table 3.7		Pearson goodness of fit test (R^2) Linearity of trend	Pearson goodness of fit test *p*-value	Spearman rank (rs) Strength of relationship between completeness and articulation	Spearman rank *p*-value	Intercept of the trend line with the y-axis (T)
Confuciusornis	Total	0.41	1.3x10-8	0.69	1.1x10-9	2.71 (Trend 2)
	Right forelimb	0.40	7.7x10-8	0.68	1.4x10-8	2.59 (Trend 2)
	Left forelimb	0.42	1.3x10-8	0.67	6.9x10-9	2.50 (Trend 2)
	Right hindlimb	0.08	1.6x10-2	0.28	2.4x10-2	3.76 (Trend 3)
	Left hindlimb	0.42	8.3x10-9	0.60	2.8x10-7	2.64 (Trend 2)
	Cervical vertebrae	0.22	8.5x10-5	0.38	2.4x10-3	3.34 (Trend 3)
	Dorsal vertebrae	0.11	8.4x10-3	0.35	1.0x10-2	3.49 (Trend 3)
	Caudal vertebrae	0.19	1.2x10-3	0.48	5.7x10-4	2.42 (Trend 2)
	Skull	0.33	1.1x10-7	0.50	6.0x10-5	2.82 (Trend 2)
	Ribs	0.36	9.6x10-5	0.67	1.7x10-5	1.96 (Trend 2)
microraptorines	Total	0.56	1.3x10-4	0.76	1.7x10-4	3.06 (Trend 3)
	Right forelimb	0.35	3.3x10-3	0.65	2.0x10-3	2.49 (Trend 2)
	Left forelimb	0.65	1.2x10-5	0.78	4.7x10-5	1.60 (Trend 2)
	Right hindlimb	0.35	4.4x10-3	0.41	8.3x10-2	3.34 (Trend 3)
	Left hindlimb	0.58	8.4x10-5	0.53	1.9x10-2	2.46 (Trend 2)
	Cervical vertebrae	0.23	2.2x10-2	0.40	8.7x10-2	3.75 (Trend 3)
	Dorsal vertebrae	0.08	1.00	0.00	1.00	3.63 (Trend 3)
	Caudal vertebrae	-	2.0x10-2	-	NA	4.00 (Trend 3)
	Skull	0.22	1.6x10-2	0.40	3.0x10-2	3.06 (Trend 3)
	Ribs	0.21	8.8x10-2	0.54	8.7x10-2	2.22 (Trend 2)

Table 3.8:

Descriptive statistics of the taphonomic trends for total specimens of *Confuciusornis*

and microraptorines in different orientations.

Table 3.8		R^2	*p*-value	Rs	*p*-value	T
Confuciusornis	Dorsoventral	0.44	5.9x10-5	0.73	8.8x10-6	2.75
	Oblique orientation	0.40	2.8x10-3	0.70	1.2x10-3	2.99
	Lateral orientation	0.17	0.12	0.53	9.0x10-2	2.25
microraptorines	Dorsoventral	1.00	1.9x10-2	1.00	0.33	3.33
	Oblique orientation	-0.31	0.83	0.41	0.49	3.12
	Lateral orientation	0.36	2.9x10-2	0.75	7.4x10-3	2.97

Table 3.9:

Corrected p-values of a non parametric multiple analysis of variance comparing the

relative magnitude of articulation and completeness for specimens of *Confuciusornis*

in different orientations.

Table 3.9			
Confuciusornis			
	Dorsoventral	Oblique	Lateral
Dorsoventral		0.3975	0.3975
Oblique	0.3975		0.0360
Lateral	0.3975	0.0360	
Permutations		9999	
Total sum of squares		32.1	
Within group sum of squares		27.23	
F		4.919	
P (same)		0.0063	

Table 3.10:

Corrected p-values of a non parametric multiple analysis of variance comparing the

relative magnitude of articulation and completeness for specimens of microraptorines

in different orientations.

Table 3.10			
microraptorines			
	Dorsoventral	Oblique	Lateral
Dorsoventral		1	1
Oblique	1		
Lateral	1	1	1
Permutations		9999	
Total sum of squares		9.482	
Within group sum of squares		9.265	
F		0.1873	
P (same)		0.9057	

Table 3.11:

Results summary of generalised linear model with Poisson distribution on the

relationship between specimen orientation and the difference between *Confusiusornis*

completeness and articulation data.

Table 3.11				
Deviance Residuals:				
Min	1st Quartile	Median	3rd Quartile	Max
-1.3629	-1.1941	-1.1941	0.3203	2.6876
Coefficients:				
	Estimate	Std. Error	z value	Pr(>|z|)
(Intercept)	-0.3383	0.1554	-2.177	0.0295 *
Forelimb or hindlimb	-31.1831	2551.5077	-0.012	0.9902
Orientation	0.2644	0.3126	0.846	0.3977
Forelimb or hindlimb: Orientation	32.1733	2551.5078	0.013	0.9899
Null deviance	148.21 on 102 degrees of freedom			
Residual deviance	136.80 on 99 degrees of freedom			
Akaike information criteria	263.18			

Table 3.12:

Results summary of Chi Squared tests. To determine if any one point of interunit
articulation is more or less likely to be found disarticulated than other points.
Distribution of each category of inter unit articulation among the 8 inter unit
articulation points is shown. Note: Numbers not in brackets are percentages of the
total number of the inter unit articulation joint recorded for each inter unit articulation
score. Number in brackets are total number of IUAs in each category, numbers in
square brackets are standardised residuals denoting deviation of observed distribution
of scores in each category from expected scores.

Table 3.12				
	Interunit articulation score			
Points of IUA	Fully disarticulated (0)	Partially articulated (0.5)	Fully articulated (1)	Total
Confuciusornis				
Rfl-a	36 (22) [0.36]	21 (13) [0.12]	43 (26) [-0.44]	100
Lfl-a	43 (26) [1.64]	23 (14) [0.54]	33 (20) [-2.00]	100
Rhl-a	33 (20) [-0.13]	18 (11) [-0.50]	48 (29) [0.53]	100
Lhl-a	41 (24) [1.16]	17(10) [-0.78]	42 (25) [-0.45]	100
s-cv	23 (14) [-1.90]	13 (8) [-1.53]	63 (38) [3.06]	100
cv-d	20 (11) [-2.45]	38 (21) [3.33]	43 (24) [-0.38]	100
d-cu	43 (21) [1.38]	14 (7) [-1.19]	43 (21) [-0.35]	100
Total	138	84	183	(405)
Df: 12	**X^2: 26.5329**	**P-value: 0.009016**		
Microraptorines				
Rfl-a	40 (8) [0.48]	50 (10) [2.66]	10 (2) [-2.86]	100
Lfl-a	65 (13) [3.01]	10 (2) [-1.75]	25 (5) [-1.37]	100
Rhl-a	35 (7) [-0.03]	20 (4) [-0.65]	45 (9) [0.61]	100
Lhl-a	35 (7) [-0.03]	20(4) [-0.65]	45 (9) [0.61]	100
s-cv	50 (5) [-1.04]	15 (3) [-1.20]	20 (12) [2.10]	100
cv-d	10(2) [-2.55]	40 (8) [1.56]	50 (10) [1.11]	100
d-cu	37 (7) [0.16]	26 (5) [0.04]	37 (7) [-0.19]	100
Total	272	196	232	(405)
Df: 12	**X^2: 27.4305**	**P-value: 0.006696**		

Table 4.1:

Composition of bottled mineral water taken from table of ingredients.

	mg/l
Calcium	55.0
Magnesium	4.4
Potassium	8.2
Sodium	31.2
Bicarbonate	193.0
Chloride	19.1
Sulphate	45.7
Nitrate	0
Flouride	<0.1
Dry residue at 180ºC	287
pH at source	7.85

Table 4.2:

Descriptive statistics for Shapiro wilks test for normality of each set of measurements

subset by decay stage.

		W	p value
Pterylae dermis thickness	Fresh	0.82	1.8×10^{-4}
	Stage one	0.82	6.6×10^{-3}
	Stage two	0.87	8.3×10^{-6}
	Stage three	0.48	0.48
Apterylae dermis thickness	Fresh	0.81	5.5×10^{-3}
	Stage one	0.93	0.16
	Stage two	0.83	3.4×10^{-2}
	Stage three	0.89	2.7×10^{-2}
Muscle diameter	Fresh	1.00	0.77
	Stage one	0.99	7.5×10^{-6}
	Stage two	0.93	7.1×10^{-14}
	Stage three	0.97	0.66
Muscle area	Fresh	0.95	1.2×10^{-4}
	Stage one	0.22	2.2×10^{-16}
	Stage two	0.92	2.0×10^{-8}
	Stage three	0.78	2.2×10^{-16}
Gecko dermis thickness	Fresh	0.95	0.43
	Stage one	0.93	0.01
	Stage two	0.90	5.6×10^{-8}
	Stage three	0.93	0.17
Pigmented layer of gecko dermis	Fresh	0.81	1.3×10^{-3}
	Stage one	0.92	5.8×10^{-3}
	Stage two	0.92	8.4×10^{-7}
	Stage three	0.90	3.9×10^{-2}

Table 4.3:

Reported decay stages for each tissue category of zebra finch skin in each thin section, where relevant.

ZEBRA FINCH DATA							
Sampling interval	FINCH	Sample	Slide	Tissue category decay stage			
				dermis	adipose	muscle	feather
FRESH	Q	3	1	FRESH	FRESH	FRESH	FRESH
			2	FRESH	FRESH	FRESH	FRESH
		8	1	FRESH	FRESH	FRESH	FRESH
			2	FRESH	FRESH	FRESH	FRESH
		9	1	FRESH	FRESH	FRESH	FRESH
			2	FRESH	FRESH	FRESH	FRESH
		12	1	FRESH	FRESH	FRESH	FRESH
			2	FRESH	FRESH	FRESH	FRESH
1 WEEK OF DECAY	F	3	1	2	N/A	2	N/A
			2	2	1	2	N/A
		4	1	2	1	2	1
			2	2	1	1	N/A
			3	1	2	1	2
			4	2	1	1	1
			5	1	2	1	1
	G	1	1	1	1	1	N/A
			2	1	1	1	1
			3	1	N/A	1	N/A
			4	1	1	1	1
		2	1	2	N/A	1	N/A
			2	2	2	1	N/A
			3	N/A	N/A	1	N/A
		3	1	1	1	1	1
			2	1	1	1	1
	H	3	1	1	1	N/A	1
			2	1	1	N/A	1
			3	1	1	N/A	1
		7	1	1	2	1	N/A
			2	1	2	1	1
		8	1	N/A	1	1	N/A
			2	N/A	1	1	1
2 WEEKS OF DECAY	I	4	1	2	2	3	N/A
			2	2	3	N/A	2
		11	1	3	3	3	3
			2	2	3	2	N/A
		12	1	2	2	3	N/A
			2	N/A	2	3	N/A
	J	1	1	3	N/A	2	N/A
			2	2	N/A	2	N/A
		2	1	1	N/A	1	N/A
		4	1	N/A	N/A	2	N/A
		7	1	N/A	3	2	N/A
			2	N/A	N/A	2	N/A

Sampling interval	FINCH	Sample	Slide	Tissue category decay stage			
				dermis	adipose	muscle	feather
2 WEEKS OF DECAY	K	1	1	3	3	N/A	N/A
			2	2	3	N/A	1
		2	1	1	4	N/A	N/A
			2	2	2	N/A	N/A
			3	2	3	N/A	1
			4	2	2	N/A	1
		3	1	1	1	2	1
			2	1	1	2	1
			3	1	1	2	1
		4	1	2	3	1	N/A
			2	2	2	1	N/A
		8	1	3	2	N/A	N/A
			2	3	2	N/A	N/A
4 WEEKS OF DECAY	L	1	1	2	2	3	3
			2	2	3	3	3
			3	3	2	3	3
			4	3	2	3	3
		2	1	2	3	3	N/A
			2	3	4	3	3
			3	3	4	3	N/A
			4	N/A	N/A	3	N/A
		3	1	2	4	3	N/A
			2	3	3	3	3
			3	3	3	3	3
			4	2	3	3	3
	M	1	1	2	2	N/A	N/A
			2	2	3	N/A	N/A
		3	1	3	3	3	N/A
			2	3	2	3	2
			3	3	2	3	2
			4	3	2	3	N/A
		5	1	2	4	2	N/A
			2	2	4	3	N/A
	N	4	1	2	4	2	N/A
			2	2	3	3	N/A
		14	1	3	3	3	N/A
			2	3	2	3	N/A

Table 4.4:

Reported decay stages for gecko skin in each thin section, where relevant.

GECKO DATA				
Sampling interval	GECKO	Sample	Slide	Gecko skin decay stage
FRESH	A	2	1	FRESH
		4	1	FRESH
		7	1	FRESH
		10	1	FRESH
1 WEEK OF DECAY	B	3	1	2
			2	1
		4	1	1
			2	1
		5	1	2
	C	2	1	1
			2	1
			3	2
		5	1	1
			2	1
			3	1
			4	1
	D	1	1	1
			2	1
			3	1
		5	1	1
			2	1
			3	1
2 WEEKS OF DECAY	E	2	1	2
			2	2
		8	1	2
			2	2
			3	1
			4	1
			5	2
			6	2
			7	2
	F	2	1	2
			2	2
		6	1	2
			2	2
		7	1	2
			2	2
			3	2
			4	2
	G	2	1	2
			2	2
			3	3
		6	1	2
			2	2
			3	2

4 WEEKS OF DECAY	H	1	1	3
			2	3
			3	2
		5	1	2
			2	2
			3	2
	I	5	1	2
			2	3
			3	3
		9	1	2
			2	2
			3	2
	J	3	1	2
			2	2
			3	2
		5	1	2
			2	3
			3	3

Table 5.1:

How features needed for the accurate imaging of decayed tissues are distributed among the three imaging methods discussed (Electron microscopy, Light microscopy and Micro-computed tomography).

	Requirements for accurate imaging of decayed tissues			
	High resolution images	Image exterior and interior of sample	Visualise tissue in three dimensions	Produce images in which structures can be recognised post-decay
Electron microscopy	YES	YES		YES
Light microscopy	YES	YES	YES	YES
Micro-computed tomography	YES	YES	YES	

The Taphonomy of Dinosaurs and Birds of the Jehol Biota

Christopher S. Rogers

Supplementary information on usb

Appendix chapter 3

Supplementary information 3.1: Photographs of specimens of *Confuciusornis* and microraptorines.

Supplementary information 3.2: Microsoft Excel file including the list of specimens and the skeletal taphonomy data sourced from each.

Appendix chapter 4

Supplementary information 4.1: Microsoft Excel file including the list of samples collected, thin sections produced from each sample and the measurements taken, where relevant of photographs of those thin sections.

Supplementary information 4.2: Histological images: Photographs of thin sections organised into folders by tissue category and sample.

Supplementary information 4.3: SEM 1 and SEM 2, PDFs with SEM images of epidermis at various stages of decay and clusters of keratinocytes that have separated from the epidermis. PDF with description of images in SEM 1 and SEM 2.